Landfill Emission Potential: Modeling, Uncertainty, and Geophysical Insights

Wang, L.

DOI
10.4233/uuid:0f57ad34-8aa9-4095-b88e-3231f993386b

Publication date
2025

Document Version
Final published version

Citation (APA)
Wang, L. (2025). *Landfill Emission Potential: Modeling, Uncertainty, and Geophysical Insights*. [Dissertation (TU Delft), Delft University of Technology]. https://doi.org/10.4233/uuid:0f57ad34-8aa9-4095-b88e-3231f993386b

Landfill Emission Potential: Modeling, Uncertainty, and Geophysical Insights

LIANG WANG

Landfill Emission Potential: Modeling, Uncertainty, and Geophysical Insights

Landfill Emission Potential: Modeling, Uncertainty, and Geophysical Insights

Dissertation

for the purpose of obtaining the degree of doctor
at Delft University of Technology
by the authority of the Rector Magnificus, prof.dr.ir. T.H.J.J. van der Hagen,
chair of the Board for Doctorates
to be defended publicly on
Tuesday, 9 September 2025 at 10:00 o'clock

by

Liang WANG

Master of Science in Geotechnical Engineering,
Southeast University, China,
born in Jiangsu, China

This dissertation has been approved by the promotors.

Composition of the doctoral committee:

Rector Magnificus,	chairperson
Prof.dr.ir. T.J. Heimovaara,	Delft University of Technology, *promotor*
Dr. J. Gebert,	Technische Universität Braunschweig, *promotor*
Independent members:	
Other members:	
Prof. dr. A. Weerts,	Deltares
Prof. dr. ir. E.C. Slob,	Delft University of Technology
Prof. dr. ir. F.C. Vossepoel,	Delft University of Technology
Dr. M. Hrachowitz,	Delft University of Technology
Dr. ir. Y. van der Velde,	Vrije Universiteit Amsterdam

Prof.dr.ir. T.J. Heimovaara of Delft University of Technology has contributed greatly to the preparation of this dissertation.

Keywords: Landfill emission potential, Stochastic modelling, Uncertainty quantification, Travel time distribution, Particle filtering, Electrical resistivity tomography, Hydrogeophysics, Bayesian inference

Printed by: Johannes Gutenberg

Cover by: Beautiful cover art that captures the entire content of this thesis in a single illustration.

ISBN 978-94-6384-829-9

An electronic copy of this dissertation is available at https://repository.tudelft.nl/.

To my beloved family.

CONTENTS

SUMMARY

The long-term environmental management of closed landfills presents significant challenges due to persistent uncertainty regarding residual contamination and pollutant release processes. While conventional aftercare practices, such as those mandated by the European Landfill Directive, focus on emission monitoring and maintenance of engineered barriers, they often overlook the complex subsurface dynamics of pollutant mobility within landfill waste bodies. Accurately quantifying the internal releasable pollutant content, referred to as the *emission potential*, is essential for developing realistic and scientifically-grounded aftercare strategies.

In this dissertation, I present an integrated framework to estimate and predict landfill emission potentials by combining stochastic modeling, Bayesian uncertainty quantification, data assimilation, and hydrogeophysical measurements. The research introduces a stochastic Lagrangian-based travel time modeling approach to simulate the heterogeneous water flow and solute transport within landfill bodies. This method, unlike traditional grid-based models, captures preferential flow phenomena and accommodates the spatial variability inherent in landfill waste structures.

The model calibration is performed using Bayesian inference, employing long-term observational data of leachate production and quality from the Braambergen landfill in the Netherlands. This probabilistic calibration explicitly quantifies uncertainties in model parameters and outputs, providing more credible risk assessments and long-term predictions of leachate emissions.

Recognizing the risk of error accumulation in history-matching methods, I further implement data assimilation techniques, notably the Weakly Coupled Particle Filter (WCPF) and a hybrid Particle Filter–Markov Chain Monte Carlo (PF-MCMC) method. These approaches enable sequential updating of model parameters and system states as new data become available, improving the predictive performance and reducing uncertainty over time. The PF-MCMC method, in particular, can estimate parameters and hidden processes, which is very helpful for understanding the dynamics in the landfill.

To further enhance the accuracy of emission potential estimations, the framework integrates hydrogeophysical data obtained through Electrical Resistivity Tomography (ERT). Using a Bayesian evidential learning approach, resistivity measurements are directly mapped into probabilistic

water storage estimates within landfill waste bodies. This additional constraint strengthens the characterization of subsurface hydrological conditions, distinguishing between leachable and isolated water fractions.

The dissertation is structured across six chapters, beginning with an overview of the landfill aftercare problem, followed by the development of the stochastic modeling framework, the application of particle filtering and PF-MCMC, the incorporation of ERT data through Bayesian evidential learning, and concluding with a synthesis of findings and recommendations for future research.

Overall, this work advances the scientific understanding of landfill emission dynamics by offering a unified methodological framework that integrates stochastic modeling, data assimilation, and hydrogeophysical surveying. The contributions herein support the development of more robust, data-driven, and cost-effective strategies for landfill aftercare, ensuring long-term environmental protection and sustainability.

SAMENVATTING

Het langetermijnbeheer van gesloten stortplaatsen brengt aanzienlijke uitdagingen met zich mee vanwege de voortdurende onzekerheid over resterende verontreiniging en processen van verontreinigingsafgifte. Hoewel conventionele nazorgpraktijken, zoals voorgeschreven door de Europese Stortplaatsrichtlijn, zich richten op emissiebewaking en het onderhouden van technische barrières, negeren zij vaak de complexe ondergrondse dynamiek van verontreinigingsmobiliteit in de stortplaatsmassa. Een nauwkeurige kwantificering van de intern vrijmaakbare hoeveelheid verontreinigingen, het zogenaamde *emissiepotentieel*, is essentieel voor het ontwikkelen van realistische en wetenschappelijk onderbouwde nazorgstrategieën.

In dit proefschrift presenteer ik een geïntegreerd raamwerk om emissiepotentiëlen van stortplaatsen te schatten en te voorspellen door stochastische modellering, Bayesiaanse onzekerheidskwantificering, data-assimilatie en hydrogeofysische metingen te combineren. Het onderzoek introduceert een stochastische, op Lagrange gebaseerde reistijdmodellering om de heterogene waterstroming en het opgeloste transport binnen stortplaatslichamen te simuleren. Deze methode, in tegenstelling tot traditionele roostergebaseerde modellen, vangt preferentiële stromingsverschijnselen en houdt rekening met de ruimtelijke variabiliteit die inherent is aan afvalstructuren.

De modelkalibratie wordt uitgevoerd met behulp van Bayesiaanse inferentie, waarbij langjarige observatiegegevens van percolaatproductie en -kwaliteit van de stortplaats Braambergen in Nederland worden gebruikt. Deze probabilistische kalibratie kwantificeert expliciet de onzekerheden in modelparameters en -uitkomsten, wat leidt tot betrouwbaardere risicobeoordelingen en langetermijnvoorspellingen van percolaatemissies.

Met het oog op het risico van foutaccumulatie in history-matching methoden implementeer ik bovendien data-assimilatietechnieken, met name het Weakly Coupled Particle Filter (WCPF) en een hybride Particle Filter–Markov Chain Monte Carlo-methode (PF-MCMC). Deze benaderingen maken het mogelijk modelparameters en systeemtoestanden sequentieel bij te werken zodra nieuwe gegevens beschikbaar komen, waardoor de voorspellende prestaties verbeteren en de onzekerheid in de loop van de tijd afneemt. De PF-MCMC-methode kan in het bijzonder zowel parameters als verborgen processen schatten, wat zeer nuttig is om de dynamiek in de stortplaats te begrijpen.

Om de nauwkeurigheid van emissiepotentieelinschattingen verder te

vergroten, integreert het raamwerk hydrogeofysische gegevens die zijn verkregen via Electrical Resistivity Tomography (ERT). Met behulp van een Bayesiaanse evidential learning-benadering worden resistiviteitsmetingen direct omgezet in probabilistische schattingen van de wateropslag in de afvalmassa. Deze extra beperking versterkt de karakterisering van de ondergrondse hydrologische omstandigheden en maakt onderscheid tussen uitloogbare en geïsoleerde waterfracties.

Het proefschrift is opgebouwd uit zes hoofdstukken, beginnend met een overzicht van het nazorgprobleem bij stortplaatsen, gevolgd door de ontwikkeling van het stochastische modelleringsraamwerk, de toepassing van deeltje-filtering en PF-MCMC, de integratie van ERT-gegevens via Bayesiaanse evidential learning, en afsluitend met een synthese van bevindingen en aanbevelingen voor toekomstig onderzoek.

Al met al vergroot dit werk het wetenschappelijke inzicht in de emissiedynamiek van stortplaatsen door een verenigd methodologisch raamwerk te bieden dat stochastische modellering, data-assimilatie en hydrogeofysische verkenning integreert. De hier gepresenteerde bijdragen ondersteunen de ontwikkeling van robuustere, datagedreven en kosteneffectieve strategieën voor nazorg, waarmee langdurige milieubescherming en duurzaamheid worden gewaarborgd.

1

INTRODUCTION

1

1.1. CURRENT STATE OF LANDFILL AFTERCARE

Landfills have long been the primary method of waste disposal in Europe, resulting in a large number of legacy sites requiring ongoing aftercare to protect human health and the environment. This aftercare typically involves monitoring emissions such as leachate and landfill gas, as well as maintaining the cover layers and collection systems. The European Landfill Directive (EC, 1999) mandates a minimum 30-year post-closure care period, though regulatory authorities may extend or shorten this period based on site-specific conditions. Law and Ross (2021) emphasize the importance of long-term care even beyond this period, which currently remains under-regulated and underfunded.

To end this costly and time-consuming aftercare phase, clear criteria must be established to evaluate potential risks. Laner *et al.* (2012a) proposed a site-specific framework for determining aftercare completion. This approach considers factors such as waste emission behavior, system performance, pollutant migration modeling through soil and groundwater, and compliance with environmental quality standards.

Several studies have reviewed strategies for either terminating or extending aftercare. For instance, Turner *et al.* (2017) used a life cycle assessment (LCA) to explore how different aftercare strategies impact long-term environmental outcomes. Their findings suggest that landfills managed with higher moisture content or infiltration outperform those capped with low-permeability barriers. Other researchers (Butt *et al.*, 2008; Laner *et al.*, 2012b) advocate for risk-based assessments to evaluate potential harm, offering more adaptive and evidence-based approaches to aftercare.

In most cases, aftercare consists of post-closure emission monitoring and maintenance of landfill systems. However, quantitative predictions of future emissions are critical to assess long-term risks. Barlaz *et al.* (2002) support using technical criteria based on time-series data of leachate composition, and leachate and gas production rates. One crucial criterion is the presence and ongoing performance of barrier systems, especially basal barriers, which cannot be maintained after closure and thus pose substantial long-term risks if they fail.

A research program aiming to achieve a significant reduction in emissions from Municipal Solid Waste landfills is currently being carried out in the Netherlands (Stichting Duurzaam Storten, 2013). More information on this program can be found at the website of the research program (Stichting Duurzaam Storten, 2025). In order to assess the success of the stabilization measures, site-specific Environmental Protection Criteria have been derived (Brand *et al.*, 2016; Storten, 2022). These criteria are defined to be the maximum allowable concentration of contaminant in the drainage system below the waste body, which will not lead to a concentration in the groundwater 20 m downstream of the

landfill that damages human health or the ecosystem.

Notably, much of the current research focuses on monitoring emissions rather than the pollutants remaining inside the landfill. This is understandable, given the inaccessibility of the landfill's interior. However, without understanding the residual contamination, long-term risk assessments remain uncertain. Laner *et al.* (2011a) highlight the importance of evaluating the remaining substance release potentials. This assessment should be site-specific and consider the type of deposited waste, local hydrogeological conditions, and the integrity of barrier systems. They propose a continuous emission model, assuming status quo conditions post-cap installation, based on a first-order decay model by Belevi and Baccini (1989). Although Laner *et al.* (2011b) outline methods for quantifying these residual release potentials, no supporting experimental data are currently available. How to estimate the environmental risk from the perspective of the pollutants remaining in the landfill's interior remains a challenge.

1.2. MODELING PROGRESS IN EMISSION POTENTIAL ESTIMATION

In this thesis, we introduce the term *emission potential* to describe the total mass of substances that can be released from a landfill's waste body. It represents the source term within a modeling framework designed to predict leachate flux and leachate concentration over time. By incorporating the emission potential, such models can more accurately reflect the temporal evolution of landfill emissions under varying environmental conditions. For conservative solutes, we hypothesize that the initial emission potential can be quantified by fitting a water balance model to measured outflow time series.

Fellner and Brunner (2010) give an overview of modeling approaches available in the literature for quantifying leachate production. Due to the large spatial heterogeneity in waste bodies of landfill, it is generally known that the contaminants are leached out from waste through preferential flow (Fellner & Brunner, 2010; Uguccioni & Zeiss, 1997). A simplified 2D two-domain grid-based model has been developed by Fellner and Brunner (2010) to simulate the preferential flow pattern in the landfill. However, this model cannot estimate water flow heterogeneity as it simply categorizes waste into two groups with their own hydraulic properties, which could not be correct in real landfills. Traditional grid-based models need to incorporate the heterogeneous hydraulic, chemical, and mechanical properties of the waste, arising from waste type, composition, and placement compaction, which requires multi-source high-quality data to quantify (Høyer *et al.*, 2019). To describe the heterogeneous flow and transport through waste bodies,

stochastic methods like Lagrangian-based travel time models attract more attention (Malmström *et al.*, 2004; Rosqvist & Destouni, 2000; Zacharof & Butler, 2004a, 2004b). Lagrangian modeling of water flow and solute transport is widely used in catchment hydrology field (Benettin & Bertuzzo, 2018; Benettin *et al.*, 2015, 2017; Harman, 2015; Rinaldo *et al.*, 2015a, 2015b). It has advanced significantly due to its ability to efficiently and intuitively represent flow and solute transport through heterogeneous environments, capturing travel time variability and complex reactions under uncertainty. Therefore, Lagrangian modeling offers a promising approach for estimating landfill emission potential by accounting for the inherent heterogeneity and transport dynamics of waste systems.

1.3. UNCERTAINTY QUANTIFICATION

Uncertainty is inherent in any landfill modeling effort due to the complex and heterogeneous nature of waste bodies, incomplete knowledge about physical processes, and the measurement and sampling errors in field data. Despite advances in modeling approaches—such as Lagrangian-based travel time models—to capture the dynamics of flow and solute transport, quantifying the associated uncertainty remains essential for accurate risk assessment and robust decision-making.

1.3.1. NEED FOR UNCERTAINTY QUANTIFICATION

Leachate generation and transport models, whether grid-based or Lagrangian, rely on numerous parameters (e.g., hydraulic conductivity, parameters in travel time distributions) that are often poorly constrained. Field measurements can be noisy, further complicating parameter estimation. As a result, deterministic model predictions—single "best-guess" outputs—may fail to capture the true variability and risks posed by landfill emissions. By conducting uncertainty quantification (UQ), modelers and policymakers can improve risk assessments by providing confidence intervals for predicted emission potential and leachate emissions.

1.3.2. MARKOV CHAIN MONTE CARLO (MCMC) METHODS

One widely used approach for uncertainty quantification is Markov Chain Monte Carlo (MCMC). It is especially relevant in the context of complex landfill models where parameters may exhibit strong non-linear interactions. The key idea of MCMC is to sample the model's parameter space using a probability-driven, iterative procedure by comparing model results with available measurements. Thus, it provides a robust

and flexible way to propagate parameter uncertainty through landfill models, enabling a deeper understanding of how uncertain inputs influence predictions. However, obtaining parameters by fitting or "history-matching" to data is generally a batch processing method that defines the best fit in an average way. This implies that we get the best fit of the measured data over the whole time range rather than the best estimation of model states (Liu & Gupta, 2007).

1.3.3. DATA ASSIMILATION METHODS

While MCMC methods are effective for exploring parameter uncertainty, they are computationally intensive and do not update predictions in real time. These methods typically sample from the full posterior $p(x_{0:T} \mid y_{0:T})$ in batch mode, without leveraging the model dynamics to perform sequential updates once new observations are available. In contrast, *data assimilation* (DA) methods aim to reduce uncertainty dynamically by continuously integrating new observation information into models. Data assimilation (DA) refers broadly to Bayesian inference approaches that integrate dynamic models with observational data to estimate time-evolving system states and/or parameters. It includes both filtering methods (e.g., Ensemble Kalman, Particle filter) that estimate the current state x_t using data up to time t, and smoothing methods (e.g., Rauch–Tung–Striebel smoother, Ensemble smoothers) that estimate past states using data over a longer window. What unifies DA methods is their reliance on the forecast–update cycle, where the model-generated forecast serves as a prior for Bayesian updating. While MCMC algorithms technically perform similarly to Bayesian smoothing, they are not usually considered data assimilation methods because they do not exploit or preserve the recursive information assimilation that characterises DA in operational settings. By systematically incorporating real-time or periodic monitoring data, DA methods can quantify uncertainties in both model parameters and states, thereby improving the accuracy and robustness of landfill emission potential predictions.

Among the main DA techniques, the *Ensemble Kalman Filter* (EnKF) (Evensen, 2003) and the *Particle Filter* (PF) (Kitagawa, 1996) are widely used for nonlinear and high-dimensional systems. EnKF updates states and/or parameters using an affine transformation that assumes a multivariate Gaussian distribution of states and observations (Hamid *et al.*, 2005; Sun *et al.*, 2020; Zhang *et al.*, 2017). This assumption can lead to suboptimal updates or even violations of physical constraints in systems that exhibit strong nonlinearity or non-Gaussianity.

Particle filtering, on the other hand, avoids this limitation by updating the system by reweighing particles based on their likelihood, given new observations. This approach maintains physical consistency and allows

for fully nonlinear data assimilation. As a result, particle filters have gained popularity in hydrological applications (Abbaszadeh *et al.*, 2019; Plaza Guingla *et al.*, 2013; Vrugt *et al.*, 2013; Zhang *et al.*, 2017).

Two main challenges must be overcome when applying particle filters: degeneracy and sample impoverishment (van Leeuwen *et al.*, 2019). Degeneracy refers to the situation where a small number of particles have significantly higher weights than the rest, rendering most particles ineffective. To mitigate this, particle filters use a resampling step, where particles with higher weights are replicated while those with low weights are discarded. While this improves sampling efficiency, it introduces the problem of sample impoverishment, characterized by a lack of particle diversity due to repeated replication of the same particles. This issue is particularly severe when estimating static parameters, as resampling alone does not provide a mechanism for parameter evolution. Localization has been introduced as a strategy to alleviate both issues, particularly in high-dimensional systems (Vossepoel & Jan van Leeuwen, 2007). By restricting the influence of observations to nearby state variables, localization reduces the effective dimensionality of the assimilation problem, helping to maintain a greater number of particles with meaningful weights and thus reducing degeneracy. However, when estimating truly static global parameters, the sample impoverishment problem is still significant.

To address this, Moradkhani *et al.* (2005) proposed perturbing parameters after resampling to maintain diversity. Building on this idea, Moradkhani *et al.* (2012) introduced a hybrid PF-MCMC method that uses Metropolis-Hastings steps to avoid excessive perturbation. This hybrid approach improves parameter sampling efficiency and has demonstrated enhanced performance in hydrological modeling (Yan *et al.*, 2015). Crucially, PF-MCMC maintains mass balance by generating all model states through forward simulations using perturbed parameters.

In scenarios involving coupled environmental systems, such as a hydrochemical model for landfill, *Coupled Data Assimilation* (CDA) becomes essential. CDA, which is mainly applied in coupled ocean-atmosphere problems, allows each subsystem to receive information from observations in both its own and other domains (Laloyaux *et al.*, 2016; Penny *et al.*, 2019; Penny & Hamill, 2017; Smith *et al.*, 2015; Tardif *et al.*, 2015).

In *weakly coupled DA* (WCDA), model states are propagated jointly via a coupled forward model but updated independently within each subsystem. The updated states are then reintegrated into the coupled system for the next forecast cycle (Penny & Hamill, 2017).

In contrast, *strongly coupled DA* (SCDA) updates all states across domains simultaneously using all available measurements (Ng *et al.*, 2009). Although SCDA is theoretically optimal, its application is limited in practice due to challenges in defining cross-domain error covariances.

Some ensemble-based methods estimate these correlations from ensemble forecasts, but their low-rank approximations may not adequately represent the actual error structure (Županski, 2017). Even in PF-based SCDA, the "curse of dimensionality" and degeneracy issues persist due to the high-dimensional joint state space. Evensen *et al.* (n.d.) convincingly shows that iterative ensemble smoothers that respect coupling between components can lead to more accurate and coherent state estimation in multiscale, strongly interacting systems. However, the assimilation window length must balance between being long enough to allow cross-covariance to develop and short enough to avoid nonlinear distortions

Han *et al.* (2013) showed that in a simplified 5-variable test, SCDA outperformed WCDA only when the ensemble size exceeded 10^4. Given such computational demands, most practical CDA applications favor the weakly coupled formulation (Zhang *et al.*, 2020).

Together, MCMC and data assimilation techniques could strengthen the predictive power of landfill emission models by accounting for and reducing uncertainty. This integrated approach provides a more robust and transparent basis for landfill aftercare decisions, ensuring that estimates of leachate flux, concentration, and long-term emission potential are both credible and actionable.

1.4. HYDROGEOPHYSICAL MEASUREMENTS

Hydrogeophysical surveys provide an additional, complementary source of information for estimating subsurface water storage in landfill bodies. Electrical Resistivity Tomography (ERT) is particularly attractive for these settings due to its ability to infer water content from measured resistivities, which can be linked to saturation through Archie's Law. Since the pollutant mass is the product of leachate volume and concentration, this extra water storage estimation gives us more insight into the emission potential.

ERT has been applied successfully to map moisture content, leachate distribution, and landfill gas accumulation in multiple studies (Feng *et al.*, 2017; Hu *et al.*, 2019; Neyamadpour, 2019). For instance, Zhan *et al.* (2019) demonstrated how ERT delineates leachate plumes in a controlled landfill cell, while Hu *et al.* (2019) used time-lapse ERT surveys to monitor changes in water content during landfill dewatering operations. These applications highlight ERT's utility for qualitatively tracking hydrological processes within waste bodies.

An emerging technique is hydrogeophysical joint inversion, where water storage and other hydraulic parameters (e.g., saturation, petrophysical coefficients) are derived directly from ERT data without requiring a separate inversion of the resistivity field (Linde & Doetsch, 2016). Treating ERT measurements within a coupled hydrogeophysical

model leverages explicit petrophysical relationships (like Archie's Law) to reduce uncertainty from intermediate inversion steps. However, challenges remain. Landfill waste layers often lack the well-defined water table assumed by many joint inversion algorithms, and extreme heterogeneity can undermine standard petrophysical models. Nevertheless, the potential for more accurate water content estimation is evident, making hydrogeophysics a powerful asset for improving emission potential predictions.

From a modeling perspective, ERT-based water storage estimates can be incorporated into the data assimilation methods discussed in previous sections (e.g., EnKF, PF, or PF-MCMC). However, in landfill models, fitting model parameters to observations typically allows us to estimate only the portion of water that is leachable. Some water may be stored in isolated zones, which have no influence on leachate emissions. Using ERT data enables the estimation of total water storage, including both the leachable and isolated fractions. This provides an important insight: it allows us to assess how different these two portions of water might be. In some cases, a significant amount of isolated water could be present in landfills, which would not contribute to the emission potential.

1.5. AIMS AND OBJECTIVES

The overarching aim of this thesis is to *estimate and predict the emission potential of landfills* by integrating *stochastic modeling*, *hydrogeophysical surveys*, and *uncertainty quantification methods*. This research spans from model development and validation to advanced data assimilation and ultimately leverages hydrogeophysical measurements (ERT) to improve water storage characterization in landfills. In detail, the objectives of this thesis are:

1. Develop a stochastic modeling framework: formulate a Lagrangian-based travel time model to capture the heterogeneous nature of water flow and contaminant transport in landfill waste bodies.

2. Implement uncertainty quantification (UQ) approaches: apply Markov Chain Monte Carlo (MCMC) to optimize the model first. Secondly, implement coupled particle filtering methods to estimate model states, parameters, and hidden processes.

3. Integrate hydrogeophysical (ERT) measurements: demonstrate how Electrical Resistivity Tomography can serve as an additional constraint for estimating water storage in landfill waste, including both leachable and isolated fractions.

4. Provide guidelines for practical application: outline how stochastic modeling, UQ, and ERT can be integrated into landfill management workflows to improve aftercare strategies.

These objectives collectively enable a more *realistic, data-informed* assessment of landfill emission potentials, providing a foundation for optimizing aftercare strategies and ensuring long-term environmental protection.

1.6. OUTLINE OF THE THESIS

This thesis is organized into *six main chapters*. Following a brief introduction and literature review in Chapter 1, the remaining chapters are outlined as follows:

- Chapter 2 focuses on the development of a *stochastic model* for landfill emissions. Here, a Lagrangian-based travel time framework is used to represent flow heterogeneity and pollutant release dynamics in landfill waste bodies.
- Chapter 3 builds upon that model to implement a *Particle Filter* for real-time state estimation. It demonstrates how sequential data assimilation can reduce predictive uncertainty in emission potential, leachate fluxes, and concentrations.
- Chapter 4 extends the scope to *PF–MCMC* techniques, integrating Markov Chain Monte Carlo steps into the Particle Filter. It aims to enable joint estimation of model parameters, hidden states, and processes without violating fundamental mass balances.
- Chapter 5 addresses *hydrogeophysical measurements*, with particular emphasis on applying Electrical Resistivity Tomography (ERT) to infer landfill water storage. A Bayesian evidential learning method is used to predict the water storage in waste bodies with uncertainty estimation directly with measured ERT data.
- Chapter 6 concludes the thesis by synthesizing the key results from all four chapters, reflecting on methodological contributions and practical implications for landfill aftercare. Prospects for future research—such as incorporating reactive transport processes or advanced field measurements—are also discussed.

Some redundancy exists in the introduction and methods sections of each chapter, as they were originally prepared as standalone journal articles.

REFERENCES

Abbaszadeh, P., Moradkhani, H., & Daescu, D. N. (2019). The Quest for Model Uncertainty Quantification: A Hybrid Ensemble and Variational Data Assimilation Framework. *Water resources research*, *55*(3), 2407–2431. https://doi.org/10.1029/2018WR023629

Barlaz, M. A., Rooker, A. P., Kjeldsen, P., Gabr, M. A., & Borden, R. C. (2002). Critical Evaluation of Factors Required To Terminate the Postclosure Monitoring Period at Solid Waste Landfills. *Environmental Science and Technology*, *36*(16), 3457–3464. https://doi.org/10.1021/es011245u

Belevi, H., & Baccini, P. (1989). Long-term behavior of municipal solid waste landfills. *Waste Management & Research*, *7*(1), 43–56. https://doi.org/10.1016/0734-242X(89)90007-4

Benettin, P., & Bertuzzo, E. (2018). Tran-SAS v1.0: A numerical model to compute catchment-scale hydrologic transport using StorAge Selection functions. *Geosci. Model Dev*, *11*(4), 1627–1639. https://doi.org/10.5194/gmd-11-1627-2018

Benettin, P., Kirchner, J. W., Rinaldo, A., & Botter, G. (2015). Modeling chloride transport using travel time distributions at Plynlimon, Wales. *Water Resources Research*, *51*(5), 3259–3276. https://doi.org/10.1002/2014WR016600

Benettin, P., Soulsby, C., Birkel, C., Tetzlaff, D., Botter, G., & Rinaldo, A. (2017). Using SAS functions and high-resolution isotope data to unravel travel time distributions in headwater catchments. *Water Resources Research*, *53*(3), 1864–1878. https://doi.org/10.1002/2016WR020117

Brand, E., de Nijs, T. C. M., Dijkstra, J. J., & Comans, R. N. J. (2016). A novel approach in calculating site-specific aftercare completion criteria for landfills in The Netherlands: Policy developments. *Waste Management*, *56*, 255–261. https://doi.org/10.1016/j.wasman.2016.07.038

Butt, T. E., Lockley, E., & Oduyemi, K. O. K. (2008). Risk assessment of landfill disposal sites – State of the art. *Waste Management*, *28*(6), 952–964. https://doi.org/10.1016/j.wasman.2007.05.012

EC. (1999). Council directive 1999/31/ec of 26 april 1999 on the landfill of waste. *Official Journal of the European Communities*, *182*, 1–19. https://doi.org/10.1039/ap9842100196

Evensen, G. (2003). The Ensemble Kalman Filter: Theoretical formulation and practical implementation. *Ocean dynamics*, *53*(4), 343:367. https://doi.org/10.1007/s10236-003-0036-9

Evensen, G., Vossepoel, F. C., & van Leeuwen, P. J. (n.d.). Iterative ensemble smoothers for data assimilation in coupled nonlinear multiscale models.

Fellner, J., & Brunner, P. H. (2010). Modeling of leachate generation from MSW landfills by a 2-dimensional 2-domain approach. *Waste Management*, *30*(11), 2084–2095. https://doi.org/10.1016/j.wasman.2010.03.020

Feng, S.-J., Bai, Z.-B., Cao, B.-Y., Lu, S.-F., & Ai, S.-G. (2017). The use of electrical resistivity tomography and borehole to characterize leachate distribution in Laogang landfill, China. *Environmental Science and Pollution Research*, *24*(25), 20811–20817. https://doi.org/10.1007/s11356-017-9853-0

Hamid, Sorooshian, S., Gupta, H. V., & Houser, P. R. (2005). Dual state-parameter estimation of hydrological models using ensemble Kalman filter. *Advances in Water Resources*, *28*(2), 135–147. https://doi.org/10.1016/j.advwatres.2004.09.002

Han, G., Wu, X., Zhang, S., Liu, Z., & Li, W. (2013). Error covariance estimation for coupled data assimilation using a lorenz atmosphere and a simple pycnocline ocean model. *Journal of Climate*, *26*(24), 10218–10231. https://doi.org/10.1175/JCLI-D-13-00236.1

Harman, C. J. (2015). Time-variable transit time distributions and transport: Theory and application to storage-dependent transport of chloride in a watershed. *Water Resources Research*, *51*(1), 1–30. https://doi.org/10.1002/2014WR015707

Høyer, A.-S., Klint, K., Fiandaca, G., Maurya, P., Christiansen, A., Balbarini, N., Bjerg, P., Hansen, T., & Møller, I. (2019). Development of a high-resolution 3D geological model for landfill leachate risk assessment. *Engineering Geology*, *249*, 45–59. https://doi.org/10.1016/j.enggeo.2018.12.015

Hu, J., Wu, X. W., Ke, H., Xu, X. B., Lan, J. W., & Zhan, L. T. (2019). Application of electrical resistivity tomography to monitor the dewatering of vertical and horizontal wells in municipal solid waste landfills. *Engineering Geology*, *254*, 1–12. https://doi.org/10.1016/j.enggeo.2019.03.021

Kitagawa, G. (1996). Monte carlo filter and smoother for non-gaussian nonlinear state space models. *Journal of computational and graphical statistics*, *5*(1), 1–25.

Laloyaux, P., Balmaseda, M., Dee, D., Mogensen, K., & Janssen, P. (2016). A coupled data assimilation system for climate reanalysis. *Quarterly Journal of the Royal Meteorological Society*, *142*(694), 65–78. https://doi.org/10.1002/qj.2629

Laner, D., Crest, M., Scharff, H., Morris, J. W. F., & Barlaz, M. A. (2012a). A review of approaches for the long-term management of municipal solid waste landfills. *Waste Management*, (3). https://doi.org/10.1016/j.wasman.2011.11.010

Laner, D., Fellner, J., & Brunner, P. H. (2011a). Environmental compatibility of closed landfills - assessing future pollution hazards. *Waste Management & Research*, *29*(1), 89–98. https://doi.org/10.1177/0734242X10387655

Laner, D., Fellner, J., & Brunner, P. H. (2012b). Site-specific criteria for the completion of landfill aftercare. *Waste Management & Research*, *30*(9_suppl), 88–99. https://doi.org/10.1177/0734242X12453610

Laner, D., Fellner, J., & Brunner, P. H. (2011b). Future landfill emissions and the effect of final cover installation – A case study. *Waste management*, *31*(7), 1522–1531. https://doi.org/10.1016/j.wasman.2011.02.022

Law, H. J., & Ross, D. E. (2021). Importance of long-term care for landfills. *Waste Management & Research*, *39*(4), 525–527. https://doi.org/10.1177/0734242X21999288

Linde, N., & Doetsch, J. (2016). Joint Inversion in Hydrogeophysics and Near-Surface Geophysics. In *Integrated Imaging of the Earth* (pp. 117–135). American Geophysical Union (AGU). https://doi.org/10.1002/9781118929063.ch7

Liu, Y., & Gupta, H. V. (2007). Uncertainty in hydrologic modeling: Toward an integrated data assimilation framework. *Water resources research*, *43*(7), 2006WR005756. https://doi.org/10.1029/2006WR005756

Malmström, M. E., Destouni, G., & Martinet, P. (2004). Modeling expected solute concentration in randomly heterogeneous flow systems with multicomponent reactions. *Environmental Science and Technology*, *38*, 2673–2679. https://doi.org/10.1021/ES030029D/SUPPL_FILE/ES030029D_S.PDF

Moradkhani, H., DeChant, C. M., & Sorooshian, S. (2012). Evolution of ensemble data assimilation for uncertainty quantification using the particle filter-markov chain monte carlo method. *Water Resources Research*, *48*(12), 2012WR012144. https://doi.org/10.1029/2012WR012144

Moradkhani, H., Hsu, K. L., Gupta, H., & Sorooshian, S. (2005). Uncertainty assessment of hydrologic model states and parameters: Sequential data assimilation using the particle filter. *Water Resources Research*, *41*(5), 1–17. https://doi.org/10.1029/2004WR003604

Neyamadpour, A. (2019). 3D monitoring of volumetric water content using electrical resistivity tomography in municipal solid waste landfill. *Environmental Earth Sciences*, *78*(14), 1–9. https://doi.org/10.1007/s12665-019-8436-4

Ng, G.-H. C., McLaughlin, D., Entekhabi, D., & Scanlon, B. (2009). Using data assimilation to identify diffuse recharge mechanisms from chemical and physical data in the unsaturated zone. *Water resources research*, *45*(9), 2009WR007831. https://doi.org/10.1029/2009WR007831

Penny, S. G., Bach, E., Bhargava, K., Chang, C. C., Da, C., Sun, L., & Yoshida, T. (2019). Strongly Coupled Data Assimilation in Multiscale Media: Experiments Using a Quasi-Geostrophic Coupled Model. *Journal of Advances in Modeling Earth Systems*, *11*(6), 1803–1829. https://doi.org/10.1029/2019MS001652

Penny, S. G., & Hamill, T. M. (2017). Coupled data assimilation for integrated earth system analysis and prediction. *Bulletin of the American Meteorological Society*, *98*(7), ES169–ES172. https://doi.org/10.1175/BAMS-D-17-0036.1

Plaza Guingla, D. A., De Keyser, R., De Lannoy, G. J., Giustarini, L., Matgen, P., & Pauwels, V. R. (2013). Improving particle filters in rainfall-runoff models: Application of the resample-move step and the ensemble Gaussian particle filter. *Water Resources Research*, *49*(7), 4005–4021. https://doi.org/10.1002/wrcr.20291

Rinaldo, A., Benettin, P., Harman, C. J., Hrachowitz, M., McGuire, K. J., van der Velde, Y., Bertuzzo, E., & Botter, G. (2015a). Storage selection functions: A coherent framework for quantifying how catchments store and release water and solutes. *Water Resources Research*, *51*(6), 4840–4847. https://doi.org/10.1002/2015WR017273

Rinaldo, A., Benettin, P., Harman, C. J., Hrachowitz, M., McGuire, K. J., van der Velde, Y., Bertuzzo, E., & Botter, G. (2015b). Storage selection functions: A coherent framework for quantifying how catchments store and release water and solutes. *Water Resources Research*, *51*(6), 4840–4847. https://doi.org/10.1002/2015WR017273

Rosqvist, H., & Destouni, G. (2000). Solute transport through preferential pathways in municipal solid waste. *Journal of Contaminant Hydrology*, *46*(1), 39–60. https://doi.org/10.1016/S0169-7722(00)00127-3

Smith, P. J., Fowler, A. M., & Lawless, A. S. (2015). Exploring strategies for coupled 4D-Var data assimilation using an idealised atmosphere-ocean model. *Tellus A: Dynamic Meteorology and Oceanography*, *67*(1), 27025. https://doi.org/10.3402/tellusa.v67.27025

Stichting Duurzaam Storten. (2013). *Duurzaam stortbeheer* [Available at: https://duurzaamstorten.nl/en/]. Retrieved May 9, 2025, from https://duurzaamstorten.nl/en/

Stichting Duurzaam Storten. (2025). *Duurzaam stortbeheer* [Available at: https://www.duurzaamstortbeheer.nl/]. Retrieved May 9, 2025, from https://www.duurzaamstortbeheer.nl/

Storten, S. D. (2022). *The dutch foundation for sustainable landfilling.* (research rep.). Dutch Sustainable Landfill Foundation. https://duurzaamstorten.nl/en/

Sun, Y., Bao, W., Valk, K., Brauer, C. C., Sumihar, J., & Weerts, A. H. (2020). Improving Forecast Skill of Lowland Hydrological Models Using Ensemble Kalman Filter and Unscented Kalman Filter. *Water Resources Research*, *56*(8), e2020WR027468. https://doi.org/10.1029/2020WR027468

Tardif, R., Hakim, G. J., & Snyder, C. (2015). Coupled atmosphere–ocean data assimilation experiments with a low-order model and CMIP5 model data. *Climate Dynamics*, *45*(5-6), 1415–1427. https://doi.org/10.1007/s00382-014-2390-3

Turner, D. A., Beaven, R. P., & Woodman, N. D. (2017). Evaluating landfill aftercare strategies: A life cycle assessment approach. *Waste Management*, *63*, 417–431. https://doi.org/10.1016/j.wasman.2016.12.005

Uguccioni, M., & Zeiss, C. (1997). Improvement of leachate prediction through municipal solid waste layers1. *JAWRA Journal of the American Water Resources Association*, *33*, 1265–1278. http://onlinelibrary.wiley.com/doi/10.1111/j.1752-%201688.1997.tb03551.x/abstract

van Leeuwen, P. J., Künsch, H. R., Nerger, L., Potthast, R., & Reich, S. (2019). Particle filters for high-dimensional geoscience applications: A review. *Quarterly Journal of the Royal Meteorological Society*, (April), 2335–2365. https://doi.org/10.1002/qj.3551

Vossepoel, F. C., & Jan van Leeuwen, P. (2007). Parameter estimation using a particle method: Inferring mixing coefficients from sea level observations. *Monthly weather review*, *135*(3), 1006–1020.

Vrugt, J. A., ter Braak, C. J. F., Diks, C. G. H., & Schoups, G. (2013). Hydrologic data assimilation using particle Markov chain Monte Carlo simulation: Theory, concepts and applications. *Advances in Water Resources*, *51*, 457–478. https://doi.org/10.1016/j.advwatres.2012.04.002

Yan, H., DeChant, C. M., & Moradkhani, H. (2015). Improving soil moisture profile prediction with the particle filter-Markov chain Monte Carlo method. *IEEE Transactions on Geoscience and Remote Sensing*, *53*(11), 6134–6147. https://doi.org/10.1109/TGRS.2015.2432067

Zacharof, A. I., & Butler, A. P. (2004a). Stochastic modelling of landfill leachate and biogas production incorporating waste heterogeneity. Model formulation and uncertainty analysis. *Waste Management*, *24*(5), 453–462. https://doi.org/10.1016/j.wasman.2003.09.010

Zacharof, A. I., & Butler, A. P. (2004b). Stochastic modelling of landfill processes incorporating waste heterogeneity and data

uncertainty [Publisher: Elsevier]. *Waste Management*, *24*(3), 241–250. https://doi.org/10.1016/j.wasman.2003.12.001

Zhan, L.-t., Xu, H., Jiang, X.-m., Lan, J.-w., Chen, Y.-m., & Zhang, Z.-y. (2019). Use of electrical resistivity tomography for detecting the distribution of leachate and gas in a large-scale MSW landfill cell. *ENVIRONMENTAL SCIENCE AND POLLUTION RESEARCH*, *26*(20), 20325–20343. https://doi.org/10.1007/s11356-019-05308-6

Zhang, H., Hendricks Franssen, H.-J., Han, X., Vrugt, J. A., & Vereecken, H. (2017). State and parameter estimation of two land surface models using the ensemble Kalman filter and the particle filter. *Hydrology and Earth System Sciences*, *21*(9), 4927–4958. https://doi.org/10.5194/hess-21-4927-2017

Zhang, Z., Pan, X., Fang, Y., Wang, Y., Zhang, Y., & Xu, H. (2020). Laboratory study on the hydraulic characteristics of mechanically and biologically treated waste in China. *Waste Management*, *102*, 686–697. https://doi.org/10.1016/j.wasman.2019.11.026

Županski, M. (2017). Data Assimilation for Coupled Modeling Systems. In S. K. Park & L. Xu (Eds.), *Data Assimilation for Atmospheric, Oceanic and Hydrologic Applications (Vol. III)* (pp. 55–70). Springer International Publishing. https://doi.org/10.1007/978-3-319-43415-5_2

2

QUANTIFICATION OF EMISSION POTENTIAL OF LANDFILL WASTE BODIES USING A STOCHASTIC LEACHING FRAMEWORK

Sanitary engineered landfills require extensive aftercare to safeguard human health and the environment. This involves monitoring emissions like leachate and gas, maintaining cover layers, and managing leachate and gas collection systems. Quantifying emission potential, a key concept integrating various processes influencing emissions, is essential for managing and predicting landfill impacts. In this study, we developed a stochastic travel time model based on water life expectancies. The model is used to predict leachate production rates and leachate chloride concentrations from landfill waste bodies. We present new data for long-term time series of leachate production and leachate quality for Landfill Braambergen in the Netherlands. By analyzing the parameters and evolution of model states, we obtain a deeper understanding of the water and mass balance of the waste bodies. We demonstrate that the model can be used to quantify the emission potential, and the estimated values of total mass match data quantified by sampling from the waste body. The results confirm that emissions with leachate are dominated by preferential flow infiltrating from the cover layer.

Parts of this chapter have been published in Heimovaara and Wang (2025)

2.1. INTRODUCTION

Landfills have long been the primary method of waste disposal in Europe, resulting in a large number of legacy landfills that require aftercare to protect human health and the environment. Aftercare typically involves monitoring emissions such as leachate and gas, as well as maintaining the cover layer and collection systems. The European Landfill Directive (EC, 1999) mandates a minimum 30-year aftercare period, but regulatory authorities may choose to shorten or extend this period based on a range of factors. To aid in decision-making, several authors have reviewed different approaches to ending or prolonging landfill aftercare (Barlaz *et al.*, 2002; Laner *et al.*, 2011). Several authors (Butt *et al.*, 2008; Laner *et al.*, 2012) have advocated for using risk-based assessments to evaluate the potential for harm. By exploring these and other solutions, we can work towards reducing the environmental impact of legacy landfills while ensuring the continued protection of public health.

In many cases the aftercare of sanitary engineered landfills consists of post-closure monitoring of emissions (e.g. leachate and gas) and maintenance of the cover layer and leachate and collection systems. Laner *et al.* (2012) postulate that post-closure care can end once a landfill no longer poses a threat to human health and the environment. Quantitative predictions of future emissions are important in order to assess future threats. Barlaz *et al.* (2002) advocate the use of technical criteria based on measured time series of leachate composition, and leachate and gas production rates. One such technical criterion is the presence of barrier systems which require maintenance during the aftercare period. Laner *et al.* (2011) address the importance of assessing the remaining substance release potentials. The assessment should be site-specific and take into account the deposited waste and the relevant boundary conditions that influence the flow of water through the landfill, including the performance of the barrier systems. They propose a continuous emission model assuming that the status quo persists (after installation of a cover layer) based on a first-order decay rate as proposed by Belevi and Baccini (1989). Although Laner *et al.* (2011) give suggestions on how to quantify the remaining substance source term, no experimental data are provided.

A research program aiming to achieve a significant reduction in emissions from Municipal Solid Waste landfills is currently being carried out in the Netherlands (Kattenberg *et al.*, 2013). More information on this program can be found at the website of the research program (Storten, 2022a, 2022b). In this program, different approaches to stabilize waste bodies by irrigation of water, recirculation and discharge of leachate, and aeration of the waste body are being tested. The approaches are tested at full scale at three different landfills. In order to assess the success of the stabilization measures, site-specific Environmental

Protection Criteria have been derived (Brand *et al.*, 2016; Dijkstra *et al.*, 2018). These criteria are defined to be the maximum allowable concentration of contaminant in the drainage system below the waste body, which will not lead to a concentration in the groundwater 20 meters downstream of the landfill which damages human health or the ecosystem. The underlying modeling approach assumes that the source term for all compounds in the drainage system remains constant over the complete evaluation period of 500 years.

In all the papers cited above, there is a common agreement that it is important to have a quantitative understanding of the source term controlling emissions of the contaminants present in the waste body. In this chapter, we would like to propose some definitions in order to clarify different approaches to quantify the source term.

The total mass of different compounds can be measured in the laboratory from samples taken from the field using destructive analytical techniques. Because contaminants can be bound in solids, total mass can lead to a significant overestimation of leachable mass. Leachable mass can be quantified in the laboratory using different types of leaching methods (Kosson *et al.*, 2002; van der Sloot *et al.*, 2017). However, characterization of heterogeneous landfill waste bodies using sampling and laboratory analysis requires a large amount of samples because of the inherent uncertainty caused by spatial variability (Sormunen *et al.*, 2008a, 2008b). In addition to the spatial variability, it is also important to realize that waste bodies most likely contain zones or pockets which isolate volumes of waste from mobile water, such as waste stored in a closed plastic bag. The presence of dead zones implies that not all contamination present in the waste body will be released from the waste body. Consequently, laboratory techniques to assess the source term of contaminants may overestimate the amounts that can be released.

In this work, we introduce the term emission potential in order to describe the amount of mass that can be released from the waste body. The emission potential is the result of all processes involved in causing emissions of compounds from waste bodies. It is related to the multi-physical coupling between fluid flow, solute transport, biogeochemical transformations, waste body settlements, and many more. The emission potential is the source term in a modeling framework that is able to describe the leachate flux and leachate concentration as a function of time. The emission potential can be quantified by fitting models to measured time series. Finally, using these models allows us to quantify the emission from the waste body under different scenarios, for example, over a time period of 500 years.

Fellner and Brunner (2010) give an overview of modeling approaches available in the literature for quantifying leachate production. They show that preferential flow is a dominant process in waste bodies and needs to be incorporated in models in order to describe landfill

leachate production dynamics (Fellner & Brunner, 2010; Uguccioni & Zeiss, 1997). In order to describe the heterogeneous flow and transport through waste bodies, several Lagrangian-based travel time models have been developed (Malmström *et al.*, 2004; Rosqvist & Destouni, 2000; Zacharof & Butler, 2004a, 2004b). Lagrangian modeling of water flow and solute transport in catchment systems has seen significant progress since then (Benettin & Bertuzzo, 2018; Benettin *et al.*, 2015, 2017; Harman, 2015; Hrachowitz *et al.*, 2016; Rinaldo *et al.*, 2015). The advantage of these Lagrangian approaches is that they allow for describing water flow and solute transport in large-scale systems where heterogeneity is captured through probability distributions.

Given the large heterogeneity present in landfills, we have developed a stochastic Lagrangian travel time modeling framework to simulate landfill water and mass balances in order to quantify the emission potential of waste bodies. The parameters in the model are calibrated using time series measurements of leachate volumes pumped from the drainage system and bi-weekly chemical analyses of chloride concentrations in pumped leachate. Measuring pumped leachate volumes and leachate quality is standard procedure for landfill operators in the Netherlands, and as such, obtaining these time series is much easier and cheaper than taking samples from the landfill for analysis in the laboratory. The source term in the model, after calibration, is considered to be the emission potential. Long-term extrapolations using the calibrated model provide insight into how the emission potential impacts future leachate quality. The generic feasibility and applicability of the proposed concept are demonstrated using data from four different waste bodies.

2.2. THEORY AND METHODS

In order to develop the model equations, we hypothesize that the solute concentration in (pumped) leachate is mainly controlled by dilution of highly concentrated base flow from the waste body, with infiltrating water originating from rainfall. We assume that the waste body is a causal system for leachate production and solute transport. This implies that the output of the system at any given time depends only on the input and the system's past behavior and consequently, the flow of water and transport of solutes through the waste body can be modeled using travel time probability distributions. In this work, we assume that the travel time probability density functions (pdf) are constant in time. The approach we follow is similar to the one described by Benettin *et al.* (2015).

If we follow a water parcel that enters the waste body at time t_{in} and exits the waste body at time t_{ex} then the total time in the waste body ($T_T = t_{ex} - t_{in}$) at any moment in time can be characterized by its age

(or residence time) indicated as T_R and the time it will still remain in the waste body before it exits the waste body (its life expectancy) is indicated as T_E. Residence time and life expectancy are related to the total travel time T_T by:

$$T_T = T_R + T_E. \tag{2.1}$$

Each day as the water parcel moves through the waste body, its residence time increases with 1 day and its life expectancy decreases with one day, which can be written as:

$$\frac{\mathrm{d}T_R}{\mathrm{d}t} = 1, \quad \frac{\mathrm{d}T_E}{\mathrm{d}t} = -1. \tag{2.2}$$

Equation 2.2 can be seen as a celerity with unit value, where the sign determines which property is described.

2.2.1. WATER BALANCE

The upper boundary of the landfill is its surface, where water can enter as rainfall and leaves as evapotranspiration. The lower boundary consists of the drainage system, where water is pumped out of the landfill as leachate. To simplify the problem, we assume that we can model the landfill as a one-dimensional, 2-layered column, where the first layer represents a cover layer and the second layer is the waste body.

The water storage in the landfill is defined as:

$$V_{total} = \frac{S_{total}}{A_{lf}} = V_{cl} + V_{wb},$$

in which S_{total} is the volume of water in a landfill and A_{lf} is the surface area of the landfill and V_{cl} and V_{wb} are the water storage in the cover layer and waste body respectively.

WATER BALANCE OF THE COVER LAYER

The water balance of the cover layer links water entering the landfill as rain and leaving the landfill as evapotranspiration to the amount of water infiltrating in to the waste body:

$$\frac{\mathrm{d}V_{cl}(t)}{\mathrm{d}t} = q_{rf}(t) - q_{ev}(t) - q_{inf}(t), \tag{2.3}$$

where V_{cl} is the storage in the cover layer.

The infiltration flux is assumed to be a nonlinear function of the storage in the cover layer.

$$q_{inf} = -K_{cl}\left(S_{eff}\right)^{b_{cl}} \tag{2.4}$$

where S_{eff} is the effective storage which ranges from zero to one and is defined as:

$$S_{eff} = \frac{V_{cl} - V_{cl_{min}}}{V_{cl_{max}} - V_{cl_{min}}}$$

where K_{cl} is the hydraulic conductivity of the cover layer [m d^{-1}], $V_{cl_{max}}$ is the maximum achievable storage in the cover layer, $V_{cl_{min}}$ is the minimum storage in the cover layer above which water will still freely drain and b_{cl} is a dimensionless empirical parameter which is larger than 0. When b_{cl} is less than 1, drainage from the cover layer predominantly occurs at low effective storage values, whereas if it is larger than 1, drainage predominantly occurs at high effective storage values.

The actual evapo-transpiration is calculated from the potential evapotranspiration:

$$q_{ev} = E_{pot}\ C_f\ f_{red}, \tag{2.5}$$

where E_{pot} is the potential evaporation [m/day], C_f is an empirical crop factor which is assumed to be a landfill specific constant and f_{red} is a factor allowing evapo-transpiration to be reduced in order to prevent the storage in the cover layer to become negative.

This model assumes that flow is caused by gravity only, i.e. gradients in the hydraulic head of the soil do not drive water flow. The magnitude of flow is strongly controlled by the storage in the cover layer.

WATER BALANCE OF THE WASTE BODY

The water balance of the waste body is calculated as:

$$\frac{\mathrm{dV_{wb}(t)}}{\mathrm{d}t} = q_{inf}(t) - q_{leach}(t), \tag{2.6}$$

where q_{leach} is the leachate flux from the waste body to the drainage system.

We can rewrite equation (2.6) as a function of life expectancies using a probability distribution of life expectancies $p_{V_{wb}}(T_E, t)$ using:

$$\frac{\mathrm{d}V_{wb}(T_E, t)}{\mathrm{d}t} = \frac{\partial V_{wb}(T_E, t)}{\partial t} + \frac{\mathrm{dT_E}}{\mathrm{d}t}\frac{\partial V_{wb}(T_E, t)}{\partial T_E},$$

to get

$$\frac{\mathrm{dV_{wb}(T_E, t)}}{\mathrm{d}t} = q_{inf}(t) p_{q_{inf}}(T_E, t) - q_{leach}(t) \tag{2.7}$$

where

$$q_{leach}(t) = V_{wb}(0, t) \tag{2.8}$$

which states that the leachate flux is equal to all the water present in the waste body with a life expectancy of 0 at time t. Please note that

after we have solved for $V_{wb}(T_E, t)$ we can calculate $p_{V_{wb}}(T_E, t)$ with:

$$p_{V_{wb}}(T_E, t) = \frac{V_{wb}(T_E, t)}{V_{wb}(t)}.$$

In order to numerically solve equation (2.7), we need to discretize along life expectancies (T_E). T_E can range from 0 to infinity. To simplify implementation we chose to discretize T_E in a discrete number of daily values from $T_{E,0}$ to $T_{E,n_{tt}}$. $V_{wb}(T_{E,i}, t)$ represent water storage cells with a life expectancy $T_{E,i}$ at time t. $V_{wb}(T_{E,n_{tt}}, t)$ represents a bulk cell containing all water with a life expectancy larger than n_{tt} days. All water with $T_E > T_{E,n_{tt}}$ is assumed to be added to the storage in the bulk of the waste body V_{bulk}:

$$V_{bulk}(t) = V_{wb}(T_E \geq T_{E,n_{tt}}, t) \tag{2.9}$$

The consequence of this choice is that an additional water flux needs to be added to the model the rate of change in $V_{bulk}(t)$. We call this flow, base flow and assume that it is a function of V_{bulk}. The base flow (q_{bF}) controls the leachate flow from the landfill in prolonged drought periods, however, it cannot continue indefinitely because of the finite amount of water stored in the bulk of the waste body. To take this finite amount in to account, we apply a gamma distribution function in order to allow q_{bF} to reduce gradually after the bulk storage reaches a critical level:

$$q_{bF}(V_{bulk}) = q_{bF_0} \frac{f_{bF}(V_{bulk})}{\mu_{bF}}, \tag{2.10}$$

where

$$f_{bF}(V_{bulk}) = \frac{x^{\sigma_{bF}-1} e^{-(V_{bulk}-V_{bulk,min})}}{\Gamma(\sigma_{bF})}$$

where $V_{bulk,min}$ is the minimal storage in the bulk where the base flow drops to zero, μ_{bF} [m] is a scaling factor for the the bulk storage and σ_{bF} [m] determines the shape of the base flow function.

Including the base flow in equation 2.7 leads to:

$$\frac{\mathrm{dV_{wb}(T_E, t)}}{\mathrm{d}t} = q_{inf}(t) p_{q_{inf}}(T_E, t) + q_{bF}(V_{bulk}(t)) p_{q_{bF}}(T_E, t) - V_{wb}(0, t) \tag{2.11}$$

where we have two distinct sources for the water travelling through the waste body: 1) water infiltrating from the cover layer, q_{inf} and 2) the base flow released from the bulk of the waste, q_{bF}.

The probability distribution $p_{q_{inf}}(T_E, t)$ describes the life expectancies along a large number of trajectories in the waste body along which water is moving. Following Rosqvist and Destouni (2000), we assume that the ensemble of the life expectancies of all particles infiltrating from the cover layer can be described with a bimodal log-normal probability

density function. We assume that this bimodal probability distribution function is time invariant.

$$p_{q_{inf}}(T_E) = \beta p_{q_{inf},fast}(T_E) + (1-\beta) p_{q_{inf},slow}(T_E) \tag{2.12}$$

$$p_{q_{inf},i}(T_E) = \frac{1}{T_E \sigma_i \sqrt{2\pi}} \exp\left(\frac{-(\ln(T_E) - \ln(\tau_i))^2}{2\sigma_i^2}\right) \tag{2.13}$$

In these, $p_{q_{inf},fast}(T_E)$ and $p_{q_{inf},slow}(T_E)$ are log-normal probability distribution functions for fractions of water experiencing fast flow and slow flow respectively (indicated with index i in equation 2.13), where β is the fraction of water following the fast flow probability distribution function.

The probability distribution function for the life expectancies of the base flow is assumed to be a time-invariant gamma distribution, in which Γ is the gamma function and a_{bF} is a value between 0 and 1:

$$p_{bF}(T_E) = \frac{x^{a_{bF}-1} e^{-x}}{\Gamma(a_{bF})} \tag{2.14}$$

where x is a normalized life expectancy of the water released from the bulk waste, defined as:

$$x = T_E / T_{E,norm} \tag{2.15}$$

.

As stated before, assumptions underlying this approach are that the flow in the waste body is considered to be a causal process and that both travel time distributions are assumed to be time invariant. This implies that the flow occurs along specific paths or streamlines and that the flow rates in these paths remain constant in time. Harman (2015) shows that it is relatively simple to relax the assumption of time-independent pdfs, for example by making T_E a function of the storage.

WATER BALANCE OF THE DRAINAGE LAYER

In the landfills analyzed for this work, leachate is actively pumped from the drainage system by an automatic system that maintains the water level between a minimum and a maximum value. As a consequence, water levels in the drainage system are are nearly constant and we can assume that the flux from the drainage system is identical to the flux entering the drainage system:

$$q_{drain} = q_{leach} \tag{2.16}$$

2.2.2. SOLUTE MASS BALANCE

In order to demonstrate the concept, we chose to consider only conservative solutes (Chloride) for this work. This implies that the mass flux is fully controlled by water flow. Because the probability distribution of life expectancies implicitly takes account of the dispersion that occurs as water flows through the system, we neglect solute diffusion as a separate process because it is very slow. The solute flux can therefore be written as:

$$\boldsymbol{q}_M = \boldsymbol{q}_w\, c \tag{2.17}$$

The solute mass balance of the cover layer can be calculated as:

$$\frac{\mathrm{d}M_{cl}(t)}{\mathrm{d}t} = c_{rain}(t)q_{rf}(t) - c_{cl}(t)q_{inf}(t). \tag{2.18}$$

The solute mass balance can be defined with:

$$\frac{\mathrm{d}M_{wb}(T_E,t)}{\mathrm{d}t} = c_{inf}(t)q_{inf}(t)p_{q_{inf}}(T_E,t) + c_{bulk}(t)q_{bF}(V_{bulk}(t))p_{q_{bF}}(T_E,t) - M_{wb}(0,t) \tag{2.19}$$

where M_{cl} and M_{wb} are the total mass of conservative species present in the cover layer and waste body [kg/m^2], respectively. As we only consider old landfills which no longer accept waste, and we assume that the concentration of conservative solutes in rain in the Netherlands is much lower than those found in landfill leachate, we take influx of solutes with rainfall to be zero. In the waste body, each water parcel with a specific life expectancy is associated with a specific mass ($M_{wb}(T_E,t)$ similar to the storage in the waste body. The concentration of conservative species for the cover layer is:

$$c_{cl}(t) = \frac{M_{cl}(t)}{V_{cl}(t)},$$

and the concentrations of the water parcels in the waste body are:

$$c_{wb}(T_E,t) = \frac{M_{wb}(T_E,t)}{V_{wb}(T_E,t)}.$$

2.2.3. SOLUTION ALGORITHM FOR COVER LAYER

Implementing the equations for the cover layer as a differential equation results in a model that requires quite a lot of time to solve. In order to have a fast model which allows for a large number of runs in a Monte-Carlo simulation framework, we chose to simulate the flows for the cover layer with an algorithmic implementation based on the equations in paragraph 4.1.1. Rainfall data and potential evapotranspiration data are available as daily average fluxes. The implementation is shown in Algorithm 1 using a time step Δt of 1 day.

Algorithm 1 Implementation of the water balance algorithm for the cover layer.

1. Estimate infiltration flux with equation (2.4) and estimate the new storage
$$V_{cl_{est_{n+1}}} = V_{cl_n} + (q_{rf_{n+1}} - q_{inf_n} + q_{Ev_{n+1}})\ \Delta t. \tag{2.20}$$

2. If the estimated amount of water in the cover layer is larger than the maximum available storage capacity, $V_{cl_{est_{n+1}}} > V_{cl_{max}}$, we need to increase the amount of infiltration by short-circuiting the flow to the waste body and and then recalculating $V_{cl_{est_{n_1}}}$ with the corrected q'_{inf_n}
$$q'_{inf_n} = q_{inf_n} + (V_{cl_{max}} - V_{cl_{est_{n+1}}})\ /\Delta t, \tag{2.21}$$
$$V_{cl_{est_{n+1}}} = V_{cl_n} + (q_{rf_{n+1}} - q'_{inf_n} + q_{Ev_{n+1}})\ \Delta t. \tag{2.22}$$

3. However if ($V_{cl_{est_{n+1}}} < 0$ and $V_{cl_n} > V_{cl_{min}}$) then we need to limit the amount of infiltration (there is not enough water in the cover layer to sustain infiltration) and perhaps also reduce the amount of evaporation:
$$q'_{inf_n} = (V_{cl_{min}} - V_{cl_n})\ /\Delta t \tag{2.23}$$
after which we again calculate $V_{cl_{est_{n+1}}}$ using equation (2.22).

4. If the estimated storage after correction is still negative, ($V_{cl_{n+1}} < 0$), we need to limit the amount of evaporation and then recalculate $V_{cl_{est_{n+1}}}$
$$q'_{Ev_{n+1}} = q_{Ev_{n+1}} + V_{cl_{n+1}}\ /\Delta t, \tag{2.24}$$
$$V_{cl_{est_{n+1}}} = V_{cl_n} + (q_{rf_{n+1}} - q'_{inf_n} + q'_{Ev_{n+1}})\ \Delta t. \tag{2.25}$$
This approach implicitly implements the f_{red} term in equation 2.5.

5. All conditions should now be fulfilled so we have a new update of the storage in the cover layer:
$$V_{cl_{n+1}} = V_{cl_{est_{n+1}}} \tag{2.26}$$

2.2.4. SOLUTION ALGORITHM FOR THE WASTE BODY

In order to solve equation 2.11 we discretize it over both time dimensions where we use a daily time step $dt = 1$ day and for each time step, the life expectancy is distributed over $n_{tt} + 1$ values ranging from 0 to n_{tt}. This approach is illustrated in Figure 2.1. Each day, water infiltrating from the cover layer is distributed among the cells in the waste body using $p_{q_{inf}}(T_E)$ and water flowing from the bulk as base flow using $p_{bF}(T_E)$.

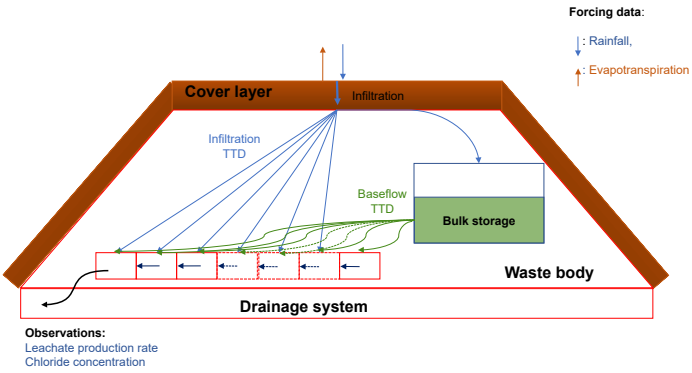

Figure 2.1.: Illustration of the conceptual model of the landfill system. The cover layer allows rainwater to be buffered so that evaporation can also occur on days without rainfall. Water subsequently infiltrates into the waste body. In the waste body, the infiltrated water is distributed over a discrete number of life-expectancy cells, and the remainder is added to the bulk. On a daily basis, water in the cell with a life expectancy (T_E) of zero is emptied in the drainage system from where it is immediately removed as leachate.

At $t = 0$, all cells are initialized with an initial amount of storage V_{ini}. Then every daily time step, all cells are shifted in life expectancy, i.e. the cell with $T_E = 1$ becomes 0, the cell with $T_E = n_{tt}$ becomes $n_{tt} - 1$ days and the cell with $T_E = n_{tt} - 1$ is filled with water from the bulk waste depending on the base flow.

2.2.5. MODEL CALIBRATION USING BAYESIAN INFERENCE

Before we can use this model to simulate leachate production rate and quality, we need to quantify the parameters. The parameters can be obtained by history matching of simulated leachate volumes and leachate concentrations to those obtained from measurements. We inferred the values of the parameters with the Multiple-try DREAM(ZS) package Laloy and Vrugt (2012), implemented in pyDREAM (Shockley *et al.*, 2018). DREAM (Vrugt, 2016) applies a Bayesian inference scheme

to obtain the distribution of model parameters ($\boldsymbol{\theta}$) which optimally describe the measured data in a probabilistic framework. Bayesian inference,

$$p(\boldsymbol{\theta}|\hat{\boldsymbol{y}}) \propto p(\boldsymbol{\theta}) \cdot L(\boldsymbol{\theta}|\hat{\boldsymbol{y}}), \tag{2.27}$$

allows us to calculate the joint posterior probability distribution ($p(\boldsymbol{\theta}|\hat{\boldsymbol{y}})$) of the set of parameters using the measured data. The posterior distribution is calculated using the prior distribution of the parameters ($p(\boldsymbol{\theta})$) and the likelihood of the parameters given the measured data ($L(\boldsymbol{\theta}|\hat{\boldsymbol{y}})$).

For the likelihood function, we applied the generalized likelihood function proposed by Schoups and Vrugt (2010):

$$L(\boldsymbol{\theta}|\hat{\mathbf{y}}) = -n \ln \frac{2\sigma_\xi \omega_\xi}{\xi + \xi^{-1}} - \sum_{t=1}^{n} \sigma_t - c_\beta \sum_{t=1}^{n} |a_{\xi,t}|^{2/(1+\beta)}. \tag{2.28}$$

For a detailed description and explanation of the parameters in this function we refer to Schoups and Vrugt (2010). We chose to use the generalized likelihood function because it allows for an improved handling of residual errors, which can be correlated, heteroscedastic, and non-Gaussian with varying degrees of kurtosis and skewness. As a result, this approach allows for a correct statistical description of the data and residual errors, without the need for separating the different error sources. In equation 2.28, we defined the measurement error as $\sigma_t = \sigma_0 + \sigma_1 y_t(\boldsymbol{\theta})$, $a_{\xi,t}$ is an independently and identically distributed random error with zero mean and unit standard deviation, described by a skew exponential power (SEP) density using parameters ξ and β to account for non-normality, scalars ω_β, σ_ξ, and c_β are derived from values of ξ and β which are a skewness and kurtosis parameter respectively and $\boldsymbol{\phi} = \{\phi_1, \ldots, \phi_4\}$ stores coefficients for an auto-regressive model of error residuals.

The generalized likelihood function is based on an additive non-linear regression model:

$$\mathbf{Y} = \mathbf{E} + \mathbf{e}$$

where $\mathbf{Y}$ is a vector of n observations, $\mathbf{E}$ is a corresponding vector of expected values; and $\mathbf{e}$ is a vector of zero mean random errors or residuals. The vector $\mathbf{e}$ includes measurement error, model input, and model structural errors. In order to account for heteroscedastic errors, Schoups and Vrugt (2010) suggest to include multiplicative bias factors in order to account for systematic deviations in model predictions:

$$E_t = Y_{h,t}(\mathbf{X}|\boldsymbol{\theta}_h)\mu_t. \tag{2.29}$$

In this equation, we assume that expected values can be modelled with a mass-balanced base flow model h, which yields simulated values $\boldsymbol{Y}_h$ as function of an observed input $\boldsymbol{X}$ and a vector of model parameters

$\boldsymbol{\theta}_h$. In this equation the simulated flow $Y_{h,t}$, and bias factor μ_t vary as a function of time. Schoups and Vrugt (2010) suggest to amplify the non-linearity in the response of the leachate production using

$$\mu_t = \exp(\mu_1 Y_{h,t}), \tag{2.30}$$

but we found that we obtained the best results by not including this bias factor so we kept μ_1 to zero.

As suggested by Vrugt (2016), we include σ_0, σ_1, β, ξ, $\boldsymbol{\phi}$ and y_{min} as so-called nuisance variables in the inference, together with all the other unknown parameters.

The generalized likelihood function was applied to both the time series of leachate production volumes and concentration data. The prediction of the cumulative total was constrained by adding a third normal likelihood term based on the cumulative leachate production over the inference period as a likelihood based on a sum of squares:

$$L_{cum}(\boldsymbol{\theta}|\hat{y}_{cum}) = -\frac{1}{2}\ln(y_{cum} - \hat{y}_{cum})^2. \tag{2.31}$$

The total likelihood, L_{tot} is the sum of the three likelihood values.

2.2.6. BOUNDARY CONDITIONS

The model is driven by daily rainfall and evaporation data, which we downloaded from the Royal Dutch Meteorological Institute (KNMI, 2022).

2.2.7. INITIALIZATION OF THE MODEL

Initial values for the model states need to be defined before we can keep track of the change in states, which are driven by the varying boundary conditions. The important states are the storage in the cover layer, V_{cl}, the storage in the waste body, V_{wb} and the solute mass in the cover layer and waste body, respectively, M_{cl} and M_{wb}. The model is started in the past, well before measurements become available, so that the effect of the initial conditions has been minimized by the seasonally varying boundary conditions. For the scenarios presented here, we start the simulation on the first of January 2003. The model is driven by daily precipitation and potential evapotranspiration data.

In order to facilitate a physical interpretation of the initial storage states, we relate them to the average water-filled porosity and heights of the cover layer and waste bodies. In addition, we estimate the initial mass present in the cover layer and waste body using an average concentration. The effect of initializing with average values will become smaller over time due to the cyclic seasonality in the meteorological boundary conditions.

The initial states are calculated with:

$$V_{cl} = \theta_{w_{cl}} * H_{cl} \tag{2.32}$$

$$V_{wb} = \theta_{w_{wb}} * H_{wb} \tag{2.33}$$

$$M_{cl} = V_{cl}\ c_{cl} \tag{2.34}$$

$$M_{wb} = V_{wb}\ c_{wb} \tag{2.35}$$

where subscripts cl and wb indicate cover layer and waste body. $\theta_{w_{cl}}$ and $\theta_{w_{wb}}$ are the volumetric water contents in the cover layer and waste body [-], H_{cl} and H_{wb} are the thickness of the cover layer and waste body [m]. M_{cl} and M_{wb} are the solute masses in the cover layer and waste body per unit landfill area. The maximum saturation of the cover layer is then parameterized using the maximum volumetric water content ($\theta_{w_{cl,max}}$) which is equal to the porosity of the cover layer. In order to ensure that the minimum storage in the cover layer is always less the maximum storage, it is initialized as a fraction of $\theta_{w_{cl,max}}$: $f_{w_{cl,min}}$. The saturation of the cover layer is initialized as to be half the difference between $V_{cl_{max}}$ and $V_{cl_{min}}$, and the saturation of the waste body was initialized directly. The minimum bulk storage, $V_{bulk_{res}}$ is parameterized in a similar manner with $f_{w_{wb,min}}$.

Each life expectancy cell and the bulk storage in the waste body are initialized with the same initial concentration from which the initial mass present in the waste body is calculated. The amount of mass removed every time step with the leachate is the amount of mass present in the cell with a life expectancy of 0 days. Mass can only enter the life expectancy cells from the bulk with the base flow. The mass in the bulk is updated every time step with the amount removed with the base flow. The mass in the life expectancy cells remains constant with time, infiltrating water from the cover layer only leads to dilution of the concentration.

2.3. SITE-SPECIFIC DATA AND PRIOR DISTRIBUTIONS OF UNKNOWN PARAMETERS

2.3.1. LANDFILLS

All data are from two landfills, which are currently part of the Natural Biodegradation Research Program on Dutch Landfills (Stichting Duurzaam Storten, 2017). The Wieringermeer landfill is near Medemblik, and the Braambergen landfill is near Almere, both in the Netherlands. Details for these landfills are given in Table 2.1. Both landfills are operated by Afvalzorg N.V.

Table 2.1.: General background information on the landfill cells

	Braambergen	**Wieringermeer**
Town	Almere	Medemblik
Compartment ID	11Z, 11Z and 12	VP06
Area basal drainage system [m^2]	11Z: 34,802 11Z: 35,188 12: 30,000	28,355
Time in operation	1999–2008	1992–1998
Total amount of waste [ton]	1,216,723	281,083
Volume of landfill cell [m^3]	11Z: 345,426.2 11Z: 388,981.9 12: 315,254.4	323,094
Average Height of landfill [m]	11Z: 9.9 11Z: 11.1 12: 10.5	12.2
Current landfill cover	Soil, incinerator bottom ash, jet grout (1.5 m)	Soil (1.5 m)
Landfill gas extraction	36 gas wells	2 gas wells + 1 shared
Bottom liner	Combination of mineral (50 cm sand bentonite) and 2 mm HDPE foil	Single 2 mm HDPE foil
Leachate drainage and collection	3 separate drainage systems for 11Z, 11Z, 12 (3 pump pits)	Separate drainage system for compartment 6, single pump pit
Aeration system	Installed Nov 2016–Jan 2017, expanded 2022 11Z: 65→113 wells, spacing 20→10 m 11Z: 114→163 wells, spacing 15→7 m 12: 56 wells, spacing 20 m Filter: 2 m long, depth 1 m above drainage system	Installed Oct 2016 109 wells, spacing 14 m Filter: 2 m long, depth 1.4 m above drainage system

Geo-referencing available as-built drawings to background maps and recent high-resolution areal photographs in a GIS package allowed us to estimate the surface area of the basal drainage system and the heights and surface areas of the landfills. The heights of the basal drains were measured in 2016. As the topography of the sites is variable, we estimated the volume of the waste body from the GIS derived data and then calculated the average height of the waste body by dividing the volume by the area of the basal drainage system. Background data for the four landfill cells can be found in Table 2.1.

Detailed monitoring of produced leachate volumes and leachate quality is carried out in the context of the biodegradation research program by the landfill operator since March 2012.

Data available for model calibration and verification were the cumulative leachate production measured every 15 minutes from 14 June 2012 to 1 November 2024 and chloride concentrations measured in a commercial laboratory over the same period. Laboratory analyses were performed on leachate samples that were taken once every two weeks.

By testing different attempts to infer the parameters from the data, we found that the best results were obtained when cumulative leachate production is transformed to weekly leachate production rates by differentiation of the cumulative production. This transformation allows the model to capture the weekly dynamics in the data.

Rainfall and potential evaporation data are downloaded from automatic weather stations operated by the Royal Dutch Meteorological Institute (KNMI, 2022). For the Wieringermeer landfill, we used the data from the Berkhout station; for Braambergen, we used the data from the Lelystad station. Daily rainfall and calculated reference evapo-transpiration were used for the water balance analysis.

Between October 2016 and February 2017, a large number of wells were installed at both landfills through which the waste body is aerated. As the aim of aeration is to ultimately improve leachate quality, the filters of the wells are installed deep in the waste body (about 1 to 2 m above the top of the drainage system. In 2023, additional wells were installed at Braambergen.

2.3.2. PRIOR DISTRIBUTION RANGES

In order to use Bayesian inference, we require prior distributions of uncertain model parameters. We chose to initialize the optimization with uniformly distributed priors over a predefined search range (Table 2.2). The initial ranges were defined based on the expected physical values and sometimes by trial and error. In this last case, when it became apparent during the optimization that the initial prior was too constrained, the boundaries of the distribution were extended. For

priors where variation is expected to vary across orders of magnitude, the ranges were initialized using the log-10 values of the parameters.

The number of finite travel times (n_{tt}) was set to be equal 1825 days (or 5 years). The model bias factor μ_1 in equations 2.29 and 2.30 was set to zero as first inference attempts indicated that model bias was not important.

In order to minimize the effect of the initial parameters on the calibration with measured data, we started the model on January 1st, 2003. This 'burn-in' time allows for the base flow from the bulk that initiated on January 1st 2003, to have moved completely across all 1825 cells before the results are compared to any measurement values. As such the solute mass and volume of water in the travel time cells are by then fully constrained by the base flow from the bulk waste five years earlier.

The model was calibrated using measured leachate volumes and chloride concentrations from the 1st of January 2014 to the 31st of December 2020. The remaining available data from the complete data set from 12 June 2012 until 1 November 2024 were used to assess the model performance beyond the calibration range.

Calibration was initially started, allowing the pyDREAM to randomly sample from the prior distributions. Once the inference had converged, pyDREAM was restarted with the final values of the 3 chains as an initial guess until the Gelman-Rubin criterion indicating convergence was met (Vrugt, 2016). The data were analyzed using the final distributions from this last optimization. The convergence and consequently the parameter distributions were assessed using the final 50% of the length of each chain (Vrugt, 2016). The optimal parameter set is the Pareto optimal of the three likelihoods calculated for leachate cumulative outflow, leachate outflow rate, and leachate concentration.

2.4. RESULTS AND DISCUSSION

2.4.1. SIMULATED LEACHATE OUTFLOW RATE AND LEACHATE CONCENTRATION VALUES

After convergence in pyDREAM, we may assume that all likelihood values in the final parameter set are samples from the distribution of likelihood values in the model that fit the measurements best. Because the inference is carried out in a hyperspace with 29 dimensions, different parameters can be highly correlated with each other.

As a result, we cannot use averaged parameter values from the posterior joint probability distributions. Instead, we need to select individual parameter vectors from the total converged distribution of parameters.

In order to provide insight into how well the model is able to describe

Table 2.2.: Priors for the Parameter Distributions Used in the Bayesian Inference

Parameter	Minimum	Maximum	^{10}log
Cover layer			
C_f	0.75	1.5	–
$\theta_{w_{cl},max}$	0.3	0.5	–
$f_{w_{cl},min}$	0.0001	1	–
K_{cl}	-5	3	x
b_{cl}	0	8	–
$c_{ini_{cl}}$	-4	-4	x
Waste body			
τ_{fast}	1	730	–
σ_{fast}	-5	2.5	x
$\Delta\tau_{slow}$	0	9125	–
σ_{slow}	-5	3	x
β_f	0	1	–
$\theta_{wb_{ini}}$	0.0	0.5	–
$f_{wb_{min}}$	0.0	0.5	–
bF_0	-5	-2	x
$c_{ini_{wb}}$	2	6	x
μ_{bF}	0	15	–
σ_{bF}	0	15	–
a_{bF}	-9	0	x
t_{norm}	0	1825	–
Generalized likelihood			
σ_0	-8	2	x
σ_1	-8	2	x
μ_1	0	–	–
β	-1	1	–
ξ	0.1	10	–
$\phi_{1,\text{leachate}}$	-1	1	–
$\phi_{1,\text{conc}}$	-1	1	–
$[\phi_2, \phi_3, \phi_4]$	[0, 0, 0]	–	–

Note. Priors are uniform distributions. The column ^{10}log indicates which parameters have a range defined by the ^{10}log values. Parameters with only a minimum value have not been inferred; the given values are used as a constant. The parameters for the generalized likelihood function are the same for both the leachate flow and the concentration data, except for the correlation parameter ϕ_1, which was maximized based on trial and error.

the measured data, we decided to present model estimations based on the posterior likelihood for parameter vectors where the density is 1, and close to 0.95, 0.5, and 0.05 from the converged distribution. The cumulative distribution of likelihood values is shown in Figure S1 in Appendix for the four waste bodies analyzed in this chapter. The likelihood values corresponding to the probability quantiles of the lines in the following graphs are reported in the legends of the figures.

The results of the simulated values of leachate production and leachate chloride concentration are compared with measured values for the Braambergen 11Z waste body in Figure 2.2. In the Appendix (Figure S2), we present similar figures for the Braambergen 11N and 12 and the Wieringermeer VP06 waste bodies.

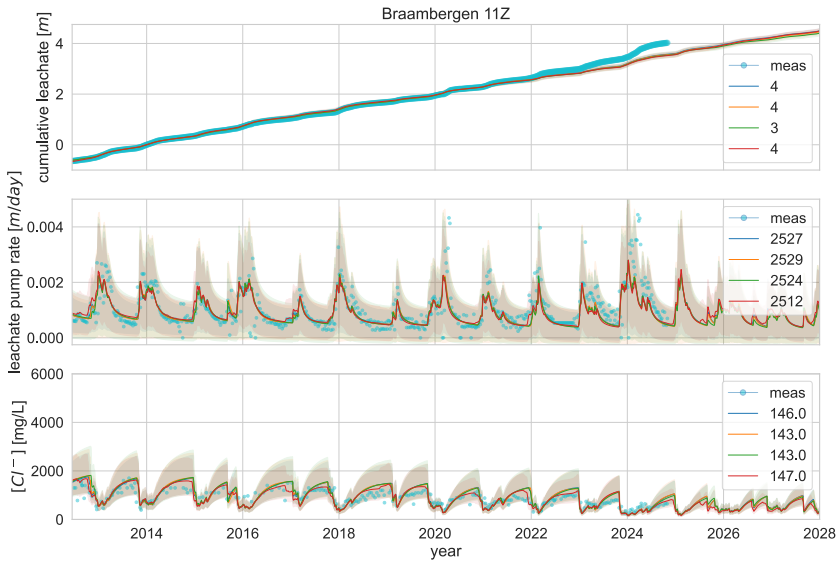

Figure 2.2.: Simulated and measured values of cumulative leachate production (CL [m]), leachate pump rate (LPR [m/day]) and leachate chloride concentration (conc [kg/m^3] for Braambergen 11Z. The four colors are the results of four scenarios corresponding to distinct values of likelihood from the converged parameter set. The shaded areas are the 95% confidence intervals estimated from the generalized likelihood model. The legends give the likelihood of the parameter set for the three objective functions used for optimization.

The generalized likelihood model of Schoups and Vrugt (2010) allows us to calculate a simulated measurement error with the forward model. For all sites the model is able to describe cumulative leachate production and leachate flow dynamics with similar accuracy. The uncertainty

estimated with the 95% confidence intervals is able to capture the spread in the measurement data for the data set used for the calibration.

In the generalized likelihood model of Schoups and Vrugt (2010), heteroscedasticity is explicitly accounted for by assuming that the measurement error increases linearly with the expected value:

$$\sigma_t = \sigma_0 + \sigma_1 E_t.$$

The inferred parameters in the generalized likelihood model ($\sigma_{0,leachate}$, $\sigma_{1,leachate}$, $\sigma_{0,conc}$, and $\sigma_{1,conc}$) of which the log10 values are reported in table 2.3, allow us to calculate the estimated measurement error for the simulated leachate production rates and leachate concentrations. For the concentration data, this calculation is less straightforward because the measurement error is estimated using the log10 transform of the measured concentration data. These uncertainties can be estimated for the other waste bodies as is graphically shown in Figure S3.

Although the uncertainty in the simulated values is significant, the estimates of the expected values give a good description of both measured time series. Please note that the calibration was carried using data that were measured between 1-1-2014 and 31-12-2020.

The estimates of the leachate production rates do not capture the extremes in the measured data. This is due to several reasons. The first is because the optimal parameter set is a pareto optimum of both leachate production rates and chloride concentrations. The simulation represented by the red line in Figure 2.2 for the Braambergen 11Z waste body is a clear example, with a high likelihood for the concentration data, but a lower one for the leachate data. An important reason for this ambiguity lies in the fact that the model is an initial boundary value problem in which many of the waste body properties cannot vary with time. Early attempts, where first only leachate production data were used in the objective criterion, gave better fits of measured leachate production values, however attempts to subsequently describe the concentration data with fixed optimal parameters for the leachate production rate simulation led to poor results for the concentration data (results not shown). This implies that the assumption of purely convective flow for chloride is not completely true or that the parameters in the model vary with time. When inferring the parameters from both time series, leachate production rates need to be smoothed in the model to a certain extent. Another example of the initial boundary condition problem can be seen in the early predictions of the concentration data (before the start of the calibration period in 2014), where the simulated concentrations poorly describe the measured values for Braambergen 11Z, 12, and Wieringermeer waste bodies.

The second reason is related to the quality of the measurement data. Leachate levels in the pump-pits of the waste body cells are allowed to vary over a narrow bandwidth of 10 cm. When the maximum level

is reached, the pump will be switched on; when the minimum level is reached, it switches off. During pumping, flow is cumulatively recorded. Since the start of monitoring in April 2012, several problems were encountered with the pumps, causing them to be switched off, leading to a zero flow. As a consequence, the drainage system buffered the leachate. As soon as the issues were fixed, the pumps quickly pumped the excess water until the set-points were reached. Pumping excess water led to much higher flow rates temporarily. In order to minimize this effect in the data, flow rates were obtained by taking backward differences of the cumulative data over a period of 7 days.

Because measurements of $q_{rf}(t)$ and $q_{leach}(t)$ were used to calibrate the model, and the uncertainty in the water balance is mainly associated with the estimation of $q_{ev}(t)$. In the approach we used, the final estimate of $q_{ev}(t)$ is determined by multiple (correlated) parameters in the model. For most of the time $q_{ev}(t)$ is equal to the estimated potential evapotranspiration, but there are moments when evaporation becomes zero due to insufficient water present in the cover layer.

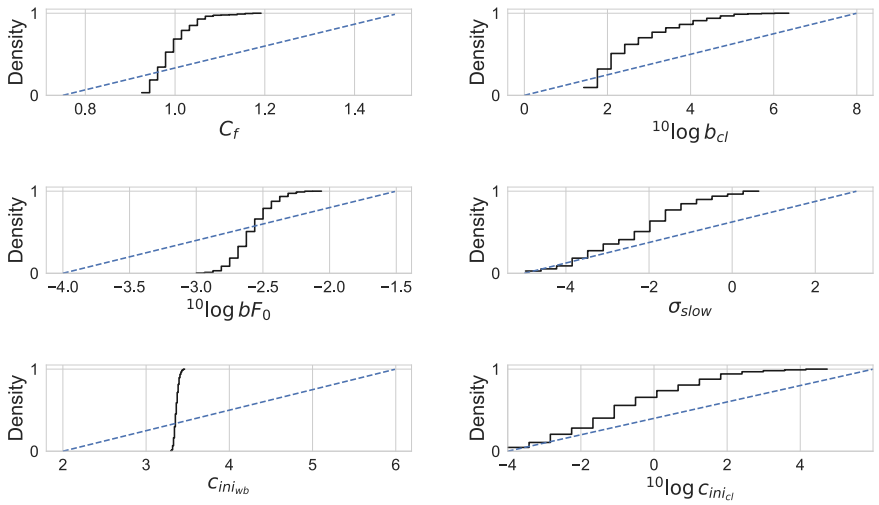

Figure 2.3.: Posterior (black) and prior (dashed blue) cumulative distributions of selected parameters for Braambergen 11Z. The left column gives examples of sensitive parameters that have converged to narrow posterior distributions, the right column gives examples of parameters that are highly correlated with other parameters or that are not sensitive and therefore are close to the prior.

The posterior distributions of the model parameters indicate the model sensitivity of the system to the parameter values within the optimal likelihood parameter set. Figure 2.3 gives examples of

Table 2.3.: Statistics and optimal parameter values after optimization with DREAM(ZS), Braambergen 11Z, number of samples in converged parameter set = 15000

	mean	std	min	25.00%	50.00%	75.00%	max	*1*	0.975	0.5	0.025
C_f	1.0	0.04	0.93	0.97	0.99	1.02	1.19	1.01	1.02	1.06	0.94
$\theta_{w_{cl,max}}$	0.39	0.02	0.35	0.38	0.39	0.4	0.44	0.39	0.39	0.38	0.36
$f_{w_{cl,min}}$	0.21	0.03	0.1	0.2	0.22	0.23	0.27	0.23	0.23	0.22	0.18
$^{10}\log K_{cl}$	1.22	0.32	0.49	0.97	1.23	1.45	2.14	1.21	0.81	1.44	0.89
b_{cl}	2.74	1.0	1.43	1.96	2.39	3.26	6.36	2.09	1.65	2.41	4.21
τ_{fast}	40.15	5.28	27.24	36.34	39.21	43.64	59.7	36.57	34.43	38.95	30.78
$^{10}\log \sigma_{fast}$	0.19	0.06	0.06	0.15	0.18	0.23	0.35	0.13	0.08	0.17	0.25
$\Delta\tau_{slow}$	2537.39	399.88	1683.64	2226.64	2562.19	2816.19	3703.74	2329.4	1967.03	2480.16	1986.02
$^{10}\log \sigma_{slow}$	-2.15	1.28	-4.97	-3.2	-2.0	-1.31	0.64	-2.52	-1.44	-1.42	-0.85
β_f	0.72	0.07	0.51	0.67	0.71	0.77	0.93	0.68	0.65	0.73	0.68
$\theta_{wb_{ini}}$	0.44	0.04	0.34	0.41	0.44	0.47	0.5	0.45	0.43	0.41	0.45
V_{min}	0.13	0.05	0.02	0.1	0.13	0.16	0.26	0.13	0.04	0.12	0.11
$^{10}\log bF_0$	-2.55	0.15	-3.0	-2.65	-2.57	-2.45	-2.06	-2.69	-2.54	-2.7	-2.4
$^{10}\log c_{ini_{cl}}$	-0.55	1.84	-4.0	-1.93	-0.79	0.75	4.74	-3.13	-1.76	0.47	-0.96
$^{10}\log c_{ini_{wb}}$	3.37	0.03	3.3	3.35	3.37	3.39	3.46	3.33	3.34	3.35	3.39
μ_{bF}	3.34	1.05	1.57	2.57	3.08	3.88	6.57	2.82	3.59	2.93	1.94
σ_{bF}	1.97	0.41	1.11	1.69	1.93	2.19	3.76	1.9	1.95	1.62	3.05
$^{10}\log a_{bF}$	-2.56	1.29	-6.05	-3.65	-2.46	-1.54	-0.02	-2.42	-3.46	-4.29	-3.22
$T_{E,norm}$	1403.17	156.77	907.43	1296.37	1407.54	1523.52	1752.52	1419.21	1620.3	1431.87	1391.85
$^{10}\log \sigma_{0,leachate}$	-3.73	0.04	-3.87	-3.76	-3.73	-3.71	-3.58	-3.75	-3.76	-3.73	-3.65
$^{10}\log \sigma_{1,leachate}$	-0.39	0.09	-0.71	-0.45	-0.39	-0.33	-0.15	-0.35	-0.28	-0.34	-0.5
$\beta_{leachate}$	0.92	0.07	0.57	0.89	0.94	0.97	1.0	0.95	0.98	0.84	0.91
$\xi_{leachate}$	1.22	0.08	0.97	1.17	1.21	1.26	1.57	1.2	1.18	1.1	1.2
$\phi_{1,leachate}$	0.26	0.04	0.15	0.24	0.26	0.29	0.37	0.22	0.3	0.23	0.27
$^{10}\log \sigma_{0,conc}$	-5.43	0.91	-7.47	-5.97	-5.51	-4.96	-2.08	-5.66	-5.55	-6.3	-6.09
$^{10}\log \sigma_{1,conc}$	-1.5	0.04	-1.63	-1.53	-1.5	-1.48	-1.38	-1.52	-1.5	-1.46	-1.49
β_{conc}	0.95	0.04	0.76	0.93	0.96	0.98	1.0	0.97	0.97	0.96	0.92
ξ_{conc}	1.25	0.12	0.88	1.16	1.25	1.33	1.59	1.22	1.24	1.29	1.29
$\phi_{1,conc}$	0.65	0.04	0.51	0.62	0.66	0.68	0.7	0.67	0.69	0.62	0.59
L_{tot}	2617.21	3.88	2597.87	2615.21	2617.52	2619.87	2626.13	2626.13	2622.75	2617.52	2610.57

posterior cumulative parameter distributions (in black) compared to the prior distributions in blue: the left column shows the inferred distributions for C_f, b_{F0}, and $c_{ini_{wb}}$ which are examples that have narrow distributions compared with the prior ranges given in table 2.2. This narrow distribution implies that the measured data contain sufficient information to infer these parameters. The total water balance depends strongly on the crop factor, C_f, because the surface area of the landfill is fixed, and the crop factor is the only parameter that can limit or enhance the evapotranspiration. Outflow concentrations strongly depend on the amount of solute mass present in the waste body, which is controlled by the initial concentration $c_{ini_{wb}}$ and the base flow, b_{F0}, which constrains the lowest flow rate during dry periods.

The parameters in the right column of Figure 2.3 are examples of poorly inferred parameters because the posterior distribution is very similar to the uniform prior distribution in table 2.2. The outflow concentration does not depend on the initial concentration in the cover

layer, $c_{ini_{cl}}$, in 2003. The simulation results show that any conservative solute in the cover layer is quickly removed. The posterior distribution can also be similar to the prior when the parameter is highly correlated with another one. A good example of this is the distribution of the mobile fraction in the cover layer, b_{cl}, which is highly correlated with residual water content in the cover layer. The last example of a poorly inferred parameter is the posterior distribution for σ_{slow}, which does have a narrower range than the prior, however, the final parameter range is still uniform over a wide range. σ_{slow} value controls the spread or variability of life expectancy values of water parcels traveling slowly through the landfill waste. When the slow-flow component has a very long mean travel time (large τ_{slow}), water from this slow pathway may rarely or never exit during the calibration period. As a consequence, observed data (leachate concentration and volume) provide little or no insight into this parameter.

2.4.2. ERROR MODEL

In order to check if the parameters in the error model are correctly inferred, we follow the approach used by Schoups and Vrugt (2010), where different aspects of the residuals are evaluated. Figure 2.3 presents the results of this analysis for the Braambergen 11Z waste body. For the error model, we assume that the errors are heteroscedastic; the left plots show the residuals as a function of the expected values of measured leachate production rates and concentrations. The errors are nicely distributed around zero, indicating that there is no bias in the results. The middle plots show that the distributions of errors are well described using the inferred parameters in the Skewed Exponential Power distribution of the generalized likelihood model. Clearly, the error model does not follow a normal distribution. Finally, the autocorrelation in the residuals is adequately captured with the autocorrelation parameter, even though the range for this parameter was constrained by a maximum value of 0.7. In addition, the different chains show similar results, demonstrating that the final parameter set is indeed from a converged distribution.

2.4.3. EXTRAPOLATION TO THE YEAR 2066

The model allows us to make predictions of how emissions vary in the future while taking the uncertainty in the inferred model parameters into account. The results for the Braambergen 11Z waste body are shown in Figure 2.5, for the other waste bodies we refer to the Supporting Information, Figure S3 in the Appendix. For all waste bodies, simulated results for selected parameter sets lie close to each other in the time range used to infer the parameters, but before and after the measurement time range, the results can diverge. This is most

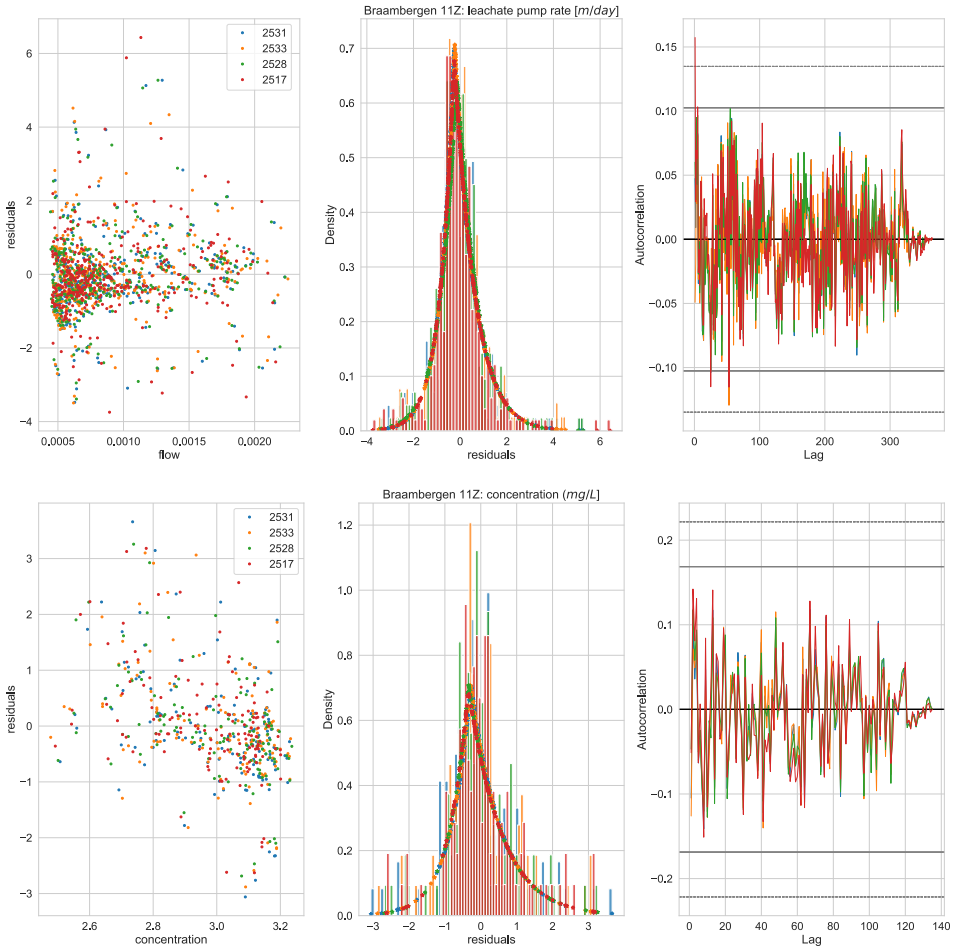

Figure 2.4.: Braambergen 11Z. Plots of the residuals as a function of leachate production rate or concentration, distribution of the errors and auto-correlation in the errors for the flow data (top row) and concentration data (bottom row).

clearly seen in the plot of the cumulative leachate production because small differences in the simulated cumulative over time. For the time range used for the parameter inference, these small differences are compensated, so the results for the different parameter sets do not diverge from each other. Similar effects also occur for leachate production rates and leachate concentration data. However, as the effects do not accumulate as quickly as for the cumulative leachate production, it will take a much longer time series to see the effects in the graphs.

The simulated cumulative leachate production starts to deviate significantly from the measured cumulative flow after 2022 and in spring 2024 we see that measured flow rates fall above the 95% intervals. This is due to the fact that the past years have moved from exceptionally dry to exceptionally wet in a very short time. An additional factor is that in 2022, additional wells were installed on Braambergen.

One of the most important assumptions in developing this approach is that the probability density functions of the travel time distributions do not change with time. It is likely that this assumption is too strict. Apparently, the waste body is not able to store more water as rainfall increases; instead, preferential flow to the drainage system seems to increase as well. Measurement artifacts also play a role. Because of the excess amount of water due to heavy rainfall, the landfill operator had to reduce the discharge to the water treatment plant by reducing the pump rate from the drainage system for a couple of weeks. The reduced flow of water may have led to a higher leaching of chloride.

In order to capture time-dependent changes in the properties of the waste body and boundary conditions, other approaches are required than those used for this work. Parameter distributions can be adjusted so that they become time-dependent. This could be done by making them depend on the storage in the waste body as suggested by Harman (2015) or by inferring parameters and states in time using a particle filter as suggested by Wang and Heimovaara (2025).

The long-term predictions (Figure 2.5) indicate that chloride is gradually leached from the waste body, and the concentration varies with the seasonal variation in infiltration. All scenarios (see also Figure S3 in the Appendix) indicate that water storage in all waste bodies reaches a long-term dynamic steady state where base-flow is compensated by storage from infiltration with life-time expectancies above n_{tt} or 1825 days.

The concentration in the leachate is controlled by chloride mass and the amount of water draining from the bulk volume of the waste body as base flow. The base flow rate is controlled by the volume of water stored in the bulk volume. Figure 2.6 shows the base flow as a function of the bulk storage. Figure 2.7 shows the simulated base flow over time, and Figure 2.8 shows the bulk concentration, which is the ratio of the solute

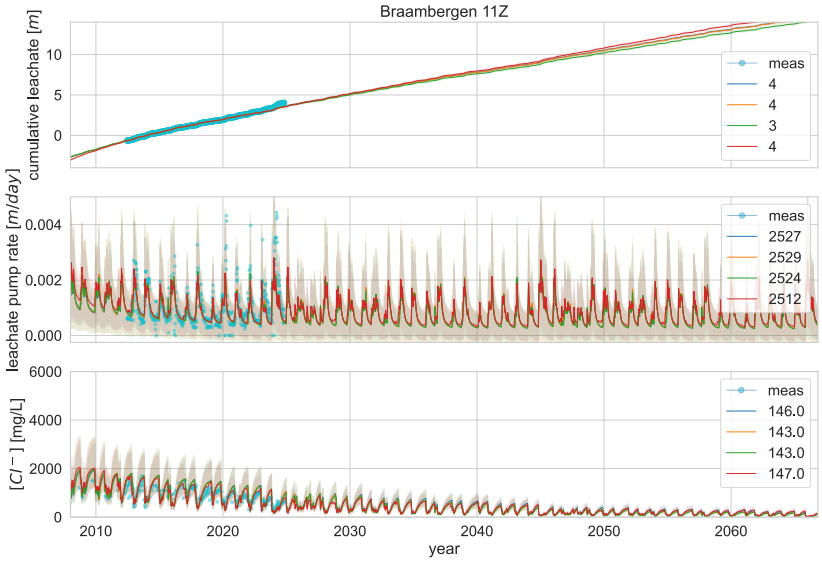

Figure 2.5.: Long term extrapolation of cumulative leachate production (CL [m]), leachate pump rate (LPR [m/day]) and leachate chloride concentration (conc [kg/m^3] for Braambergen 11Z. The scenarios are identical to the ones presented in figure 2.2

mass and storage. Each parameter set results in base flows with a different magnitude; however, as the model is simulating both the water balance and the chloride mass-balance, final outcomes are very similar (see figures 2.2 and 2.5). The differences in magnitudes for the base flow are caused by the fact that concentration is the ratio of solute mass to water storage. A higher concentration leads to a higher water mass, which therefore will lead to higher bulk storage values and, therefore, a different base flow function to achieve similar base flow mass rates. A clear indication of the mass balance is the similar magnitudes of the variations in the bulk storage (V_{bulk}) in Figure 2.8.

The oscillations in the base flow (Figure 2.6) can be explained by the the seasonal variation in the infiltration leading to a variation in the bulk storage (Figure 2.8) and the slope of the base flow function (Figure 2.6).

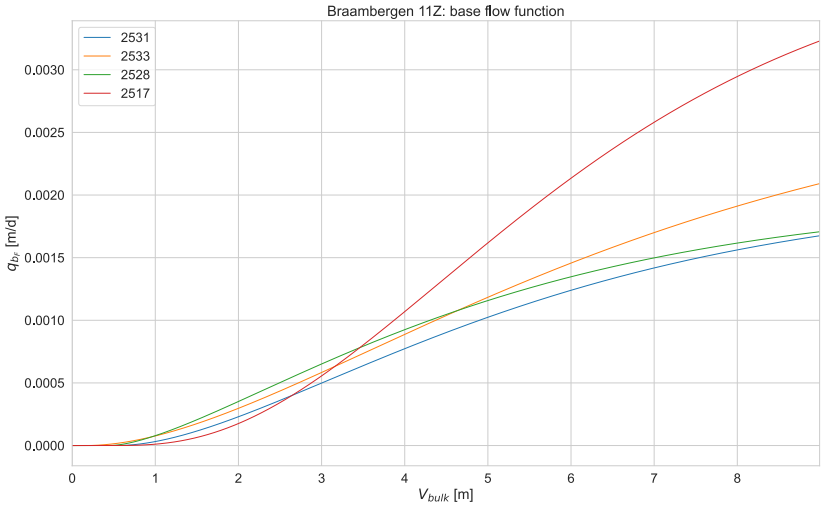

Figure 2.6.: Base flow (b_F) functions for Braambergen 11Z using equation 2.10

2.4.4. LIFE EXPECTANCY DISTRIBUTIONS

In figure 2.9, cumulative density functions are plotted for the life expectancy time distributions used to partition the water from the infiltration flux from the cover layer and the base flow from the bulk. Until a life expectancy of 2500 days, the probability density functions for q_{inf} are completely determined by the fast flow fraction for all scenarios except the green one. Apparently, the slow fraction only has an impact on water with a life expectancy which is much larger than 2500 days. Given the fact that all water with a life expectancy older than $n_{tt} = 1825$

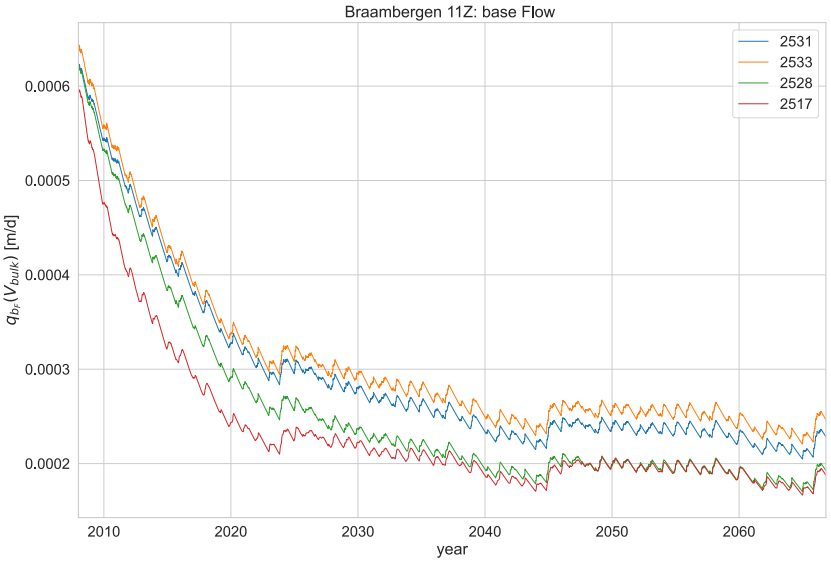

Figure 2.7.: Simulated base flow (b_F)for Braambergen 11Z.

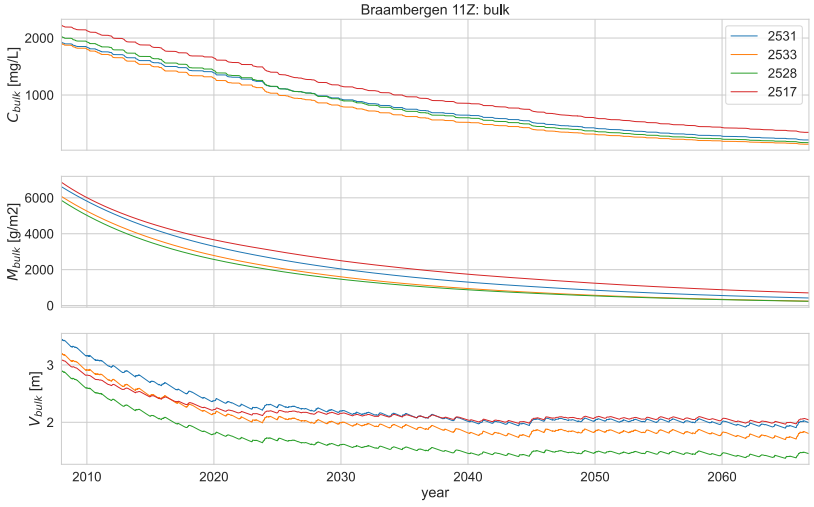

Figure 2.8.: Simulated chloride concentration, mass and total storage in the bulk of the waste body for Braambergen 11Z.

days is added to the bulk, the results imply that about 40 % of the infiltrating water is added to the bulk of the waste body, and that about 20% of the infiltrating water will have left the waste body as leachate after about 45 days. The same is true for the green scenario, as the jump occurs after 1900 days.

The cumulative density function for the base flow indicates that in all scenarios, except for the 100% probability scenario (blue with a likelihood of 2531) are directly added to the cell with a life expectancy of 1825 days, which is consistent with convective transport of the water.

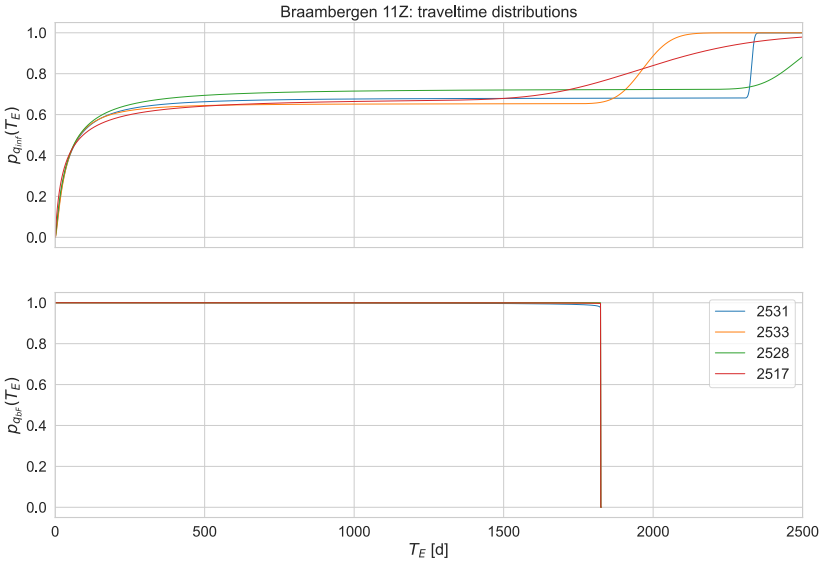

Figure 2.9.: Cumulative densities of the travel time distributions for the infiltration flux from the cover layer (q_{inf}) using Equation 2.12 and the base flow from the bulk (q_{bF}) using Equation 2.14.

Because 20% of the water infiltrating from the cover layer has a life expectancy of less than 45 days, leachate concentration dynamics are dominated by this water moving preferentially through the waste body. This preferential flow explains why in winter, concentrations are low and in summer, concentrations are high. In the Netherlands, evapo-transpiration is high in summer, leading to no or very low infiltration fluxes from the cover layer, and solute present in cells with short life expectancy is not diluted. In winter, evapo-transpiration is very low, leading to high infiltration fluxes, which significantly dilute the solute present in the cells with short life expectancy.

2.4.5. EMISSION POTENTIAL

The model keeps track of the mass balances of water and chloride in the waste body. The dynamics in the long-term leachate production rates and leachate chloride concentrations are controlled by the mass present in the bulk. The only source for chloride in the leachate is the mass present at initialization, and water is added via precipitation and subsequent infiltration into the waste body. These assumptions lead to a gradual decrease in chloride mass, which then leads to a gradual reduction in leachate concentrations as well.

Figure 2.10 shows the simulated totals of chloride mass, water storage, and corresponding chloride concentrations for the waste body of Braambergen 11Z. Clearly, the mass shows an exponential decrease with time, which is to be expected.

The leachate volume in the waste body decreases from 4.8 *m* to values between 2 and 2.6 *m*. The concentration is the ratio of the mass to the volume. As long as base flow occurs, the total mass in the waste body will decrease. The rate of decrease is controlled by the magnitude of the base flow and the concentration in the bulk. Similar patterns have been found for the other waste bodies in this study as well.

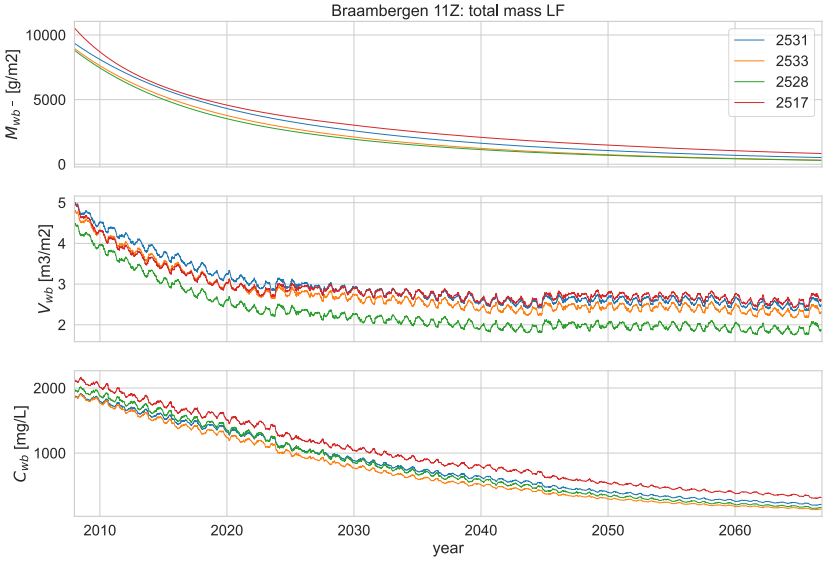

Figure 2.10.: Total chloride mass, total storage and solute concentration in the waste body of Braambergen 11Z.

These results indicate that our approach provides insight in the mass controlling long-term emissions from waste bodies. The total mass

in Figure 2.10 shows the emission potential of this waste body as a function of time. This mass controls the concentration in the leachate, and as no new mass is added to the waste body, it will also control future emissions.

2.4.6. IMPLICATIONS FOR MANAGING LANDFILL AFTER CARE

The model and parameter inference approach based on life-expectancy modeling is a viable approach to describe measured time series of leachate production rates and leachate concentration dynamics. Because the parameter inference approach provides us with uncertainty estimates, we also obtain insight in the uncertainty of the simulated values. The inferred parameters allow us to understand the uncertainty in the parameters controlling the emission of solutes from the waste body. The model allows us to make sense of the measured variations in leachate concentration data without having the need to smooth the data.

An important result is that this approach can provide minimum and maximum estimates of leachate concentrations over time which can be used to assess the necessity of landfill after-care measures. In addition the inferred parameter distributions allow for an estimate of amount of mass in the waste body that is controlling the long-term leachate concentrations. This information is essential for understanding long term future risk associated with leachate emissions.

The results also clearly demonstrate that concentrations in leachate are dominated by dilution with water infiltrating from the cover layer and quickly moving via preferential path ways to the drainage system. Transport of mass from the bulk of the waste body to the drainage system is a relatively slow process. Dilution is a dominating mechanism reducing the actual leachate concentrations compared with the solute concentrations present in the waste body. Enhancing preferential flow by engineered measures in the waste body, may reduce these concentrations even further because the amount of water being stored in the bulk will decrease. This then leads to a decrease in the release rate from the bulk because of a decrease in storage. However the decrease in emission potential will slow down as well.

This methodology requires long-term time series of leachate production rates and leachate concentration values in order to infer the parameters. Leachate production rates and leachate concentrations are parameters that landfill are obliged to measure in order to be compliant with the regulations. For the Wieringermeer and Braambergen landfills the landfill operator did increase the measurement frequency significantly. When applying the approach to new data sets one can start using the posterior distributions obtained published with this paper, instead of starting with fresh uninformative priors.

2.5. SUMMARY AND CONCLUSIONS

A model has been developed for simulating leachate production rates and leachate concentrations using a mass balance approach combined with a stochastic trave time approach based on life time expectancies. The model is one dimensional and consists of two layers. The first layer is a reservoir model for the cover layer, the second layer a stochastic life expectancy model. The model is driven by measured rainfall and potential evapotranspiration and is calibrated using measured leachate production rates and leachate concentrations. Posterior parameter distributions are inferred using a Bayesian MCMC approach implemented in PyDREAM (Shockley *et al.*, 2018) where the objective functions are based on the generalized likelihood model of Schoups and Vrugt (2010). The model has been applied to analyze data sets obtained from two different landfills and a total of four waste bodies.

We also propose to use emission potential as a term to describe the amount of mass that can be released from the waste body in realistic conditions. This emission potential is the source term in a modeling framework that can describe measured leachate flux and leachate concentration.

The model with posterior parameter distributions can describe the measured time series of leachate production rates and leachate chloride concentrations. In addition uncertainty bandwidths using inferred measurement errors can be determined as well. Model simulations can be carried out to extrapolate leachate production and leachate concentration in to the future allowing for assessment of the future development of concentration and leachate production volume.

Integrating biogeochemical reactions in the approach would allow the model to be used for evaluation of reactive compounds as well. This however will considerably increase the complexity of the model as well.

The results indicate that the waste bodies that have been studied, have reached seasonal steady state until 2022, where total water storage in the waste body oscillates around a constant value. From 2022 onward, the measured cumulative leachate production is larger than simulated. This implies that using time independent life-expectancy probability distributions is too strict.

The oscillations in leachate production rates and leachate concentrations are controlled by infiltration rates from the cover layer and the life time expectancy distribution. Leachate concentrations depend strongly on the simulated base flow which is controlled by the storage in the bulk of the waste body where life expectancy of water is longer than 1825 days.

Emission potential is a combination of the total mass present in the waste body and the expected future behavior of the base flow. The model can be used to plot the future development of the two parameters controlling leachate concentrations being total solute mass and total

water storage for different climate forcing scenarios. The total mass is a quantification of the emission potential. The results of such simulations can be used to assess different landfill after care scenarios.

REFERENCES

Barlaz, M. A., Rooker, A. P., Kjeldsen, P., Gabr, M. A., & Borden, R. C. (2002). Critical Evaluation of Factors Required To Terminate the Postclosure Monitoring Period at Solid Waste Landfills. *Environmental Science & Technology*, *36*(16), 3457–3464. https://doi.org/10.1021/es011245u

Belevi, H., & Baccini, P. (1989). Long-term behavior of municipal solid waste landfills. *Waste Management & Research*, *7*(1), 43–56. https://doi.org/10.1016/0734-242X(89)90007-4

Benettin, P., & Bertuzzo, E. (2018). *Tran*-SAS v1.0: A numerical model to compute catchment-scale hydrologic transport using StorAge Selection functions. *Geoscientific Model Development*, *11*(4), 1627–1639. https://doi.org/10.5194/gmd-11-1627-2018

Benettin, P., Rinaldo, A., & Botter, G. (2015). Tracking residence times in hydrological systems: Forward and backward formulations. *Hydrological Processes*, *29*(25), 5203–5213. https://doi.org/10.1002/hyp.10513

Benettin, P., Soulsby, C., Birkel, C., Tetzlaff, D., Botter, G., & Rinaldo, A. (2017). Using SAS functions and high-resolution isotope data to unravel travel time distributions in headwater catchments. *Water Resources Research*, *53*(3), 1864–1878. https://doi.org/10.1002/2016WR020117

Brand, E., de Nijs, T. C. M., Dijkstra, J. J., & Comans, R. N. J. (2016). A novel approach in calculating site-specific aftercare completion criteria for landfills in The Netherlands: Policy developments. *Waste Management*, *56*, 255–261. https://doi.org/10.1016/j.wasman.2016.07.038

Butt, T. E., Lockley, E., & Oduyemi, K. O. K. (2008). Risk assessment of landfill disposal sites – State of the art. *Waste Management*, *28*(6), 952–964. https://doi.org/10.1016/j.wasman.2007.05.012

Dijkstra, J. J., van Zomeren, A., Brand, E., & Comans, R. N. J. (2018). Site-specific aftercare completion criteria for sustainable landfilling in the netherlands: Geochemical modelling and sensitivity analysis. *Waste Management*, *75*, 407–414. https://doi.org/10.1016/j.wasman.2018.02.002

EC. (1999). Council directive 1999/31/ec of 26 april 1999 on the landfill of waste. *Official Journal of the European Communities*, *182*, 1–19. https://doi.org/10.1039/ap9842100196

Fellner, J., & Brunner, P. H. (2010). Modeling of leachate generation from MSW landfills by a 2-dimensional 2-domain approach.

Waste Management, *30*(11), 2084–2095. https://doi.org/10.1016/j.wasman.2010.03.020

Harman, C. J. (2015). Time-variable transit time distributions and transport: Theory and application to storage-dependent transport of chloride in a watershed. *Water Resources Research*, *51*(1), 1–30. https://doi.org/10.1002/2014WR015707

Heimovaara, T. J., & Wang, L. (2025). Quantification of Emission Potential of Landfill Waste Bodies Using a Stochastic Leaching Framework. *Water Resources Research*, *61*(3), e2024WR038360. https://doi.org/10.1029/2024WR038360

Hrachowitz, M., Benettin, P., van Breukelen, B. M., Fovet, O., Howden, N. J., Ruiz, L., van der Velde, Y., & Wade, A. J. (2016). Transit times-the link between hydrology and water quality at the catchment scale. *Wiley Interdisciplinary Reviews: Water*, *3*, 629–657. https://doi.org/10.1002/wat2.1155

Kattenberg, W. J., Sloot, H. A. v. d., & Heimovaara, T. J. (2013). *New dutch legislation to allow research of natural biodegradation at landfills* (Vol. 30). CISA Publisher, Italy. http://duurzaamstortbeheer.nl/wp-content/uploads/2014/06/%20Kattenberg-et-al-Sard2013-652.pdf

KNMI. (2022). Dagwaarden van weerstations. https://www.daggegevens.knmi.nl/klimatologie/daggegevens

Kosson, D., van der Sloot, H., Sanchez, F., & Garrabrants, A. (2002). An integrated framework for evaluating leaching in waste management and utilization of secondary materials [Publisher: Mary Ann Liebert, Inc.]. *Environmental Engineering Science*, *19*(3), 159–204. Retrieved June 23, 2011, from http://www.liebertonline.com/doi/abs/10.1089/109287502760079188

Laloy, E., & Vrugt, J. A. (2012). High-dimensional posterior exploration of hydrologic models using multiple-try DREAM(ZS) and high-performance computing. *Water Resources Research*, *48*(1), W01526. https://doi.org/10.1029/2011WR010608

Laner, D., Fellner, J., & Brunner, P. H. (2011). Environmental compatibility of closed landfills - assessing future pollution hazards. *Waste Management & Research*, *29*(1), 89–98. https://doi.org/10.1177/0734242X10387655

Laner, D., Fellner, J., & Brunner, P. H. (2012). Site-specific criteria for the completion of landfill aftercare. *Waste Management & Research*, *30*(9_suppl), 88–99. https://doi.org/10.1177/0734242X12453610

Malmström, M. E., Destouni, G., & Martinet, P. (2004). Modeling Expected Solute Concentration in Randomly Heterogeneous Flow Systems with Multicomponent Reactions. *Environmental Science & Technology*, *38*(9), 2673–2679. https://doi.org/10.1021/es030029d

Rinaldo, A., Benettin, P., Harman, C. J., Hrachowitz, M., McGuire, K. J., van der Velde, Y., Bertuzzo, E., & Botter, G. (2015). Storage selection functions: A coherent framework for quantifying how catchments store and release water and solutes. *Water Resources Research*, *51*(6), 4840–4847. https://doi.org/10.1002/2015WR017273

Rosqvist, H., & Destouni, G. (2000). Solute transport through preferential pathways in municipal solid waste. *Journal of Contaminant Hydrology*, *46*(1), 39–60. https://doi.org/10.1016/S0169-7722(00)00127-3

Schoups, G., & Vrugt, J. A. (2010). A formal likelihood function for parameter and predictive inference of hydrologic models with correlated, heteroscedastic, and non-Gaussian errors. *Water Resources Research*, *46*(10), 1–17. https://doi.org/10.1029/2009WR008933

Shockley, E. M., Vrugt, J. A., & Lopez, C. F. (2018). Pydream: High-dimensional parameter inference for biological models in python: Supplemental material. *Bioinformatics*, *34*, 695–697. https://doi.org/10.1093/bioinformatics/btx626

Sormunen, K., Ettala, M., & Rintala, J. (2008a). Detailed internal characterisation of two finnish landfills by waste sampling. *Waste Management*, *28*, 151–163. https://doi.org/10.1016/j.wasman.2007.01.003

Sormunen, K., Ettala, M., & Rintala, J. (2008b). Internal leachate quality in a municipal solid waste landfill: Vertical, horizontal and temporal variation and impacts of leachate recirculation. *Journal of Hazardous Materials*, *160*, 601–607. https://doi.org/10.1016/j.jhazmat.2008.03.081

Stichting Duurzaam Storten. (2017). Biodegradation research programme on dutch landfills. https://duurzaamstortbeheer.nl/english-page/

Storten, S. D. (2022a). *Natural biodegradation research programme on dutch landfills* (research rep.). Dutch Sustainable Landfill Foundation. https://duurzaamstortbeheer.nl/english-page/

Storten, S. D. (2022b). *The dutch foundation for sustainable landfilling.* (research rep.). Dutch Sustainable Landfill Foundation. https://duurzaamstorten.nl/en/

Uguccioni, M., & Zeiss, C. (1997). Improvement of leachate prediction through municipal solid waste layers1. *JAWRA Journal of the American Water Resources Association*, *33*, 1265–1278. http://onlinelibrary.wiley.com/doi/10.1111/j.1752-%201688.1997.tb03551.x/abstract

van der Sloot, H. A., Kosson, D. S., & van Zomeren, A. (2017). Leaching, geochemical modelling and field verification of a municipal solid waste and a predominantly non-degradable waste landfill. *Waste*

Management, *63*, 74–95. https://doi.org/10.1016/j.wasman.2016.07.032

Vrugt, J. A. (2016). Markov chain Monte Carlo simulation using the DREAM software package: Theory, concepts, and MATLAB implementation. *Environmental Modelling & Software*, *75*, 273–316. https://doi.org/10.1016/j.envsoft.2015.08.013

Wang, L., & Heimovaara, T. J. (2025). Quantifying landfill emission potential using a weakly coupled particle filter. *Water Resources Research*, *61*(2), e2023WR036549. https://doi.org/10.1029/2023WR036549

Zacharof, A. I., & Butler, A. P. (2004a). Stochastic modelling of landfill leachate and biogas production incorporating waste heterogeneity. Model formulation and uncertainty analysis. *Waste Management*, *24*(5), 453–462. https://doi.org/10.1016/j.wasman.2003.09.010

Zacharof, A. I., & Butler, A. P. (2004b). Stochastic modelling of landfill processes incorporating waste heterogeneity and data uncertainty [Publisher: Elsevier]. *Waste Management*, *24*(3), 241–250. https://doi.org/10.1016/j.wasman.2003.12.001

3

QUANTIFYING LANDFILL EMISSION POTENTIAL USING A WEAKLY COUPLED PARTICLE FILTER

The emission potential, which represents the total leachable mass in landfill waste body, is hard to measure directly. Therefore, we propose to quantify it by assimilating available measurements. The total water storage influences the leachate production rate in the waste body, while both total chloride mass and total water storage in the waste body influence the chloride concentration in the leachate. Thus, assimilating leachate volume and chloride concentration simultaneously will help quantify the uncertainties in emission potential. This study investigated the feasibility of using a particle filter in a concentration-volume coupled travel time distribution model to estimate the emission potential. Leachate production rates and chloride concentrations were assimilated simultaneously by a weakly coupled data assimilation(WCDA) method. The time lag issue in the travel time distribution model was solved by adding a daily model error to cover layer states. The proposed method was tested in synthetic experiments first to investigate the performance. The results show that the uncertainties in chloride mass and total water storage in the waste body were quantified and reduced. The predictions of chloride concentrations were also improved.

Parts of this chapter have been published in Wang and Heimovaara (2025)

3.1. INTRODUCTION

Municipal solid waste(MSW) landfill leachate is a primary source of pollution to the surrounding environment because it is a source of contamination for soil and groundwater (Brand, 2014; Fatoba *et al.*, 2021; Gworek *et al.*, 2016). The environmental risk of leachate is determined by its composition and the amount released to the environment. The leachate flux from old landfills is mainly controlled by the water balance of the landfill which depends on precipitation and evapotranspiration. Leachate composition is influenced by the water storage and pollutant mass present in the waste body (Grugnaletti *et al.*, 2016; Laner *et al.*, 2011; Yang *et al.*, 2015). Also, reliable predictions of leachate emissions in the long term require a quantitative assessment of total pollutant mass and water storage in the waste body. As such, this quantitative assessment is an important criterion to determine the aftercare strategy (Kattenberg & Heimovaara, 2011).

Direct measurement of pollutant mass and water storage is virtually impossible due to the size and heterogeneity of waste bodies. As a result, researchers have developed alternative approaches that use forward modeling to predict leachate flux, composition, and the evolution of pollutant mass and water storage over time. For instance, Pantini *et al.* (2014) developed a process-based landfill water balance model where biodegradation and waste compression processes are included. Grugnaletti *et al.* (2016) got more accurate leachate production predictions by carrying out a parameter calibration with available outflow measurements. Zhang *et al.* (2021) proposed a pollutant concentration, leakage rate, and a solute transport coupled model that allows the prediction of concentrations. Generally, initial values of water and pollutant storages in the models are often approximated by waste characteristics like waste initial moisture (São Mateus *et al.*, 2012; Yang *et al.*, 2015). However, these estimations could be biased because of the significant spatial variation in initial states and the lack of information on waste composition. Laboratory studies help quantify certain model parameters, but small-scale tests often fail to capture the behavior of full-scale landfills (Fellner *et al.*, 2009). Even when initial moisture levels are calibrated with observations, as in Grugnaletti *et al.* (2016), the results reflect an averaged value of the whole waste body. While these models can reasonably predict leachate production rates, they struggle to capture the dynamics of pollutant concentration in leachate.

It is generally known that the contaminants are leached out from waste through preferential flow (Fellner & Brunner, 2010). It means we may not need to explicitly consider the heterogeneity of waste properties if we can use a function to describe the preferential flow. Recent research shows that travel time distributions can be used to characterize the flow pathway heterogeneity (Rinaldo *et al.*, 2011). We have developed a travel time distribution(TTD) model to predict leachate production rate

(LPR) and chloride concentration from landfill waste bodies (Heimovaara & Wang, 2025). The preferential water flow in landfill waste bodies is primarily characterized by two travel time distributions: one for infiltration from the cover layer and another for baseflow from bulk storage. The concentration states in this model are one-way coupled to the water volume states, meaning changes in concentration levels are controlled by changes in water volume. Parameters and initial states in this model are obtained by optimization using the DREAM$_{ZS}$ algorithm (Vrugt, 2016), a Markov chain Monte Carlo (MCMC) method for Bayesian inference.

In recent years, MCMC methods have been widely applied to hydrology models. It allows for estimating the probability distribution of model parameters by comparing model results with available measurements. However, obtaining parameters by fitting or 'history-matching' to data is generally a batch processing method that defines the best fit in an average way. This implies that we get the best fit of the measured data over the whole time range rather than the best estimation of model states (Liu & Gupta, 2007). Hence, normal MCMC-like batch processing methods cannot recursively include new information when it becomes available.

Data assimilation (DA) is another class of Bayesian inference methods. It is widely used because of its power to recursively assimilate new measurements to improve understanding of immeasurable or hidden states (Carrassi *et al.*, 2018; Liu *et al.*, 2012). Most DA algorithms consist of alternating forecast and analysis steps. Model states are propagated with time using a forward model to get predictions, and then measurements are used to update the predictions in analysis steps. This sequential updating allows model states to be refined whenever new observations become available.

Filter and smoother are two main categories of data assimilation. Filters estimate current states using past and current observations, making them efficient for real-time applications. On the other hand, Smoothers use both past and future observations to improve accuracy but are more computationally demanding. For example, the ensemble Rauch-Tung-Striebel smoother (EnRTSS) (Raanes, 2016) leverages batch processing to recursively update states, making it suitable for retrospective analysis. Since our objective is to update model states once new observations are available, we focus on the more computationally efficient filtering methods

Among the main data assimilation filtering methods, the ensemble Kalman filter(EnKF) (Evensen *et al.*, n.d.) and the particle filter (PF) (Djurić *et al.*, 2003) are commonly used for nonlinear forward models. The state update performed by the EnKF is an affine transformation that is precise only when the joint distribution of states and observations follows a multivariate Gaussian distribution. If it isn't, the update is

only approximate and can violate all manner of physics. In contrast, particle filtering approaches can preserve the physics because the measurements are used to weigh particles instead of adjusting them. Due to its ability to handle fully nonlinear systems, it has been widely used in hydrology (Abbaszadeh *et al.*, 2019; Plaza Guingla *et al.*, 2013; Vrugt *et al.*, 2013; Zhang *et al.*, 2017).

A coupled data assimilation (CDA) method is typically employed when the forward model is a coupled system with different types of measurements. CDA is popular due to its ability to enable each model component to receive information from measurements in other domains (Laloyaux *et al.*, 2016; Penny *et al.*, 2019; Penny & Hamill, 2017; Smith *et al.*, 2015; Tardif *et al.*, 2015). In weakly CDA, all model states are predicted simultaneously by a coupled forward model but are updated separately within each domain (Penny & Hamill, 2017). The updated states are then propagated to the next time step by the coupled model, integrating measurement information from both domains. Conversely, in strongly CDA, states in individual domains are predicted by the coupled model and updated simultaneously using measurements from all domains (Ng *et al.*, 2009). This approach is optimal compared to weakly CDA because it leverages information from all measurements in both the prediction and update steps. However, the successful application of strongly CDA is limited due to the challenges associated with model error covariance (Zhang *et al.*, 2020). Defining error covariance in coupled data assimilation is particularly challenging because it requires defining the correlations between states in different domains, which are often the least understood. Although some ensemble data assimilation methods derive correlations through ensemble forecasts, it is difficult to determine if the low-dimensional approximation of the ensemble error covariance is acceptable (Županski, 2017). In methods where the error covariance is not explicitly defined, such as particle filter, the problem still exists because of the low quality of the fundamental Monte Carlo approximation. In addition, particle filter methods introduce issues such as the 'Curse of Dimensionality' and particle degeneracy because the state space encompasses all states in both domains in strongly CDA. The drawbacks of strongly CDA were demonstrated in a 5-variable test, where strongly CDA outperformed weakly CDA only when the ensemble size was increased to approximately 10^4 (Han *et al.*, 2013). Consequently, most CDA systems in practical applications are weakly CDA (Zhang *et al.*, 2020).

In a synthetic experiment, comparative research on weakly CDA was performed by Gharamti *et al.* (2013), where an ensemble Kalman filter was used in a 2D subsurface flow-transport coupled model. The hydraulic head and contaminant concentration observations in multiple wells are assimilated to estimate the evolution of these two states. However, the problem with the Ensemble Kalman Filter (EnKF) persists

when the states and observations do not follow a joint multivariate Gaussian distribution.

This study investigates the feasibility of using a weakly coupled particle filtering approach in a landfill TTD model for estimating the emission potential. The emission potential is determined by the waste body's pollutant mass states and water storage states. Based on our knowledge, no research has used particle filtering approaches to estimate both volume quantities and solute concentrations in hydrochemical coupled models. We also believe this is the first time data assimilation has been used to estimate landfill emission potential. Moreover, mass state estimation remains a problem in many data assimilation applications in hydrology. Six synthetic assimilation scenarios were tested to verify the proposed method and optimize the assimilation strategy. Several implementation steps of the algorithm were adjusted to make it suitable for the TTD model. The uncertainties of these hidden states were quantified, and improvement in prediction was evaluated. The chloride mass in the landfill was selected as the representative emission potential in this research.

3.2. METHODS

This data assimilation framework uses a coupled TTD model as the forward model. The weakly coupled particle filter was used as a data assimilation algorithm. The first part of this section describes the theory of weakly coupled particle filter. The second part introduces the forward model and its specific characteristics, which must be addressed in the DA application. The last part concerns synthetic experiment design, implementation procedure, and performance estimation matrices.

3.2.1. WEAKLY COUPLED PARTICLE FILTER

SEQUENTIAL IMPORTANCE SAMPLING

The weakly coupled PF is based on the sequential importance sampling (SIS) PF. Model and measurement equations are required during the state estimation process as given by Arulampalam *et al.* (2002). We take $\boldsymbol{x}_t$ to represent a state vector that contains all the model states at the current time step t. Firstly, the state vector is propagated from the former time step to the current step with the model equation

$$\boldsymbol{x}_t = M_t(\boldsymbol{x}_{t-1}) + \boldsymbol{\varepsilon}_{model} \tag{3.1}$$

where $M_t(\cdot)$ denotes the forward model, and $\boldsymbol{\varepsilon}_{model}$ represents the model error vector caused by different sources of uncertainty. The state vector will then be linked to measurements through the measurement equation

$$\boldsymbol{y}_t = H_t(\boldsymbol{x}_t) + \boldsymbol{\varepsilon}_{mea} \tag{3.2}$$

in which $H_t(\cdot)$ denotes the measurement operator that connects model states to measured states, and $\boldsymbol{\varepsilon}_{mea}$ represents the measurement error vector.

The main task of state estimation is to estimate the probability density function (pdf) of immeasurable states based on measurement series. We use the subscript $1:t$ to represent the time range from the initial step to step t. Hence, $\boldsymbol{y}_{1:t}$ are the available measurements until current step t and $p(\boldsymbol{x}_t \mid \boldsymbol{y}_{1:t})$ represents the pdf of current state vector $\boldsymbol{x}_t$ given $\boldsymbol{y}_{1:t}$. Bayes' theorem is used to calculate $p(\boldsymbol{x}_t \mid \boldsymbol{y}_{1:t})$, the so-called posterior pdf, by combining prior pdf $p(\boldsymbol{x}_t \mid \boldsymbol{y}_{1:t-1})$ from last time step with likelihood pdf $p(\boldsymbol{y}_t \mid \boldsymbol{x}_t)$ as

$$p(\boldsymbol{x}_t \mid \boldsymbol{y}_{1:t}) = \frac{p(\boldsymbol{y}_t \mid \boldsymbol{x}_t)\, p(\boldsymbol{x}_t \mid \boldsymbol{y}_{1:t-1})}{p(\boldsymbol{y}_t \mid \boldsymbol{y}_{1:t-1})} \tag{3.3}$$

$p(\boldsymbol{y}_t \mid \boldsymbol{y}_{1:t-1})$ is a normalization factor in making sure the integral of pdf is 1. If the posterior pdf $p(\boldsymbol{x}_{t-1} \mid \boldsymbol{y}_{1:t-1})$ at the previous assimilation step is known, the prior pdf $p(\boldsymbol{x}_t \mid \boldsymbol{y}_{1:t-1})$ could be calculated as

$$p(\boldsymbol{x}_t \mid \boldsymbol{y}_{1:t-1}) = \int p(\boldsymbol{x}_t \mid \boldsymbol{x}_{t-1}) p(\boldsymbol{x}_{t-1} \mid \boldsymbol{y}_{1:t-1}) d\boldsymbol{x}_{t-1} \tag{3.4}$$

Then we obtain the aim posterior pdf $p(\boldsymbol{x} \mid \boldsymbol{y}_{1:t})$ as

$$p(\boldsymbol{x}_t \mid \boldsymbol{y}_{1:t}) = \frac{p(\boldsymbol{y}_t \mid \boldsymbol{x}_t) \int p(\boldsymbol{x}_t \mid \boldsymbol{x}_{t-1}) p(\boldsymbol{x}_{t-1} \mid \boldsymbol{y}_{1:t-1}) d\boldsymbol{x}_{t-1}}{p(\boldsymbol{y}_t \mid \boldsymbol{y}_{1:t-1})} \tag{3.5}$$

The core idea of sequential importance sampling is to approximate the required pdf through N independent particles with weight w_i respectively. More specifically, sampling from $p(\boldsymbol{x}_{t-1} \mid \boldsymbol{y}_{1:t-1})$ means several particles are obtained from the previous time step. $p(\boldsymbol{x}_t \mid \boldsymbol{x}_{t-1})$ indicates propagating these particles with forward model (equation 4.1). The posterior pdf $p(\boldsymbol{x}_t \mid \boldsymbol{y}_{1:t})$ can be approximated as

$$p(\boldsymbol{x}_t \mid \boldsymbol{y}_{1:t}) \approx \sum_{i=1}^{N} w_t^i \delta(\boldsymbol{x}_t - \boldsymbol{x}_t^i) \tag{3.6}$$

In which δ represents the Dirac delta function. N is the number of particles. The w_t^i is calculated recursively as

$$w_t^i = \frac{w_{t-1}^i p(\boldsymbol{y}_t \mid \boldsymbol{x}_t^i)}{\sum_{i=1}^{N} (w_{t-1}^i p(\boldsymbol{y}_t \mid \boldsymbol{x}_t^i))} \tag{3.7}$$

The conditional probability $p(\boldsymbol{y}_t \mid \boldsymbol{x}_t)$ is often computed as a Gaussian likelihood:

$$p(\boldsymbol{y}_t \mid \boldsymbol{x}_t) = \exp\left\{-0.5[\boldsymbol{y}_t - H_t(\boldsymbol{x}_t^i)]^T R^{-1} [\boldsymbol{y}_t - H_t(\boldsymbol{x}_t^i)]\right\} \tag{3.8}$$

where $H_t(\cdot)$ is the measurement operator, R is the error covariance of the measurements (Van Leeuwen, 2009). Common statistics can be easily acquired with the posterior pdf or weighted particles. For instance, the mean of state vector $\boldsymbol{x}$ is calculated as

$$\overline{\boldsymbol{x}}_t = \sum_{i=1}^{N} w_t^i \boldsymbol{x}^i \tag{3.9}$$

SYSTEMATIC RESAMPLING

Particle degeneracy is one main limitation of sequence importance sampling, which occurs after several assimilation steps when the weights of all but one particle can be neglected (Snyder *et al.*, 2008). The effective ensemble size is used to evaluate the degeneracy problem. It is computed as

$$N_t^{eff} = \frac{1}{\sum_{i=1}^{N} (w_t^i)^2} \tag{3.10}$$

When the effective ensemble size is smaller than $N/2$, resampling should be performed. The idea of resampling is duplicating particles with high weights and discarding those with low weights. After that, all weights will be set as $1/N$. The general resampling algorithms include multinomial, stratified, systematic, and residual resampling methods. In this research, we chose systematic resampling due to its superior resampling quality and computational efficiency compared with the others. A more detailed description of resampling algorithms is given in Hol *et al.* (2006).

WEAKLY COUPLED DATA ASSIMILATION (WCDA)

Coupled data assimilation is used when there is more than one measurement type. Also, a coupled model should be available. In WCDA, a coupled model is used to predict all the model states at the current time step, while the weighting and updating steps are performed within each component domain. Then the updated states are propagated to the next step by the coupled model. Although the measurements in one model domain are used to update the states in the same domain, the coupled model propagates the information to the other domain(Zhang *et al.*, 2020). The details about the implementation of WCDA are introduced in section 3.2.7.

3.2.2. COUPLED TRAVEL TIME DISTRIBUTION MODEL

The coupled travel time distribution (TTD) model predicts leachate production rates and chloride concentrations. A detailed description and implementation of the coupled TTD model are given in Chapter 2.

Here, we briefly introduce the model to facilitate understanding of our approach.

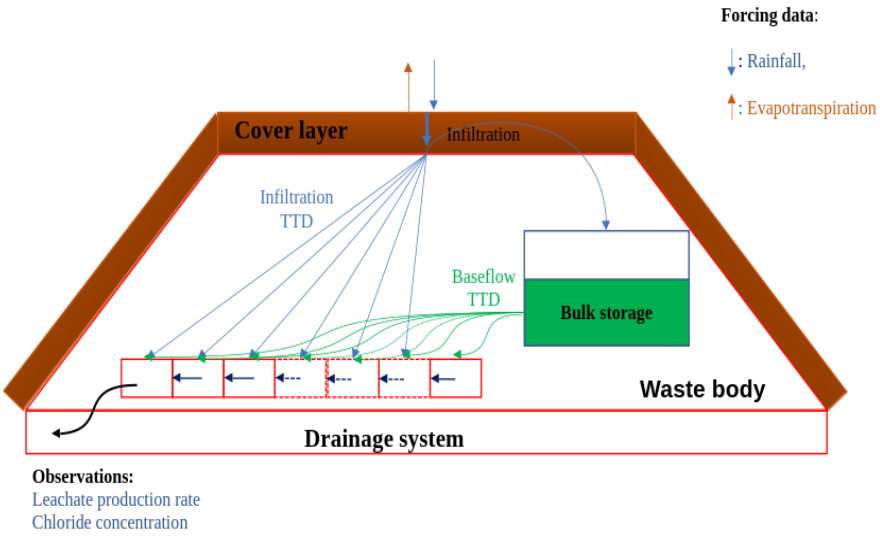

Figure 3.1.: A schematic overview of model structure.

As shown in Figure 3.1, the model consists of two layers representing a cover layer and waste body in a landfill. The forcing data at the top boundary are rainfall (R) and potential evapotranspiration (P_{ev}), which will enter or leave the landfill from the cover layer. The water storage in the cover layer determines the amount of water (q_{inf}) infiltrating the waste body. The waste body is conceptually divided into a single bulk storage and P cells to represent different travel times of water parcels before they flow out (discretization of the travel time distribution). The number of mobile cells needs to be large enough to capture the dilution pattern in the travel time distribution of cover layer infiltration but not so large that it assumes the water in the mobile part of the landfill can stay too long. The time difference between neighboring cells is one day. This means that it takes P days for leachate in the last cell to exit. It is important to note that these P cells do not refer to physical locations within the waste body, but rather represent leachate parcels with different travel times. The discretization into P cells is a method used to model the distribution of travel times.

The leachate that flows out from bulk storage is considered baseflow, and its volume is a function of bulk water storage. This baseflow is modeled by a log-normal distribution, parameterized by a shape parameter σ_{bF} and a scale parameter $\ln(\mu_{bF})$. The final baseflow value

is obtained by multiplying the output of this log-normal distribution and the maximum baseflow value bF_0. The baseflow will then be distributed to P cells according to a Gamma travel time distribution function $\Gamma(\kappa_{bF}, \theta = 1)$. Similarly, the q_{inf} from the cover layer is distributed to the waste body with another travel time distribution function. The infiltration TTD itself is modeled as a mixture distribution that combines both fast-flow and slow-flow components, each represented by a separate log-normal distribution. We use parameter β_f to describe the fast-flow fraction, and $1-\beta_f$ is the fraction of slow flow.

Similar to the transport model from Gharamti *et al.* (2013), the chloride concentration is one-way coupled in the water balance model. The concentration states in P cells are determined by time propagation, as well as distributed leachate from baseflow and infiltration from the cover layer. The parameters and initial states were optimized using DREAM(ZS) (Shockley, 2020; Vrugt, 2016). The model parameters used in this manuscript is shown in Table 3.1.

The state vector is given by

$$\boldsymbol{x_t} = [V_{cl_t}, M_{cl_t}, C_{cl_t}, v_{bulk_t}, m_{bulk_t}, c_{bulk_t}, v_{cell_t^i}, m_{cell_t^i}, c_{cell_t^i}]^T \qquad (3.11)$$

where i represents i_{th} cell state. The concentration defined as $c = m/v$ applies to all elements in the conceptual model. Also, $V_{wb_t} = v_{bulk_t} + \sum_{i=0}^{P-1} v_{cell_t^i}$ and $M_{wb_t} = m_{bulk_t} + \sum_{i=0}^{P-1} m_{cell_t^i}$ are used in the following parts to represent the entire storage states in the waste body. C_{wb} indicates the average concentration in the waste body. We use capital letters to represent the overall state variables of each layer, and we use lowercase letters to represent all internal variables. A detailed explanation of the variables in the model is presented in the nomenclature list.

3.2.3. SPECIFIC MODEL CHARACTERISTICS

ONE WAY COUPLED MODEL

The TTD model we use is based on a one-way coupling between water volume and chloride concentration. The leachate production rates only contain information on water volume states, while the concentration states depend both on water volume and solute mass. However, it is unknown how much information concentration measurements contain about water volume states. Is it possible to only assimilate concentration measurements, or do we need both the leachate outflow and concentration measurements? Gharamti *et al.* (2013) always use the concentration measurements to update the water head states, while the research does not investigate the benefits of assimilating both measurements compared with assimilating only one. Assimilating both measurements could get the best overall estimation for the

Table 3.1.: Parameters values and description in the coupled TTD model

Parameter	Values	Description
c_f	9.759×10^{-1}	An empirical crop-factor to compensate for different types of crops to close the water balance [−]
$\theta_{w_{cl},\max}$	3.437×10^{-1}	Porosity of the cover layer [−]
$f_{w_{cl},\min}$	2.472×10^{-2}	Fraction of maximum volumetric water content in cover layer representing minimum water storage [−]
K_{cl}	-1.960×10^{-1}	Saturated hydraulic conductivity of the cover layer [$m\,d^{-1}$], 10_{log}
b_{cl}	5.427	Empirical shape factor for the non-linear flow term of the cover layer [−]
τ_{fast}	3.813×10^{1}	Expected fast travel time (log-normal infiltration distribution) [d]
σ_{fast}	2.660×10^{-1}	Std. deviation of fast infiltration travel time [d], 10_{log}
$\Delta_{\tau_{slow}}$	7.934×10^{2}	Difference between τ_{fast} and τ_{slow}; $\tau_{slow} = \tau_{fast} + \Delta_{\tau_{slow}}$
σ_{slow}	2.993	Std. deviation of slow infiltration travel time [d], 10_{log}
β_f	6.281×10^{-1}	Fraction of fast flow in waste body [−]
bF_0	−3.368	Maximum baseflow from bulk storage to mobile cells [m], 10_{log}
σ_{bF}	-0.294×10^{-1}	Shape factor of log-normal baseflow function [m], 10_{log}
μ_{bF}	−0.321	Scale parameter of log-normal baseflow function [m], 10_{log}
κ_{bF}	−8.341	Shape parameter for baseflow travel-time distribution (Gamma distribution) [m]

model states, but it is not necessarily true for specific model parts. For example, when assimilating both types of measurements, the estimation results for volume states may be poorer compared with using only leachate production rate measurements. In order to explore this issue, we have designed different scenarios to investigate the optimal assimilation strategy.

TIME LAGS IN TTD MODEL

In particle filtering approaches, we can estimate hidden states in the model using measurements of observable states because the measurements contain some information about hidden states. Assuming the model is imperfect, errors will be added to both hidden states and observable states during the state propagation process. One

beneficial side effect of introducing model error is that it “rejuvenates” the ensemble of a particle filter. This means that adding model errors to hidden states enables the exploration of the hidden state space more thoroughly. The hidden states with model error will be assessed in the following time steps because they influence the measurable states. However, if this influence is weak or does not exist, the hidden states will be updated randomly, and the estimation will be poor (Plaza Guingla *et al.*, 2013).

In the forward TTD model we use, we have explicit time lags between many model states and measurements because the travel time distribution considers the time information explicitly. At each time step, the model state vector includes thousands of individual cell states as well as a bulk state, which summarizes the entire system. The time lag between the oldest and youngest cell states is determined by the infiltration travel time distribution, with a maximum lag of 5 years, as illustrated in Figure 3.2. The infiltration water with a travel time larger than 5 years is added to the bulk.

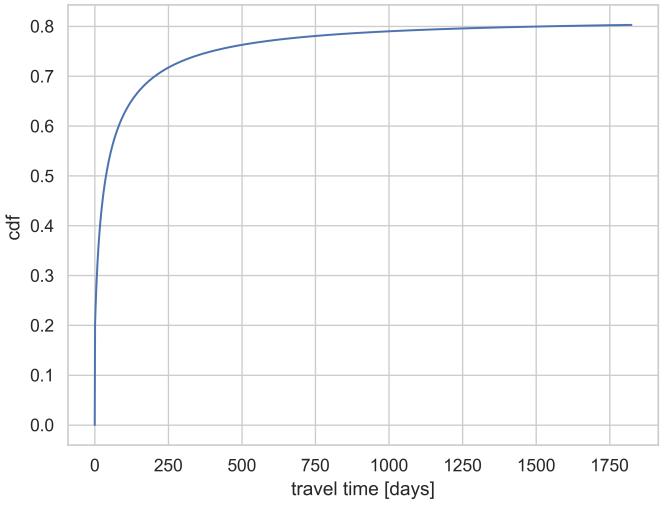

Figure 3.2.: Cumulative distribution of infiltration TTD

It’s important to distinguish between two types of time discretization here: one that tracks the evolution of model states over time and another representing the distribution of travel times for infiltration from a cover layer or baseflow from bulk to exit the system. In this context, a time lag represents the difference in these travel times. As shown in Figure 3.1, the cells mean the water parcels with different travel times rather than real physical water cells. For instance, the leachate in the oldest cell at time step t will take $P-1$ days to move to the youngest

cell at time step $t+P-1$. This means the oldest cell will only be reflected in the measurements after P days. This time lag complicates the estimation of multiple hidden states using current measurements.

Several studies are trying to solve these challenges with time-lagged measurements in data assimilation (Li *et al.*, 2013; McMillan *et al.*, 2013; Noh *et al.*, 2013, 2014). McMillan *et al.* (2013) used the current measurements to update states at previous time steps within the time lag. Noh *et al.* (2013, 2014) used the measurements after an extended time to estimate current model states to consider the time lag effect. These methods use the forward models as measurement operators to link the model states to corresponding lagged measurements. In these approaches, the assumption is that the forward models are accurate for this extended prediction; otherwise, the representation error (Janjić *et al.*, 2018) in the measurement operator should be considered. The maximum time lag in the landfill TTD model is around five years. This is much longer than those previously used in distributed catchment models. Consequently, model error accumulation is expected to be severe during the extended prediction process (Noh *et al.*, 2013, 2014), so it is unreasonable to assume a correct model for such a long prediction period. Additionally, the TTD model has thousands of states that are lagged in time due to the discretization of TTD, whereas the published applications usually have time lag issues for between two states. To overcome these issues, we have developed a specific strategy for the TTD model.

In the TTD landfill model, the cell states are propagated with time. After P (the number of cells) days, there will be a connection among all cells and bulk states. We call this implicit relationship 'history'. We can estimate hidden states by current measurements if this' history' is maintained. Hence, the initialization of particles and the model errors should guarantee this 'history'. The implementation strategy is further explained in section 3.2.7.

3.2.4. SITE AND DATA DESCRIPTION

The model parameter calibration is based on actual measurements from the Braambergen landfill in the Netherlands (Duurzaam stortbeheer, 2023). Daily meteorological forcing data (same as model resolution) are obtained from the nearest weather station affiliated with KNMI (2022). The leachate is pumped out from the drainage system, and the daily production volume is acquired. The chloride concentration is measured by sampling from the drainage layer generally with a bi-weekly frequency(with some larger intervals up to 28 days). In practical cases, there are many irregular values in daily production rate measurements because of the management of the leachate pump system by the landfill operator. When the pump system is broken, the

outflow remains in the drainage layer, resulting in an observed leachate production volume of zero. Afterward, the water is pumped out, a large leachate volume is measured. In order to limit the effect of these operational irregularities, seven days' average leachate production rates were calculated from the cumulative leachate measurements and used as measurements. The measurement equations for leachate production rate and chloride concentration are:

$$LPR_t = \frac{\sum_{i=t-6}^{t} v_{cell_{0_i}}}{7} + \varepsilon_{LPR_{mea}} \tag{3.12}$$

$$C_t = c_{cell_{0_t}} + \varepsilon_{C_{mea}} \tag{3.13}$$

3.2.5. SYNTHETIC TRUTH GENERATION

Synthetic experiments are often designed to evaluate the performance of data assimilation techniques. Artificial truth states are generated by running a known forward model. If the DA algorithm is effective, estimated states or parameters are expected to converge to the synthetic truth by assimilating the simulated measurements obtained from the forward model. The method of creating artificial truth is highly dependent on the aim of the applied DA technique and the assumption of existing underlying uncertainties. The primary sources of uncertainty for a deterministic model are errors in forcing data, initial states, model parameters, and model concepts. The most simple scenario assumes that the model is correct and only adds white noise to simulated measurements as measurement error. Weerts and El Serafy (2006) perturbed forcing data to consider the forcing data uncertainties in a state estimation problem. Plaza Guingla *et al.* (2013) further added Gaussian noise to model parameters, although only model states are updated in that research. Li *et al.* (2013) chose to perturb the state variables in a probability-distributed hydrological model. All the uncertainties above are considered to be included in state variables. Gelsinari *et al.* (2020) used the 'truth' generated from the unperturbed model, while the model used in assimilation is with a perturbed parameter set. Since we aim to assess the feasibility of estimating emission potential in the TTD model by coupled particle filter, we assume the forward model parameters to be correct in order to simplify the problem. The initial states and input data were perturbed in order to simulate a scenario where we have a poor understanding of initial states and the input measurements are inaccurate.

The initial states in 2003 were obtained from model calibration in order to generate a synthetic truth. Zero mean Gaussian error with a standard deviation of $10\% \times c_{ini}$ and $10\% \times v_{ini}$ were added to perturb the initial states.

Zero-mean Gaussian errors were added to daily rainfall and potential evapotranspiration during the simulation period from 2003 to 2021. The uncertainty range of rainfall is often chosen as $(0-15\%) \times R_t$ (Weerts & El Serafy, 2006). Here the standard deviation of random rainfall error was set as $15\% \times R_t$. The perturbation of evapotranspiration followed Plaza Guingla *et al.* (2013) where a $30\% \times Pev_t$ standard deviation was used.

Although this study primarily focuses on synthetic experiments, we aim to adapt the framework to accommodate the assimilation of real-world data for further research. Hence, the data assimilation frequency was set to be identical to the frequency of the real concentration measurements.

Once the simulation results are obtained as synthetic truth, the measurement errors should be added to observable states to simulate measurements as shown in equation 4.12 and equation 4.13. The standard deviations of Gaussian measurement error are selected as 10% of LPR_t and C_t, respectively.

All the errors are presented in Table 3.2. It is worth emphasizing that although we try to simulate the actual case in the synthetic experiment, the artificial truth is only trying to approach the natural world in the context of a proof-of-concept study (Matgen *et al.*, 2010).

Table 3.2.: Standard deviation of Gaussian random errors for truth generation

Variables	R	Pev	v_{ini}	c_{ini}
Standard deviation	$0.15 \times R_t$	$0.3 \times Pev_t$	$0.1 \times v_{ini}$	$0.1 \times c_{ini}$

v_{ini} and c_{ini} represent all the initial volume and concentration states in the model.

3.2.6. ENSEMBLE GENERATION PERFORMANCE CONTROL

The performance of DA relies on the appropriate representation of uncertainties in the prediction. More specifically, the model error in equation 4.1 should make the spread of generated ensembles realistic compared to real measurements. Following the method proposed by De Lannoy *et al.* (2006), the ensemble spread($ensp_t$), the mean square error(mse_t), and the ensemble skill($ensk_t$) are calculated as:

$$ensp_t = \frac{1}{N}\sum_{i=1}^{N}(y_t^i - \overline{\boldsymbol{y}_t})^2 \tag{3.14}$$

$$mse_t = \frac{1}{N}\sum_{i=1}^{N}(y_t^i - y_{mea_t})^2 \tag{3.15}$$

$$ensk_t = (\overline{\boldsymbol{y}_t} - y_{mea_t})^2 \tag{3.16}$$

N, i, t, y, y_{mea} represent ensemble size, ith ensemble number, assimilation time step, simulated observable states, and assimilated measurements, respectively. According to De Lannoy *et al.* (2006), to ensure the generated ensembles' statistical accuracy, the following requirements should be considered:

$$\frac{< ensk >}{< ensp >} \approx 1 \tag{3.17}$$

<> means the average over the simulation time range. More specifically, a value larger than 1 indicates insufficient ensemble spread, while a value smaller than 1 indicates excessive spread. If the truth is indistinguishable from a member of the ensemble, the following equation should be true(De Lannoy *et al.*, 2006):

$$\frac{< \sqrt{ensk} >}{< \sqrt{mse} >} \approx \sqrt{\frac{N+1}{2N}} \tag{3.18}$$

When both leachate production rate and concentration measurements are assimilated, we need a sufficiently large ensemble spread in the simulated output. This is achieved by manually optimizing the standard deviations of model error. Firstly we obtained the model error for the cover layer water storage using an interval search to get an appropriate spread in leachate production rate simulations. If the spread for concentration states is not sufficient or excessive with the chosen model error, we adjust the initial uncertainty range for the bulk concentration states. Using this approach allows us to obtain a good ensemble spread for concentration states while not making the spread in leachate production excessive.

3.2.7. IMPLEMENTATION PROCEDURE

Based on the theory and model characteristics, the implementation of sequential importance resampling in this coupled TTD model is as follows:

1. Initialization: from the model calibration results, we take one parameter set and initial states in 2003. The initial samples are sampled from Gaussian distributions where the means are the optimized initial values. Initially, the corresponding percentiles of standard deviations in Gaussian distributions are set to be the same as the ones used in the generation of synthetic initial states (see table 3.2). Subsequently, the standard deviations undergo

adjustment to meet the ensemble spread criteria, as is discussed in section 3.3.1. With a warm-up simulation, the samples are propagated to the starting date of data assimilation on the 19th June 2012, a time step 7 days earlier than the first measurement date. The reason to perform this warm-up propagation is that we need to build connections among waste body states. Otherwise, the time lag between bulk states and measurements will make the estimation unreliable.

2. Update step: all the particles are propagated to the next assimilation step with equation 4.1, where $M(\cdot)$ indicates the coupled TTD model. The forward model is discretized with a daily time step, and the assimilation frequency is the same as the real concentration measurement frequency, which is generally two weeks. The choice of model error is crucial for representing uncertainties and ensuring a good data assimilation technique performance. Most studies applying particle filter or ensemble Kalman filter choose to add a Gaussian random error to perturb forcing data, model states, and/or parameters (Mattern *et al.*, 2013; Tran *et al.*, 2020; Vrugt *et al.*, 2013; Weerts & El Serafy, 2006). Considering the time lag issue, if we add independent model error to each state directly, the accumulation of errors of states like v_{bulk} will be huge after several years' lag. Therefore, we choose to add daily error to V_{cl}. The daily errors added on day t will be propagated to waste body states since day $t+1$ according to the infiltration TTD curve with time until the next assimilation step. Therefore, we are actually adding correlated model errors to waste body states. Since the influence of error in V_{cl} on fast flow cells(cells with small travel time) can be estimated by current measurements, we can avoid adding too many unreasonable errors to old states like v_{bulk}. Additionally, this error choice maintains the total mass balance in waste body water storage($V_{wb_{t+1}} = V_{wb_t} + infiltration - outflow$). No model error is introduced to the concentration states directly. Once the initial concentration values are determined, the concentration variation is assumed to be determined by volume states only.

3. Analysis step: The particle weights are calculated by equation 4.7. Based on different assimilation strategies, we weigh the states differently. In a coupled assimilation scenario, the weights for volume w_v and concentration states w_c are calculated separately using their corresponding measurements. Both concentration and leachate volume are used to calculate w_m: $w_m = w_c * w_v$. Then w_m is normalized before estimating the mass states. If only concentration measurements are assimilated, all the model states are weighted based on the concentration measurements. When

only LPR measurements are assimilated, the weights are used to estimate all states except concentration states.

4. Resampling step: this step is similar to the analysis step, effective ensemble size N_v^{eff}, N_c^{eff} is computed according to equation 3.10. Then the volume states will be resampled when N_v^{eff} is smaller than $N/2$. The concentration states will be resampled if N_c^{eff} is smaller than $N/2$. These two resampling steps are totally separated, which means the resampling of volume states will not change the concentration states and their weights w_c, and vice versa. If volume or concentration states are resampled, the mass states will be recalculated based on the current volume and concentration states, and the weights w_m are also updated with new w_v and w_c. The resampled volume and concentration states are then used in the coupled forward model to make a prediction until the next assimilation step.

5. Iteration: all former steps after initialization are repeated until the last assimilation step.

3.2.8. PERFORMANCE ESTIMATION

Besides the evolution of hidden states, the accuracy of state estimation results is evaluated with the temporal mean root-mean-square error, which is described in equation 4.16. The L indicates the number of assimilation time steps.

$$MRMSE = \frac{\sum_{t=1}^{L} \sqrt{\sum_{i=1}^{N} w_t^i (x_t^i - x_t^{truth})^2}}{L} \tag{3.19}$$

The prediction accuracy is also evaluated using a logarithmic form(η) proposed by (Ercolani, 2017):

$$\eta = -\ln(1 - NSE) \tag{3.20}$$

Where NSE is the Nash-Sutcliffe efficiency calculated as:

$$NSE = 1 - \frac{\sum_{t=1}^{T} (y_t - y_{mea_t})^2}{\sum_{t=1}^{T} (y_{mea_t} - \overline{y_{mea}})^2} \tag{3.21}$$

where y_{mea_t} are the measurements at time step t, y_t represents the model prediction, and the over bar means the average over time. The logarithmic scale allows dealing with high NSE values(close to 1). It tends to plus infinity when the observations and predictions achieve a perfect match. The reliability of ensemble prediction is not considered here because the model error is optimized to get reliable predictions.

3.2.9. SYNTHETIC SCENARIOS

Different synthetic scenarios are designed to test the application's feasibility. As shown in table 3.3, in total six scenarios are used to test the assimilation performance and get optimal assimilation strategy. Scenarios A, D follow the proposed coupled assimilation procedure described above. In other scenarios, only LPR or concentration measurements are assimilated. The concentration observations are used to estimate all states when assimilated solely, while the LPR observations are used to update volume states solely. This is because concentration measurements contain information on both volume and concentration states, while the LPR observations only contain information on volume states. Scenarios D to F are similar to A to C but with the difference that we initialize the simulation with much smaller initial bulk volume values. These scenarios are used to test the influence of the baseflow function, which will be discussed in the following part. Two open-loop simulations are also performed to get reference results for scenarios $A-C$ and $D-E$. The open loop simulations have the same initial sample distributions and model errors as corresponding scenarios, but no measurements are assimilated to update model states.

Table 3.3.: Synthetic scenarios

Scenario	Assimilate LPR	Assimilate C	Small initial V_{bulk}
A	Yes	Yes	No
B	Yes	No	No
C	No	Yes	No
D	Yes	Yes	Yes
E	Yes	No	Yes
F	No	Yes	Yes
$OL_{A\text{-}C}$	No	No	No
$OL_{D\text{-}F}$	No	No	Yes

3.3. RESULTS AND DISCUSSION

The results of the experiment will be presented as follows. First, we present the performance of ensemble generation. Next, we discuss the hidden state estimations, including cover layer water storage, total water storage, average concentration, and total chloride mass in the waste body. Finally, we show the prediction performance results across all scenarios. Based on our experimental scenario settings, we will primarily make two types of comparisons: one between scenarios with different initial bulk storage states, and another between scenarios with the same initial bulk storage but different measurements assimilated.

3.3.1. ENSEMBLE GENERATION

The appropriateness of ensemble generation and the generated initial particles on the starting date of data assimilation, which is the 19th of June, is verified using equations 4.14 and 4.15. Based on the results of a preliminary sensitivity analysis of ensemble size, all experiments use 10240 particles to ensure stable performance. The final choice of initialization, model errors and the corresponding ensemble generation skills are presented in table 3.4.

Table 3.4.: Ensemble generation performance

Scenario	$M_{v_{bulk}}$	$\sigma_{v_{bulk}}$	$\sigma_{c_{bulk}}$	$\epsilon_{V_{cl}}$	$\frac{<ensk>}{<ensp>_{LPR}}$	$\frac{<\sqrt{ensk}>}{<\sqrt{mse}>_{LPR}}$	$\frac{<ensk>}{<ensp>_{C}}$	$\frac{<\sqrt{ensk}>}{<\sqrt{mse}>_{C}}$
A-C	4.067	0.100	0.130	0.0145	1.002	0.651	1.082	0.587
D-E	2.000	0.100	0.100	0.0135	0.998	0.624	1.013	0.583

Note. All the initial states in 2003 are sampled from Gaussian distributions $N(M, \sigma \times M)$. The distribution parameters are the same as truth generation if not explicitly defined in the table. $M_{v_{bulk}}$ represents the initial mean of bulk water storage. $\sigma_{v_{bulk}}$ and $\sigma_{c_{bulk}}$ refer to the standard deviation percentile of bulk water storage and chloride concentration, respectively. $\epsilon_{V_{cl}}$ shows the standard deviation percentile for Gaussian model error ($N(0, \epsilon_{V_{cl}} \times V_{cl})$) added to cover layer water storage. If the newly generated cover layer water storage with model error is negative, we manually set it to a small value of 0.001.

3.3.2. ASSIMILATION PERFORMANCE

ESTIMATION OF HIDDEN STATES

The hidden state estimation performance of the method is evaluated using the proposed performance matrices (equation 4.16 - 4.18). The results of total water storage in the cover layer, chloride mass, and water storage in the waste body are presented in Figure 3.3. In addition, the results of average chloride concentration are presented to understand the state update process better. Although there is a small amount of chloride in the cover layer, it can be ignored compared with the amount in the waste body.

Total water storage in cover layer

As shown in Figure 3.3, the four MRMSE values for the storage in the cover layer (V_{cl}) in A-C and OL_{A-C} scenarios are similar. This observation is supported by the standard deviations of MRMSE, which are within a magnitude of $4 \times 10^{-3} m$. Similar estimation performance is observed in scenarios D-F and OL_{D-F}, where the standard deviations of MRMSE are within a magnitude of $3 \times 10^{-3} m$. The values of the standard deviations of RMSE are in the uploaded output file. The similar behavior of cover

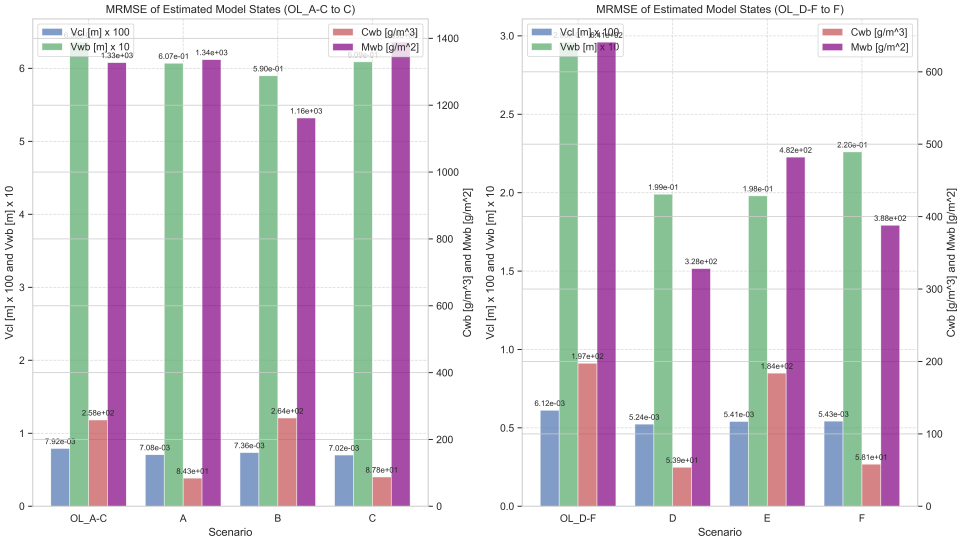

Figure 3.3.: MRMSE of hidden states in different scenarios

layer water storage is mainly caused by the buffering effect of the unsaturated soil model used to simulate V_{cl}. When saturation is high, infiltration to the waste body will be high as well. If no model error or forcing data errors were added, the V_{cl} starting with different values would converge to a same value after a period of time. The random model error added during data assimilation is the main source of the uncertainty in V_{cl}.

Total water storage in waste body

Scenarios A - C are initialized with high values for initial bulk water storage. As shown in Figure 3.3, scenario B has similar waste body water storage (V_{wb}) estimation results as scenario A because of the same assimilation procedure for volume states.

As shown in Figure 3.4, the mean estimation shows no noticeable improvement throughout the entire period in scenario A. However, when the model is initialized with a lower value for the initial bulk water storage in scenario D, the behavior differs significantly. The assimilation of new measurements corrects the biases in total water storage compared to the scenarios with large bulk water storage. Scenarios D and E also exhibit better estimation performance than open-loop simulations, unlike scenarios B and C, where only slight improvement is observed, as illustrated in Figure 3.3.

The difference in assimilation performance between the two initial values in water storage is due to the baseflow function. As discussed

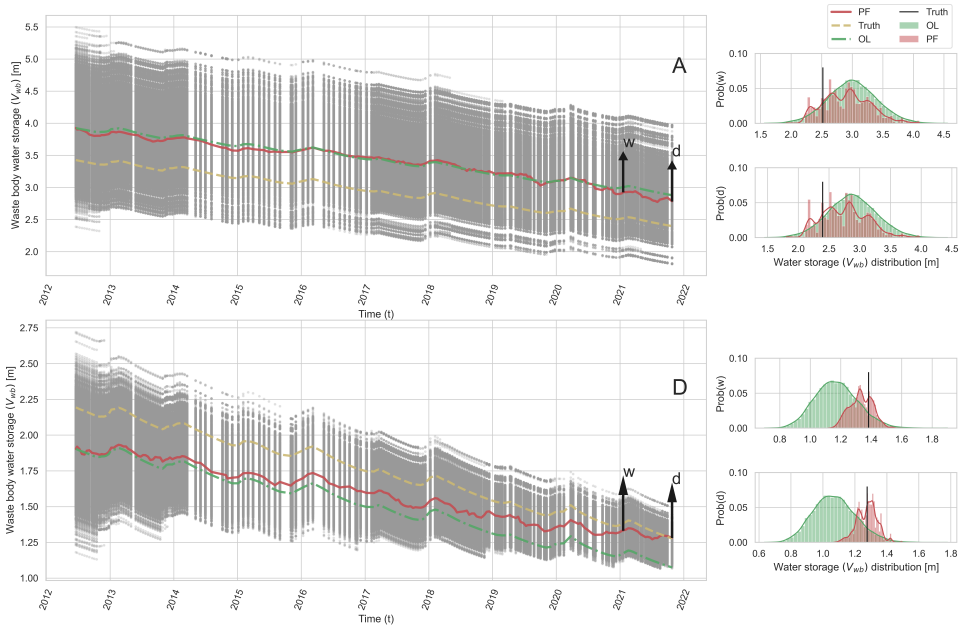

Figure 3.4.: Water storage in the waste body in scenarios A and D. The red line represents the mean estimation of the particle filter. The green and yellow lines represent the open loop results and synthetic truth, respectively. The individual particles are shown as grey points. The two black arrows point to the wet and dry period during the assimilation process, with corresponding probabilities plotted. The black vertical lines in the probability histograms are the truth at specific time steps.

regarding the time lag issue, we can only estimate hidden states if the measurements are sensitive to their variations. Figure 3.5 shows the baseflow function, which links bulk water storage to the generated baseflow volume. Bulk water storage constitutes a significant portion of the total water storage in the waste body, making its estimation crucial for accurate V_{wb} estimation. As shown, baseflow is sensitive to variations in bulk water storage only when it ranges between 0 and 2 meters. Additionally, Figure 3.6 illustrates the travel time distribution of baseflow, indicating that almost all generated baseflow is allocated to the oldest cell. This means any changes in bulk storage take five years to be reflected in simulated leachate production rates.

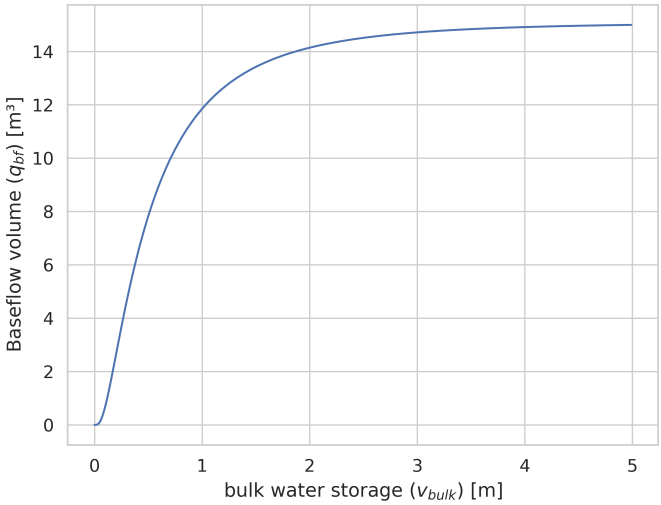

Figure 3.5.: Baseflow change with bulk water storage variation

According to the synthetic truth, the bulk water storage five years before the last measurement in scenarios A-C is around 2.18m. Obviously, the information in the measurements to quantify bulk water storage is limited. Lower values of the bulk water storage allow the baseflow to reduce during the simulation time span. As a consequence, measured leachate production rates contain information on this reduced water storage because of lower baseflow values. This improves the estimate of bulk water storage and V_{wb}, leading to lower uncertainty. It's worth noting that selecting different baseflow functions or baseflow distribution functions from the MCMC results can lead to varying state estimation outcomes. This chapter aims to investigate the feasibility of using the coupled particle filter method in a synthetic experiment, assuming our model parameters are accurate. Additionally, we will explore the influence of parameter uncertainty in subsequent research.

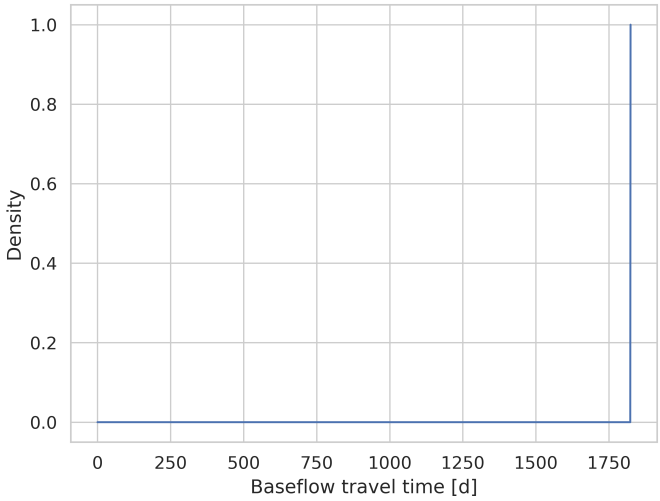

Figure 3.6.: Baseflow travel time distribution

Another influencing factor of the uncertainty quantification capacity is the measurement error. While the measurement errors are small, it can detect smaller baseflow changes. For example, the bulk water content will still influence the baseflow when it varies between 2 and 3 meters. When the measurement error is relatively large compared to the corresponding baseflow variation, most of the particle sets in this range will have close weights as they all give similar baseflow output. As shown in scenario A in Figure 3.4, only large and small particle sets are discarded with assimilation.

In scenario A, the posterior distribution in wet periods is close to the ones obtained during dry periods. This means that the estimation results of V_{wb} are stable during the last wet-dry cycle. However, in scenario D, the posterior distributions in dry periods still change compared with wet periods. This indicates that the measurements in the last cycle still contain new information content which are being assimilated to reduce the uncertainty. To further quantify the uncertainty and correct the bias in mean estimation, the time series of measured leachate production rates should be long enough to capture the effect of reducing bulk water storage values in the sensitive range.

Comparing scenarios assimilating different measurements, Figure 3.3 shows that when the information content of the measurements is high, the concentration measurements can be used to estimate V_{wb} in scenario F. Compared with scenario D, the MRMSE in scenario F is higher. It is because the weights in scenario F are calculated using concentration measurements, which are also influenced by mass states. The particles with the wrong volume and mass values but correct

concentration values are also considered with high probability.

Average chloride concentration in waste body

Estimation of the average chloride concentration in the waste body is another case where the "history" is required. All available measurements are linked to the first cell only. Nevertheless, the estimation of the average concentration becomes possible because of the "history" connection between cells and bulk.

As shown in Figure 3.3, the MRMSE values in average concentration are lower when concentration measurements are assimilated, compared with the open-loop results. As shown in Figure 3.7, in both scenarios A and D, the uncertainties are significantly reduced, and the synthetic truth is covered by the particles. Regardless of the sensitivity of baseflow to variations in bulk water storage, the chloride in the waste body bulk serves as the source for chloride in the mobile cells, enabling us to use concentration measurements to estimate the average concentration effectively.

It is worth noting that when only concentration states are assimilated in scenarios B and F, Figure 3.3 shows slightly higher MRMSE values compared with scenarios A and D, where both concentration and LPR measurements are assimilated. Similarly, the MRMSE of average concentration in scenario E is slightly better than the open-loop group. This indicates that the assimilation of LPR measurements helps improve the estimation of concentration states. Although concentration states are updated solely by concentration measurements, the updated volume states influence the prediction of concentration states at the next time step. This illustrates how weakly coupled data assimilation integrates information from both domains. We did not observe this behavior in waste body water storage estimation because our model is one-way coupled. This effect is likely not very strong, probably because our initial particles for volume states can generate good volume predictions due to optimization by MCMC. Overall, the assimilation of concentration states helps quantify the uncertainty in concentration states.

Total chloride mass in waste body

The total chloride mass in the waste body is calculated from the estimated water volume and concentration states. The uncertainty reduction in either volume states or concentration states reduces the uncertainty of mass states. On the other hand, bias in the estimation of volume or concentration states can result in bias in mass estimation, even if the other estimation is perfect.

As shown in Figure 3.3, when initial bulk water storage is small, all the synthetic experiments have better MRMSE results than open-loop simulations. Assimilating both measurements achieves the best

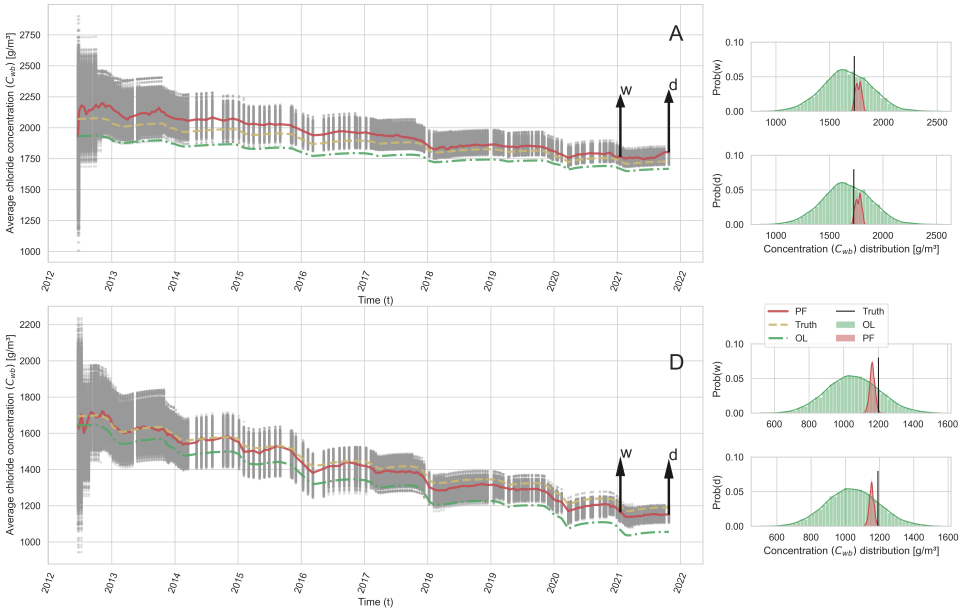

Figure 3.7.: Average concentration in the waste body in scenarios A and D. Colors of lines as in Figure 3.3.

estimation results. In contrast, when the initial bulk storage is high, the MRMSE decrease is relatively small after assimilation. This is because the uncertainty in V_{wb} is not sufficiently reduced in scenarios A, B, and C. Scenario B's MRMSE result is unusually small because it yields a higher estimation of water storage and a lower estimation of average concentration states, leading to a better mean estimation of mass states.

Following the conclusion from volume and concentration estimations, solely assimilating LPR measurements is insufficient for emission potential estimation. When the sensitivity of baseflow to bulk storage is high, we can use concentration measurements solely to estimate the M_{wb}. Assimilating both measurements achieves the best performance in the sense of both mean estimation and uncertainty reduction.

PREDICTION PERFORMANCE

Leachate production rates

Figure 3.8 shows the metrics we use to quantify the quality of the predicted states. All six scenarios have smaller MRMSE values and greater η values compared with the corresponding open-loop simulations. This indicates reduced prediction uncertainty and improved accuracy. However, the η and NSE values of three scenarios with the

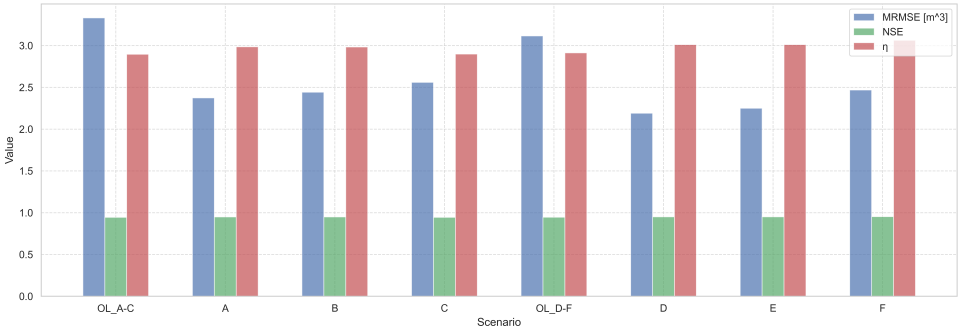

Figure 3.8.: LPR prediction performance in different scenarios.

same initial bulk storage are very close.

As discussed in section 3.2.1.1, the estimation of cover layer water storage has a relatively good consistency with the truth because of the buffering effect, which guarantees the accuracy of LPR prediction, especially in wet periods where infiltration from the cover layer takes up most of the outflow. Additionally, when the bulk storage in the waste body, v_{bulk}, reduces below 1 m (see Figure 3.5), the baseflow magnitude will reduce significantly. Under such conditions, baseflow will show a large sensitivity to infiltration from the cover layer reaching the bulk storage.

Although scenario D, as shown in Figure 3.3, provides a better estimation of waste body water storage than scenario F, scenario F has a higher η value compared to scenario D. This is likely because more uncertainty remained in the posterior distribution of scenario F, which is crucial for capturing the effect of changes in bulk storage on the baseflow. Additionally, η is calculated using synthetic measurements that include measurement errors. During the dry period, some values are smaller than the true values, which can only be accounted for by small v_{bulk} values.

Chloride concentrations

As shown in Figure 3.9, when concentration measurements are assimilated in scenarios A, C, D, and F, the values of prediction accuracy η improve significantly compared with open-loop realizations. When only LPR measurements are assimilated, we also observe the reduction of MRMSE and improvement of η. Although the improvement is very small compared with the scenarios assimilating concentrations, it shows the improvement in flow estimation can help improve the concentration prediction.

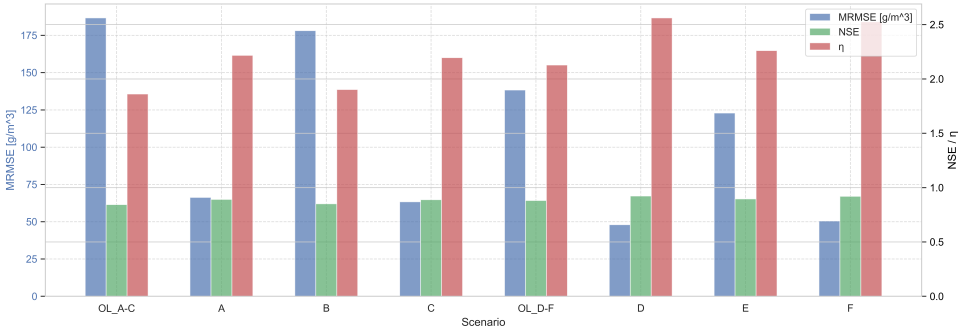

Figure 3.9.: Concentration prediction performance in different scenarios.

3.4. SUMMARY AND CONCLUSIONS

This work presents a weakly coupled particle filter framework to assimilate leachate production rates and chloride concentrations with the aim of estimating the emission potential of landfill waste bodies. The emission potential in this chapter is defined as the mass of leachable chloride present in the waste body. A concentration-coupled travel time distribution model was used as a forward model for data assimilation. Synthetic experiments were performed to investigate the feasibility of state estimation and improving prediction. Six scenarios were developed to investigate the best assimilation strategy. Two synthetic measurement data sets were generated with the same forward model using different initial bulk water content values under identical meteorological forcing conditions. On each synthetic data set, three types of Data Assimilation were carried out: DA using both Leachate Production Rate (LPR) and concentration measurements and DA using only LPR or concentration measurements.

The results from the different scenarios show that the sensitivity of baseflow to bulk water storage volume plays a vital role in controlling the assimilation performance. When the bulk water storage is within the range where its change has limited influence on baseflow, assimilating measurements cannot reduce the uncertainties in waste body water storage. This indicates that we need to record measurements over a long enough period to capture the sensitive range. Additionally, proactive measures should be implemented to stimulate the emission of bulk water storage, allowing us to reach the sensitive range more quickly.

The results also indicate that the improvement in the estimation of cover layer water storage is limited, as the open-loop realizations already have good consistency with the synthetic truth. Assimilating concentration measurements improves the estimation of average concentration states in the waste body. It also benefits the estimation of

water storage states as the concentration states are coupled to the water balance model. However, assimilation with concentration measurements alone behaves worse in water storage estimation in comparison with assimilating both LPR and concentration measurements under the assumed measurement errors in this research. In contrast, assimilating LPR helps quantify the uncertainty in water storage states in the waste body, while it doesn't reduce the uncertainties in concentration states. The proposed coupled assimilation method leads to good estimation results in both water storage and concentration states. More specifically, better concentration estimation performance is observed in coupled assimilation compared with assimilating concentration solely, which indicates the benefit of information exchange in forecast steps.

The estimation of emission potential heavily relies on an accurate estimation of the total water storage and concentration states within the waste body. Reducing uncertainties in volume or concentration states leads to a corresponding reduction in uncertainties associated with emission potential. Therefore, improving the estimation of volume and concentration states directly contributes to minimizing uncertainties in emission potential. The results show the uncertainty is reduced in all the tested scenarios where the baseflow is sensitive to bulk storage change. The LPR prediction improvement after assimilation is insignificant, as the open-loop realizations also have good predictions. In contrast, the concentration predictions improved considerably when the chloride concentration measurements were assimilated.

Overall, the results of this study indicate that the proposed coupled assimilation procedure can be used to estimate total water storage and chloride mass in the waste body. As such, Data Assimilation is demonstrated to be a viable approach for quantifying the emission potential of landfill waste bodies. The assimilation of LPR rates helped improve the accuracy of the estimation of total water storage, V_{wb}, compared to assimilating concentrations alone. The gap between volume states and mass states is filled by concentration assimilation. Although the coupled assimilation was performed at the same time steps, this method can easily be expanded to assimilate different types of measurements at different time steps. This synthetic experiment assumes a perfect model so that the time lag issue can be solved by adding daily model errors to cover layer states. In a real case study, we must combine the state and parameter estimation to account for the parameter uncertainty. We may also need to independently add model errors to all states if we consider the model conceptual error. Extra measurements, such as hydrogeophysical observations for the whole waste body, may be required to further quantify the uncertainty without suffering the time lag problem. Future studies will focus on quantifying the uncertainty caused by model parameters, which, for example, determine the sensitivity of baseflow to bulk water storage

volume.

REFERENCES

Abbaszadeh, P., Moradkhani, H., & Daescu, D. N. (2019). The Quest for Model Uncertainty Quantification: A Hybrid Ensemble and Variational Data Assimilation Framework. *Water resources research*, *55*(3), 2407–2431. https://doi.org/10.1029/2018WR023629

Arulampalam, M., Maskell, S., Gordon, N., & Clapp, T. (2002). A tutorial on particle filters for online nonlinear/non-Gaussian\nBayesian tracking. *IEEE Transactions on signal processing*, *50*(2), 174–188. https://doi.org/10.1109/78.978374

Brand, E. (2014). Development of emission testing values to assess sustainable landfill management on pilot landfills Phase 2 : Proposals for testing values.

Carrassi, A., Bocquet, M., Bertino, L., & Evensen, G. (2018). Data assimilation in the geosciences: An overview of methods, issues, and perspectives. *Wiley Interdisciplinary Reviews: Climate Change*, *9*(5), e535. https://doi.org/10.1002/wcc.535

De Lannoy, G. J., Houser, P. R., Pauwels, V. R., & Verhoest, N. E. (2006). Assessment of model uncertainty for soil moisture through ensemble verification. *Journal of Geophysical Research: Atmospheres*, *111*(10). https://doi.org/10.1029/2005JD006367

Djurić, P., Kotecha, J., Zhang, J., Huang, Y., & Bugallo, M. (2003). Particle filtering. *IEEE Signal Processing Magazine*, 19–38.

Duurzaam stortbeheer. (2023). English page [Available at: https://duurzaamstortbeheer.nl/english-page/].

Ercolani, G. (2017). Variational assimilation of streamflow data in distributed flood forecasting. *Water Resources Research*, *53*(1), 158–183. https://doi.org/10.1002/2016WR019208.Received

Evensen, G., Vossepoel, F. C., & van Leeuwen, P. J. (n.d.). Iterative ensemble smoothers for data assimilation in coupled nonlinear multiscale models.

Fatoba, J. O., Eluwole, A. B., Sanuade, O. A., Hammed, O. S., Igboama, W. N., & Amosun, J. O. (2021). Geophysical and geochemical assessments of the environmental impact of Abule-Egba landfill, southwestern Nigeria. *Modeling Earth Systems and Environment*, *7*(2), 695–701. https://doi.org/10.1007/s40808-020-00991-8

Fellner, J., & Brunner, P. H. (2010). Modeling of leachate generation from MSW landfills by a 2-dimensional 2-domain approach. *Waste Management*, *30*(11), 2084–2095. https://doi.org/10.1016/j.wasman.2010.03.020

Fellner, J., Döberl, G., Allgaier, G., & Brunner, P. H. (2009). Comparing field investigations with laboratory models to predict landfill

leachate emissions. *Waste Management*, *29*(6), 1844–1851. https://doi.org/10.1016/j.wasman.2008.12.022

Gelsinari, S., Doble, R., Daly, E., & Pauwels, V. R. N. (2020). Feasibility of improving groundwater modeling by assimilating evapotranspiration rates. *Water Resources Research*, *56*(2), e2019WR025983. https://doi.org/10.1029/2019WR025983

Gharamti, M. E., Hoteit, I., & Valstar, J. (2013). Dual states estimation of a subsurface flow-transport coupled model using ensemble Kalman filtering. *Advances in water resources*, *60*, 75–88. https://doi.org/10.1016/j.advwatres.2013.07.011

Grugnaletti, M., Pantini, S., Verginelli, I., & Lombardi, F. (2016). An easy-to-use tool for the evaluation of leachate production at landfill sites. *Waste management*, *55*, 204–219. https://doi.org/10.1016/j.wasman.2016.03.030

Gworek, B., Dmuchowski, W., Koda, E., Marecka, M., Baczewska, A. H., Bragoszewska, P., Sieczka, A., & Osiński, P. (2016). Impact of the municipal solid waste lubna landfill on environmental pollution by heavy metals. *Water*, *8*(10), 470. https://doi.org/10.3390/w8100470

Han, G., Wu, X., Zhang, S., Liu, Z., & Li, W. (2013). Error covariance estimation for coupled data assimilation using a lorenz atmosphere and a simple pycnocline ocean model. *Journal of Climate*, *26*(24), 10218–10231. https://doi.org/10.1175/JCLI-D-13-00236.1

Heimovaara, T. J., & Wang, L. (2025). Quantification of Emission Potential of Landfill Waste Bodies Using a Stochastic Leaching Framework. *Water Resources Research*, *61*(3), e2024WR038360. https://doi.org/10.1029/2024WR038360

Hol, J. D., Schön, T. B., & Gustafsson, F. (2006). ON RESAMPLING ALGORITHMS FOR PARTICLE FILTERS. *Nonlinear Statistical Signal Processing Workshop, 2006 IEEE*, 79–82. https://doi.org/DOI:10.1109/NSSPW.2006.4378824

Janjić, T., Bormann, N., Bocquet, M., Carton, J. A., Cohn, S. E., Dance, S. L., Losa, S. N., Nichols, N. K., Potthast, R., Waller, J. A., & Weston, P. (2018). On the representation error in data assimilation. *Quarterly Journal of the Royal Meteorological Society*, *144*(713), 1257–1278. https://doi.org/10.1002/qj.3130

Kattenberg, W., & Heimovaara, T. (2011). Policy process of allowing research pilots for sustainable emission reduction at landfills in the netherlands. *Proc. Thirteenth International Waste Management and Landfill Symposium,* (October 2011), 1–8.

KNMI. (2022). Dagwaarden van weerstations. https://www.daggegevens.knmi.nl/klimatologie/daggegevens

Laloyaux, P., Balmaseda, M., Dee, D., Mogensen, K., & Janssen, P. (2016). A coupled data assimilation system for climate reanalysis.

Quarterly Journal of the Royal Meteorological Society, *142*(694), 65–78. https://doi.org/10.1002/qj.2629

Laner, D., Fellner, J., & Brunner, P. H. (2011). Future landfill emissions and the effect of final cover installation – A case study. *Waste Management*, *31*(7), 1522–1531. https://doi.org/10.1016/j.wasman.2011.02.022

Li, Y., Ryu, D., Western, A. W., & Wang, Q. J. (2013). Assimilation of stream discharge for flood forecasting: The benefits of accounting for routing time lags. *Water resources research*, *49*(4), 1887–1900. https://doi.org/10.1002/wrcr.20169

Liu, Y., Weerts, A. H., Clark, M., Hendricks Franssen, H. J., Kumar, S., Moradkhani, H., Seo, D. J., Schwanenberg, D., Smith, P., Van Dijk, A. I., Van Velzen, N., He, M., Lee, H., Noh, S. J., Rakovec, O., & Restrepo, P. (2012). Advancing data assimilation in operational hydrologic forecasting: Progresses, challenges, and emerging opportunities. *Hydrology and earth system sciences*, *16*(10), 3863–3887. https://doi.org/10.5194/hess-16-3863-2012

Liu, Y., & Gupta, H. V. (2007). Uncertainty in hydrologic modeling: Toward an integrated data assimilation framework. *Water resources research*, *43*(7), 2006WR005756. https://doi.org/10.1029/2006WR005756

Matgen, P., Montanari, M., Hostache, R., Pfister, L., Hoffmann, L., Plaza, D., Pauwels, V. R., De Lannoy, G. J., De Keyser, R., & Savenije, H. H. (2010). Towards the sequential assimilation of SAR-derived water stages into hydraulic models using the Particle Filter: Proof of concept. *Hydrology and Earth System Sciences*, *14*(9), 1773–1785. https://doi.org/10.5194/hess-14-1773-2010

Mattern, J. P., Dowd, M., & Fennel, K. (2013). Particle filter-based data assimilation for a three-dimensional biological ocean model and satellite observations. *Journal of Geophysical Research: Oceans*, *118*(5), 2746–2760. https://doi.org/10.1002/jgrc.20213

McMillan, H. K., Hreinsson, E. O., Clark, M. P., Singh, S. K., Zammit, C., & Uddstrom, M. J. (2013). Operational hydrological data assimilation with the recursive ensemble Kalman filter. *Hydrology and Earth System Sciences*, *17*(1), 21–38. https://doi.org/10.5194/hess-17-21-2013

Ng, G.-H. C., McLaughlin, D., Entekhabi, D., & Scanlon, B. (2009). Using data assimilation to identify diffuse recharge mechanisms from chemical and physical data in the unsaturated zone. *Water resources research*, *45*(9), 2009WR007831. https://doi.org/10.1029/2009WR007831

Noh, S. J., Rakovec, O., Weerts, A. H., & Tachikawa, Y. (2014). On noise specification in data assimilation schemes for improved flood forecasting using distributed hydrological models. *Journal of hydrology*, *519*, 2707–2721.

Noh, S. J., Tachikawa, Y., Shiiba, M., & Kim, S. (2013). Ensemble kalman filtering and particle filtering in a lag-time window for short-term streamflow forecasting with a distributed hydrologic model. *Journal of Hydrologic Engineering*, *18*(12), 1684–1696. https://doi.org/10.1061/(ASCE)HE.1943-5584.0000751

Pantini, S., Verginelli, I., & Lombardi, F. (2014). A new screening model for leachate production assessment at landfill sites. *International Journal of Environmental Science and Technology*, *11*(6), 1503–1516. https://doi.org/10.1007/s13762-013-0344-7

Penny, S. G., Bach, E., Bhargava, K., Chang, C. C., Da, C., Sun, L., & Yoshida, T. (2019). Strongly Coupled Data Assimilation in Multiscale Media: Experiments Using a Quasi-Geostrophic Coupled Model. *Journal of Advances in Modeling Earth Systems*, *11*(6), 1803–1829. https://doi.org/10.1029/2019MS001652

Penny, S. G., & Hamill, T. M. (2017). Coupled data assimilation for integrated earth system analysis and prediction. *Bulletin of the American Meteorological Society*, *98*(7), ES169–ES172. https://doi.org/10.1175/BAMS-D-17-0036.1

Plaza Guingla, D. A., De Keyser, R., De Lannoy, G. J., Giustarini, L., Matgen, P., & Pauwels, V. R. (2013). Improving particle filters in rainfall-runoff models: Application of the resample-move step and the ensemble Gaussian particle filter. *Water Resources Research*, *49*(7), 4005–4021. https://doi.org/10.1002/wrcr.20291

Raanes, P. N. (2016). On the ensemble Rauch-Tung-Striebel smoother and its equivalence to the ensemble Kalman smoother. *Quarterly Journal of the Royal Meteorological Society*, *142*(696), 1259–1264. https://doi.org/10.1002/qj.2728

Rinaldo, A., Beven, K. J., Bertuzzo, E., Nicotina, L., Davies, J., Fiori, A., Russo, D., & Botter, G. (2011). Catchment travel time distributions and water flow in soils. *Water Resources Research*, *47*(7). https://doi.org/10.1029/2011WR010478

São Mateus, M. d. S. C., Machado, S. L., & Barbosa, M. C. (2012). An attempt to perform water balance in a Brazilian municipal solid waste landfill. *Waste Management*, *32*(3), 471–481. https://doi.org/10.1016/j.wasman.2011.11.009

Shockley, E. (2020). A Python implementation of the MT-DREAM(ZS) algorithm from Laloy and Vrugt 2012. https://github.com/LoLab-MSM/PyDREAM

Smith, P. J., Fowler, A. M., & Lawless, A. S. (2015). Exploring strategies for coupled 4D-Var data assimilation using an idealised atmosphere-ocean model. *Tellus A: Dynamic Meteorology and Oceanography*, *67*(1), 27025. https://doi.org/10.3402/tellusa.v67.27025

Snyder, C., Bengtsson, T., Bickel, P., & Anderson, J. (2008). Obstacles to high-dimensional particle filtering. *Monthly Weather Review*. https://doi.org/10.1175/2008MWR2529.1

Tardif, R., Hakim, G. J., & Snyder, C. (2015). Coupled atmosphere–ocean data assimilation experiments with a low-order model and CMIP5 model data. *Climate Dynamics*, *45*(5-6), 1415–1427. https://doi.org/10.1007/s00382-014-2390-3

Tran, V. N., Dwelle, M. C., Sargsyan, K., Ivanov, V. Y., & Kim, J. (2020). A Novel Modeling Framework for Computationally Efficient and Accurate Real-Time Ensemble Flood Forecasting With Uncertainty Quantification. *Water Resources Research*, *56*(3), 1–31. https://doi.org/10.1029/2019WR025727

Van Leeuwen, P. J. (2009). Particle filtering in geophysical systems. *Monthly Weather Review*, *137*(12), 4089–4114. https://doi.org/10.1175/2009MWR2835.1

Vrugt, J. A. (2016). Markov chain Monte Carlo simulation using the DREAM software package: Theory, concepts, and MATLAB implementation. *Environmental Modelling & Software*, *75*, 273–316. https://doi.org/10.1016/j.envsoft.2015.08.013

Vrugt, J. A., ter Braak, C. J. F., Diks, C. G. H., & Schoups, G. (2013). Hydrologic data assimilation using particle Markov chain Monte Carlo simulation: Theory, concepts and applications. *Advances in Water Resources*, *51*, 457–478. https://doi.org/10.1016/j.advwatres.2012.04.002

Wang, L., & Heimovaara, T. J. (2025). Quantifying landfill emission potential using a weakly coupled particle filter. *Water Resources Research*, *61*(2), e2023WR036549. https://doi.org/10.1029/2023WR036549

Weerts, A. H., & El Serafy, G. Y. H. (2006). Particle filtering and ensemble Kalman filtering for state updating with hydrological conceptual rainfall-runoff models. *Water resources research*, *42*(9), 1–17. https://doi.org/10.1029/2005WR004093

Yang, N., Damgaard, A., Kjeldsen, P., Shao, L. M., & He, P. J. (2015). Quantification of regional leachate variance from municipal solid waste landfills in China. *Waste management*, *46*, 362–372. https://doi.org/10.1016/j.wasman.2015.09.016

Zhang, H., Hendricks Franssen, H.-J., Han, X., Vrugt, J. A., & Vereecken, H. (2017). State and parameter estimation of two land surface models using the ensemble Kalman filter and the particle filter. *Hydrology and Earth System Sciences*, *21*(9), 4927–4958. https://doi.org/10.5194/hess-21-4927-2017

Zhang, Z., Pan, X., Fang, Y., Wang, Y., Zhang, Y., & Xu, H. (2020). Laboratory study on the hydraulic characteristics of mechanically and biologically treated waste in China. *Waste Management*, *102*, 686–697. https://doi.org/10.1016/j.wasman.2019.11.026

Zhang, Z., Chen, X., Cheng, Q., & Soulsby, C. (2021). Using StorAge selection (SAS) functions to understand flow paths and age distributions in contrasting karst groundwater systems. *Journal*

of Hydrology, *602*(December 2020), 126785. https://doi.org/10.1016/j.jhydrol.2021.126785

Županski, M. (2017). Data Assimilation for Coupled Modeling Systems. In S. K. Park & L. Xu (Eds.), *Data Assimilation for Atmospheric, Oceanic and Hydrologic Applications (Vol. III)* (pp. 55–70). Springer International Publishing. https://doi.org/10.1007/978-3-319-43415-5_2

4

UNDERSTANDING HIDDEN PROCESSES IN LANDFILLS BY APPLYING PF-MCMC IN A COUPLED TRAVEL TIME DISTRIBUTION MODEL

This study introduces a novel approach using Particle Filter coupled with Markov Chain Monte Carlo (PF-MCMC) in a weakly coupled data assimilation framework, applied within a travel time distribution-based landfill leachate emission model. The proposed method integrates sequential observations of leachate production rate (LPR) and chloride concentrations to estimate hidden model states, parameters, and underlying processes. Synthetic experiments demonstrated the effectiveness of the PF-MCMC method in significantly reducing uncertainty and improving predictions compared to open-loop simulations. Real-world application to data from Braambergen landfill in the Netherlands further confirmed these advantages, notably improving concentration predictions while offering insights into hidden landfill processes like baseflow dynamics and preferential flow distributions. The study highlights the potential of PF-MCMC as a predictive tool and an analytical instrument to diagnose model limitations and dynamically track changes in landfill behavior, thereby enhancing long-term aftercare strategies.

Parts of this chapter appear in Wang and Heimovaara (2025b)

4.1. INTRODUCTION

Modern sanitary engineered landfills, as well as legacy landfills, produce leachate even under impermeable cover layers if organic wastes are degraded. Leachate is the liquid leaving the waste body through the bottom liner or drainage system. It causes environmental concern because it may be contaminated with compounds dissolved from the waste, which may have a negative impact on human health and the environment (Fatoba *et al.*, 2021; Gworek *et al.*, 2016; Pal *et al.*, 2010). Impermeable cover layers are not only very expensive but also unsustainable as they require eternal after-care. In the Netherlands, regulations require replacement of the cover layer after 75 to 100 years.

Instead of passing the risk to former generations, we believe that long-term after-care of landfills can be improved with a better understanding of long-term developments in both leachate quantity as well as quality, and how these values vary over time (Kattenberg *et al.*, 2013). An important measure for managing long-term after-care is the concept of leachate emission potential, which is the amount of releasable contaminant mass that will leave the landfill with leachate in combination with a prediction of how concentrations vary over time (Barlaz *et al.*, 2002; Heimovaara & Wang, 2025; Laner *et al.*, 2012).

The emission potential of a landfill depends on the initial releasable mass of leachable pollutants and the reduction over time due to leachate outflow. Accurately quantifying this potential requires robust modeling tools to simulate the complex dynamics of leachate movement. Research indicates that leachate typically flows along preferential pathways within the waste body (Fellner & Brunner, 2010; Malmström *et al.*, 2004; Rosqvist & Destouni, 2000; Zhang & Yuan, 2019b). Fellner and Brunner (2010) developed a model with a fast flow in a channel domain and a slow flow in a matrix domain to simulate the leachate behavior. However, the authors acknowledge that the model cannot estimate the heterogeneity of leachate flow, which is only possible if the solute transport is integrated into the simulation. Zhang and Yuan (2019b) developed and applied a bimodal probability density model to experimentally characterize and quantify preferential flow in municipal solid waste using dye tracer and solute breakthrough tests. In our recent work, we proposed a travel time distribution-based stochastic model to simulate the leachate hydrodynamics in field-scale landfills, where chloride concentration is also incorporated. The parameters were optimized using the Markov Chain Monte Carlo (MCMC) method with leachate production rate and chloride concentration data (Heimovaara & Wang, 2025). The leachate emission potential was then quantified using this model. However, the uncertainty in estimation is a challenge.

History matching methods, such as normal MCMC, are adept at obtaining the parameter set that gives a best-fit approximation of measurements over the time they are available (Vrugt, 2016). However,

these methods cannot recursively incorporate new measurement data or account for various sources of uncertainty that can change with time (Liu & Gupta, 2007). An alternative to MCMC is data assimilation, known for accommodating errors in the model and recursively assimilating new measurements to improve estimates (Wikle & Berliner, 2007). In recent years, data assimilation has gained widespread use for prediction in hydrology (Ercolani, 2017; Tran *et al.*, 2020; Yan & Moradkhani, 2016), and estimation of state and parameters in a wide range of models (Abbaszadeh *et al.*, 2019; Eryigit, 2021; Zhang *et al.*, 2017).

Among the various data assimilation methods, the Particle Filter (PF) is particularly useful with non-Gaussian state space models (van Leeuwen *et al.*, 2019). Our previous work confirmed that a sequential importance resampling (SIR) framework can effectively improve the predictions of leachate volume and quality, assuming a correct travel-time distribution model. However, this assumption of an accurate parameter set is very strong, as the parameters in landfill models can be biased or exhibit significant temporal variation (Grugnaletti *et al.*, 2016). From this perspective, treating these parameters as special, time-varying states within the model is more pragmatic.

When particle filters are applied, two main challenges must be overcome: degeneracy and sample impoverishment (van Leeuwen *et al.*, 2019). While the resampling step in SIR can mitigate degeneracy, it often leads to particle impoverishment, which is characterized by many particles with identical values and high weights. This lack of particle diversity can lead to biased estimation results. This problem is particularly pronounced in the parameter space, as parameters are not adjusted in forward simulations. To address this issue, Moradkhani *et al.* (2005) suggested perturbing parameters after resampling to preserve parameter diversity. Subsequently, an integration of Markov Chain Monte Carlo (MCMC) methods into particle filters was proposed to improve the efficiency of parameter search. In this approach, the parameters are perturbed and a Metropolis acceptance ratio is used to avoid excessive perturbation (Moradkhani *et al.*, 2012). Yan *et al.* (2015) demonstrated enhanced estimation performance in hydrological modeling using the PF-MCMC method.

When using a PF-MCMC approach to estimate parameters, it is important to maintain mass balance in the models. The PF-MCMC method developed by Vrugt *et al.* (2013) cannot be used for our purposes since it involves adjusting the model states after forward simulation during the MCMC step, potentially disrupting the conservation of the water balance. Similarly, methods based on the Ensemble Kalman Filter (EnKF) (Gharamti *et al.*, 2013), which directly update the states in the model using measurements, are also not utilized. The PF-MCMC approach proposed by (Moradkhani *et al.*, 2012) maintains mass balance by generating all states in the model through forward simulation with

perturbed parameters.

The assimilation of leachate production rates and leachate quality dynamics represents a coupled data assimilation(CDA) challenge. Coupled data assimilation can generally be separated into two categories: weakly coupled data assimilation(WCDA) and strongly coupled assimilation(SCDA) (Zhang *et al.*, 2020). The state analysis step is performed separately in WCDA, and the information exchange between domains only happens in the forecast step. In SCDA, the analysis step also updates the coupled domains as a whole. Although SCDA shows potential to make full use of the measurement information, the successful application of SCDA is limited because of the large sampling error in cross-domain error covariance. Similarly, joint state and parameter estimation in SCDA remains ongoing research owing to the uncertain state-parameter covariance (Zhang *et al.*, 2020).

Consequently, we choose to use the WCDA for state and parameter estimation in this study. WCDA has seen many successful applications using ensemble-based methods like the Kalman filter (Liu *et al.*, 2014b, 2014a). However, the number of reported studies using particle filter methods with WCDA for state and parameter estimation is quite limited.

In this chapter, we propose to use a PF-based state and parameter estimation method in the coupled travel time distribution model developed by Heimovaara and Wang (2025). Using PF-MCMC, our aim is to estimate hidden model states and parameters, thereby gaining insights into the hidden processes in the model controlling landfill emissions. By 'hidden', we refer to model states and processes that cannot be directly measured. We initially tested the proposed method in a synthetic experiment to investigate the assimilation effect. Subsequently, the method was applied to real data monitored at cell 11Z of Braambergen landfill in the Netherlands (Stichting Duurzaam Storten, 2017). With this approach, we aim to quantify the dynamics in leachate production and the impact preferential flow has on the concentration dynamics. In addition, we will be able to quantify the releasable mass (emission potential) present in the waste body. This information is essential for making informed decisions about long-term aftercare of landfills.

4.2. METHODS

In this section, we give a summary of the methods used in this chapter. We start with the travel time distribution model, which is the forward model used to simulate leachate volume and quality as a function of time. We then describe the PF-MCMC method that is used in the coupled WCDA assimilation framework. We apply the approach to two case studies related to the same field site. The first, to test the performance of the PF-MCMC method, is a synthetic case

based on stochastically perturbed simulations of leachate volume and leachate chloride concentrations, using a model with known (optimized) parameters. The second case is based on real measurements and aims to see how the approach works in practice when both states and parameters are estimated using available measurements.

4.2.1. TRAVEL TIME DISTRIBUTION MODEL

The TTD model is a one-way coupled model that predicts leachate production rate and chloride concentration. The model is driven by its inputs, rainfall, and evapotranspiration at the surface of the landfill. Infiltration, being the net result of rainfall and evapotranspiration, is distributed into the waste body through a travel time distribution of life-expectancies (Figure 4.1). The small red cells within the waste body represent water parcels with varying life-expectancy, which indicate the remaining time before these parcels exit the waste body.

A second source for water in the life-expectancy cells comes from the flow from the bulk waste, which we call base flow and which is loaded with solutes present in the waste body. This study considers chloride as the target solute, and rainwater is assumed to be chloride-free; base flow is therefore the sole source of chloride in the model. The solution present in the life-expectancy cells is diluted by the accumulated infiltration of water from the cover layer before flowing out into the drainage system. A detailed description of the original version of this coupled travel time distribution model can be found in Heimovaara and Wang (2025). In the version used in this chapter, the travel time distribution for base flow is simplified by adding the base flow to the water parcel that infiltrates into the drainage system directly. This simplification makes the model more suitable for parameter estimation by avoiding the time lag issue of base flow identified in Wang and Heimovaara (2025a).

4.2.2. PF-MCMC

The core idea of data assimilation is assimilating information from measurements to better understand unknown states and parameters. Considering $\boldsymbol{x}_{t-1}$ as the state vector containing all model states at the previous time step $t-1$, and $\boldsymbol{\theta}_{t-1}$ as the parameter vector, the forward simulation is given by:

$$\boldsymbol{x}_t = M_t(\boldsymbol{x}_{t-1}, \boldsymbol{\theta}_{t-1}) + \boldsymbol{\varepsilon}_{\text{model}_t} \tag{4.1}$$

where $M_t(\cdot)$ denotes the forward model, and $\boldsymbol{\varepsilon}_{\text{model}_t}$ represents the model error.

By applying a measurement operator H_t, we predict measurable states, which we can compare with actual measurements $\boldsymbol{y}_t$ at time t as shown in equation 4.2:

$$\boldsymbol{y}_t = H_t(\boldsymbol{x}_t) + \boldsymbol{\varepsilon}_{\text{mea}_t} \tag{4.2}$$

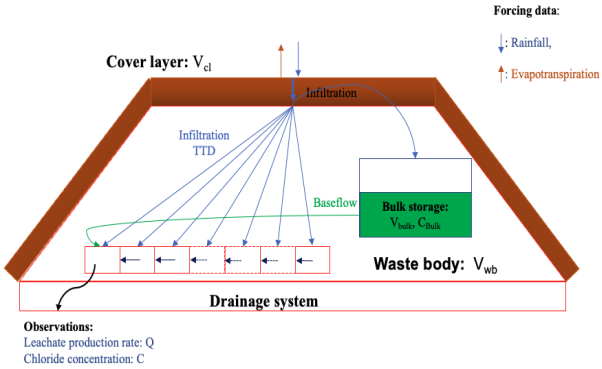

Figure 4.1.: A schematic overview of the travel time distribution model. Model states that are estimated in the PF-MCMC are the water volume in the cover layer (V_{cl}), the water volumes in the waste body with a specific life expectancy (V_{wb,T_i}) and the water volume and solute mass in the bulk of the waste body ($V_{wb,bulk}$ and $C_{wb,bulk}$).

where $\boldsymbol{\varepsilon}_{\text{mea}_t}$ denotes the measurement error vector.

The task of state estimation involves estimating the probability density function (pdf) of immeasurable states based on a series of measurements at discrete time steps. We use the subscript $1:t$ to represent the time range from the initial step to step t. Thus, $\boldsymbol{y}_{1:t}$ represents all available measurements until the current time step t, and $p(\boldsymbol{x_t}, \boldsymbol{\theta_t} \mid \boldsymbol{y}_{1:t})$ represents the pdf of the current state vector $\boldsymbol{x}$ and parameter vector $\boldsymbol{\theta}$ given $\boldsymbol{y}_{1:t}$. Bayes' theorem calculates the posterior pdf, $p(\boldsymbol{x_t}, \boldsymbol{\theta_t} \mid \boldsymbol{y}_{1:t})$, by combining the prior pdf from the last time step, $p(\boldsymbol{x_t}, \boldsymbol{\theta_t} \mid \boldsymbol{y}_{1:t-1})$, with the likelihood pdf $p(\boldsymbol{y}_t \mid \boldsymbol{x}_t, \boldsymbol{\theta_t})$:

$$p(\boldsymbol{x_t}, \boldsymbol{\theta_t} \mid \boldsymbol{y}_{1:t}) = \frac{p(\boldsymbol{y}_t \mid \boldsymbol{x}_t, \boldsymbol{\theta_t}) p(\boldsymbol{x}_t, \boldsymbol{\theta}_t \mid \boldsymbol{y}_{1:t-1})}{p(\boldsymbol{y}_t \mid \boldsymbol{y}_{1:t-1})} \tag{4.3}$$

The likelihood pdf is a quantification of how well the parameters $\boldsymbol{\theta}_t$ and states $\boldsymbol{x}_t$ describe the measurements $\boldsymbol{y}_t$. If the posterior pdf of state and parameter $p(\boldsymbol{x}_{t-1}, \boldsymbol{\theta}_{t-1} \mid \boldsymbol{y}_{1:t-1})$ at the previous assimilation step is known, the prior pdf at time step t, $p(\boldsymbol{x}_t, \boldsymbol{\theta}_t \mid \boldsymbol{y}_{1:t-1})$ can be calculated as:

$$p(\boldsymbol{x}_t, \boldsymbol{\theta}_t \mid \boldsymbol{y}_{1:t-1}) = \int p(\boldsymbol{x}_t, \boldsymbol{\theta}_t \mid \boldsymbol{x}_{t-1}, \boldsymbol{\theta}_{t-1}) p(\boldsymbol{x}_{t-1}, \boldsymbol{\theta}_{t-1} \mid \boldsymbol{y}_{1:t-1}) \, d(\boldsymbol{x}_{t-1}, \boldsymbol{\theta}_{t-1}) \tag{4.4}$$

The posterior pdf, $p(\boldsymbol{x}, \boldsymbol{\theta} \mid \boldsymbol{y}_{1:t})$, is then obtained from:

$$p(\boldsymbol{x}_t, \boldsymbol{\theta}_t \mid \boldsymbol{y}_{1:t}) = \frac{p(\boldsymbol{y}_t \mid \boldsymbol{x}_t, \boldsymbol{\theta}_t)}{p(\boldsymbol{y}_t \mid \boldsymbol{y}_{1:t-1})} \times \int p(\boldsymbol{x}_t, \boldsymbol{\theta}_t \mid \boldsymbol{x}_{t-1}, \boldsymbol{\theta}_{t-1}) p(\boldsymbol{x}_{t-1}, \boldsymbol{\theta}_{t-1} \mid \boldsymbol{y}_{1:t-1})\, d(\boldsymbol{x}_{t-1}, \boldsymbol{\theta}_{t-1}) \tag{4.5}$$

When using particle filtering, the desired pdf is approximated using the distribution of N independent discrete particles, each with weight w_i. Specifically, sampling from $p(\boldsymbol{x}_{t-1}, \boldsymbol{\theta}_{t-1} \mid \boldsymbol{y}_{1:t-1})$ means taking state and parameter particles from the previous time step. The propagation of these particles through the forward model (equation 4.1) is denoted by $p(\boldsymbol{x}_t, \boldsymbol{\theta}_t \mid \boldsymbol{x}_{t-1}, \boldsymbol{\theta}_{t-1})$. The $\boldsymbol{\theta}_t$ is also included in the equation in a parameter estimation problem, although the parameter values are not changed in forward propagation. The $p(\boldsymbol{y}_t \mid \boldsymbol{y}_{1:t-1})$ can be seen as a normalization factor ensuring that the sum of the pdf is 1. Thus, the posterior pdf $p(\boldsymbol{x}_t, \boldsymbol{\theta}_t \mid \boldsymbol{y}_{1:t})$ can be approximated as:

$$p(\boldsymbol{x}_t, \boldsymbol{\theta}_t \mid \boldsymbol{y}_{1:t}) \approx \sum_{i=1}^{N} w_t^i \delta([\boldsymbol{x}_t, \boldsymbol{\theta}_t] - [\boldsymbol{x}_t^i, \boldsymbol{\theta}_t^i]) \tag{4.6}$$

In this, δ represents the Dirac delta function. The weights w_t^i are recursively calculated from:

$$w_t^i = \frac{w_{t-1}^i p(\boldsymbol{y}_t \mid \boldsymbol{x}_t^i, \boldsymbol{\theta}_t^i)}{\sum_{i=1}^{N} (w_{t-1}^i p(\boldsymbol{y}_t \mid \boldsymbol{x}_t^i, \boldsymbol{\theta}_t^i))} \tag{4.7}$$

The likelihood term $p(\boldsymbol{y}_t \mid \boldsymbol{x}_t, \boldsymbol{\theta}_t)$ can be computed as:

$$p(\boldsymbol{y}_t \mid \boldsymbol{x}_t, \boldsymbol{\theta}_t) = \exp\left\{-0.5[\boldsymbol{y}_t - H_t(\boldsymbol{x}_t^i)]^T R^{-1} [\boldsymbol{y}_t - H_t(\boldsymbol{x}_t^i)]\right\} \tag{4.8}$$

where R is the measurement error covariance matrix.

The SIR method then resamples the particle sets with high likelihood values from the posterior distribution to avoid sample degeneracy. The implementation procedure follows Wang and Heimovaara (2025a). After the resampling step, all the particle weights are set to be $1/N$. Unlike the model states, model parameters are not changed during forward propagation, which causes sample impoverishment. We follow the approach of Moradkhani *et al.* (2005) where we add a perturbation term to parameters after resampling as:

$$\theta_t^{i,p} = \theta_t^{i+} + \varepsilon_t^i, \quad \varepsilon_t \sim N[0, sVar(\theta_t^{i-})] \tag{4.9}$$

The θ_t^{i+} means parameters after resampling, θ_t^{i-} are the parameters before analysis step and $\theta_t^{i,p}$ represents the proposed new parameters.

Larger parameter adjustments are preferred as they enable a more comprehensive parameter space exploration. However, excessive modifications must be avoided to prevent unrealistic predictions in the subsequent time step. To address this issue, Moradkhani *et al.* (2012) and Vrugt *et al.* (2013) have proposed the addition of a Markov Chain Monte Carlo (MCMC) step following resampling. A Metropolis acceptance ratio α determines whether to accept the proposed parameters.

$$\alpha = \min\left[1, \frac{p(x_t^{i,p}, \theta_t^{i,p}|y_{1:t})}{p(x_t^{i,+}, \theta_t^{i,+}|y_{1:t})}\right] \tag{4.10}$$

where $p(x_t^{i,p}, \theta_t^{i,p}|y_{1:t})$ is the proposed joint probability distribution. Roberts and Rosenthal (2001) suggested choosing optimal jump rates for a Gaussian proposal distribution as follows:

$$s = \frac{2.38}{\sqrt{2d}}. \tag{4.11}$$

Notably, the PF-MCMC method developed by Moradkhani *et al.* (2012) is adopted in our application case, as it maintains mass balance by not adjusting model states during the MCMC step. We refer readers to that paper for a detailed description of the implementation procedure. In summary, the perturbed parameters that yield more accurate predictions are accepted, while the others are kept the same as the resampled parameters without perturbation. The generated parameters are then used in the next forecasting step.

4.2.3. COUPLED ASSIMILATION FRAMEWORK

The idea of WCDA is straightforward: using the corresponding measurements to estimate and update model states accordingly. This approach extends similarly to parameter inclusion. The parameters related to volume states are estimated and resampled based on LPR measurements. Meanwhile, parameters pertaining to concentration dynamics are updated using concentration measurements. In our specific case, the TTD model is one-way coupled, where all the model parameters are related to volume states and the concentration states are controlled by volume states and initial concentration values. Hence, we update parameters and volume states based on LPR observations, update concentration states by concentration measurements, and calculate mass states based on both volume and concentration states.

4.2.4. CASE STUDY AREA AND AVAILABLE DATA

The research project is based on the Braambergen landfill in the Netherlands. Daily meteorological forcing data (same as model

resolution) are obtained from the Lelystad weather station affiliated with KNMI (2022). The leachate is collected from a landfill drainage system, and cumulative outflow volumes are automatically measured when leachate is pumped toward the water treatment plant. Chloride concentration is measured in a commercial laboratory on samples obtained from the drainage layer every two weeks (with some larger intervals up to 28 days). Gaussian measurement errors of 10% are assumed for the concentration measurements and 30% for the LPR measurements. These errors are intentionally set at lower values than the model prediction residuals because model prediction residuals account for both errors in the model structure and inaccuracies in measurements.

The values of the measured cumulative leachate production are a result of the leachate production from the waste body, but also depend on choices made by the landfill operator in managing the leachate pump system. There are periods when no outflow can be measured because no leachate is being pumped. This occurs during maintenance of the pump hardware, power failures, or problems downstream in the water treatment plant. In these cases, the observed leachate production volume is measured to be zero, and leachate is buffered in the drainage system. When pumping is restored, this excess leachate is pumped out at higher pumping rates. To limit the effect of these operational irregularities, weekly average leachate production rates were calculated from the cumulative leachate measurements and used as measurements for data assimilation. The measurement equations for leachate production rate and chloride concentration are:

$$LPR_t = \frac{\sum_{i=t-6}^{t} v_{cell_{0_i}}}{7} + \varepsilon_{LPR_{mea}} \tag{4.12}$$

$$C_t = c_{cell_{0_t}} + \varepsilon_{C_{mea}} \tag{4.13}$$

4.2.5. IMPLEMENTATION PROCEDURE

PRIOR GENERATION

The model was initialized in 2003 to simulate the warm-up period (Wang & Heimovaara, 2025a). To provide physically consistent priors for both parameters and state variables at the start of assimilation, we carried out a separate, offline Bayesian calibration. All leachate production and chloride concentration observations available were fitted with a DREAM(ZS) Markov-chain Monte Carlo algorithm, yielding a converged posterior ensemble. This posterior ensemble was taken as the initial particle cloud in the PF–MCMC experiment. This ensures the particle filter starts in a high-probability, physically consistent region of parameter space, reducing early particle degeneracy and improving

assimilation stability. The full set of posterior samples is archived and openly accessible; see the Data Availability section.

MODEL ERROR OPTIMIZATION

The model error in equation 4.1 should be tuned to generate enough spread in predicted particles during the data assimilation process. Following a similar procedure as in the Wang and Heimovaara (2025a), the ensemble spread ($ensp_t$), the mean square error (mse_t), and the ensemble skill ($ensk_t$) are calculated. According to De Lannoy *et al.* (2006), the following requirements should be considered to ensure the statistical accuracy of generated predictions,

$$\frac{< ensk >}{< ensp >} \approx 1 \tag{4.14}$$

<> means the average over the simulation time range. More specifically, a value larger than 1 indicates insufficient ensemble spread, while a value smaller than 1 indicates excessive spread. If the truth is indistinguishable from a member of the ensemble, the following equation should be true (De Lannoy *et al.*, 2006):

$$\frac{< \sqrt{ensk} >}{< \sqrt{mse} >} \approx \sqrt{\frac{N+1}{2N}} \tag{4.15}$$

To get sufficient ensemble spread for LPR predictions, we tuned the Gaussian random error added to v_{cl} first. As the concentration predictions are influenced by water volume states in the coupled TTD model, the error in v_{cl} also introduces errors to concentration states. If the ensemble spread of concentration predictions is insufficient, a Gaussian error will perturb the initial bulk concentration samples in 2003. The tuned Gaussian errors and the corresponding ensemble spread values for both synthetic and real tests are presented in Table 4.1. 10240 particles were used in all the following experiments.

Table 4.1.: Ensemble generation performance

Scenario	$\epsilon_{C_{bulk}}$	$\epsilon_{V_{cl}}$	$\frac{<ensk>}{<ensp>_{LPR}}$	$\frac{<\sqrt{ensk}>}{<\sqrt{mse}>_{LPR}}$	$\frac{<ensk>}{<ensp>_{C}}$	$\frac{<\sqrt{ensk}>}{<\sqrt{mse}>_{C}}$
Synthetic test	0.160	0.027	1.038	0.639	1.032	0.591
Real test	0.140	0.039	1.002	0.612	1.014	0.596

$cBulk_{ini}$ and v_{cl} represent the initial bulk concentration and cover layer water storage separately. The means of Gaussian distributions are zero.

ASSIMILATION PERFORMANCE ESTIMATION

In addition to the evolution of hidden states, the accuracy of state estimation results is evaluated using the temporal mean root-mean-square error (MRMSE), as described in Equation 4.16. Here, L denotes the number of assimilation time steps. This metric provides a robust measure of the deviation between the estimated and true states over the assimilation period, thereby offering a quantitative assessment of the model's performance.

$$MRMSE = \frac{1}{L}\sum_{t=1}^{L}\sqrt{\sum_{i=1}^{N} w_t^i (x_t^i - x_t^{truth})^2} \tag{4.16}$$

where L is the total number of assimilation time steps, N represents the number of particles, x_t^i denotes the estimated particle at time t, x_t^{truth} represents the true state variable at time t, w_t^i is the weight for the particle.

The prediction accuracy is also evaluated using a logarithmic form(η) proposed by (Ercolani, 2017):

$$\eta = -\ln(1 - NSE) \tag{4.17}$$

where NSE is the Nash-Sutcliffe efficiency calculated as:

$$NSE = 1 - \frac{\sum_{t=1}^{T}(y_t - y_{mea_t})^2}{\sum_{t=1}^{T}(y_{mea_t} - \overline{y_{mea}})^2} \tag{4.18}$$

where y_{mea_t} are the measurements at time step t, y_t represents the model prediction, and the overbar means the average over time. The logarithmic scale allows dealing with high NSE values(close to 1). It tends to infinity when the observations and predictions achieve a perfect match. The reliability of ensemble prediction is not considered here because the model error is optimized to get reliable predictions.

4.2.6. SYNTHETIC TRUTH GENERATION

The synthetic truth was generated by running the forward model using a single randomly selected parameter set from the converged distribution of MCMC samples. Random Gaussian noises were added to the forcing data from 2003 onward in order to account for the possible accumulation of uncertainties. The standard deviation of random rainfall error was set to be $15\% \times R_t$. The perturbation of evapotranspiration followed Plaza Guingla *et al.* (2013) where a $30\% \times Pev_t$ standard deviation was used. Finally, Gaussian measurement errors of 10% are added to the concentration predictions, and Gaussian measurement errors of 20% are added to LPR predictions to generate the synthetic measurements. We

use a smaller measurement error for LPR measurements to investigate the performance of the method under ideal measurement accuracy conditions.

4.2.7. APPLICATION TO DATA FROM THE CASE STUDY

Similarly to synthetic truth generation, we directly sampled from the MCMC results to get N particle sets. Also, we chose to sample the parameter set as a whole instead of sampling independently because we wanted to use information from MCMC to get more reliable prior samples. To achieve the initial particles on the 19th of June 2012, a time step 7 days earlier than the first measurement date, we performed a warm-up simulation starting from 2003. The same forcing error was introduced as the synthetic truth generation process.

4.3. RESULTS AND DISCUSSION

The weakly coupled PF-MCMC method was first applied in a synthetic experiment to evaluate its performance in hidden state and parameter estimation and how it improves the prediction of LPR and concentrations. Then, the method was used in a real case dataset from the Braambergen landfill.

4.3.1. SYNTHETIC EXPERIMENT

STATES

The estimation performance matrices calculated by equation 4.16 are shown in Table 4.2. The estimation evolution with time is presented in Figure 4.2.

Table 4.2.: MRMSE of estimated model states

State	$V_{cl}[m]$	$V_{wb}[m]$	$C_{bulk}[g/m^3]$	$M_{wb}[g/m^2]$
Open loop	6.421e-3	0.325	589.072	1038.556
Particle filter	6.286e-3	0.109	127.846	286.223

The estimation performance of cover layer water storage using a particle filter shows minimal improvement over open-loop results. Both approaches demonstrate a good fit with the synthetic truth. This limited difference is mainly attributed to the buffering effect of the unsaturated soil model, in which different initial conditions converge to similar water storage levels when no additional errors are introduced.

The estimation of releasable water storage in the waste body is improved compared with open-loop results. The uncertainty is reduced with time, and the mean estimation converges to the synthetic truth. The

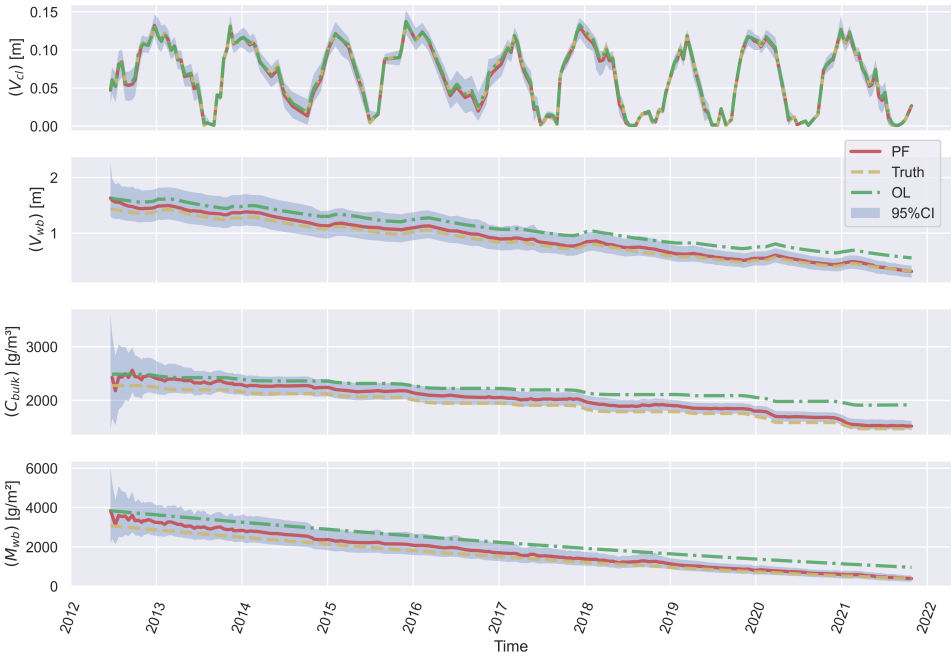

Figure 4.2.: Hidden states estimation in the synthetic experiment. The red line represents the mean estimation of the particle filter. The green and yellow lines represent the mean of open-loop results and the synthetic truth. The light grey areas represent 95% confidence intervals.

estimation of bulk chloride concentration shows a larger improvement, where the incorrect open-loop simulation is dropped, and the particle filter estimation converges to the synthetic truth. As shown in Table 4.2, the decrease in MRMSE value of bulk concentration is also greater than the one in total releasable water storage. We see a larger improvement in bulk concentration estimation because the bulk concentration states strongly correlate with concentration measurements in the outflow. At the start of the simulation, the mean estimations of both waste body water storage and bulk concentration are biased, and it takes some assimilation steps for the mean estimations to converge to the synthetic truths. This is because the model error in the cover layer water storage limits the model errors added to bulk concentration and total releasable water storage in the waste body. It avoids unrealistic perturbation of bulk concentration states but also constrains the capacity to correct the particles while some initial bias in the estimation exists. As the total chloride mass is controlled by the chloride concentration and water storage of the waste body, we also see the decreased MRMSE of M_{wb} in Table 4.2 and the mean estimation converges to the truth in Figure 4.2.

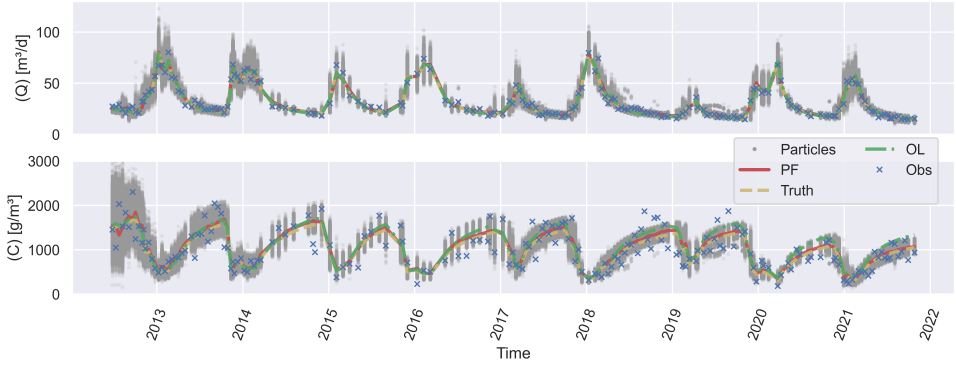

Figure 4.3.: Prediction performance in the synthetic experiment. The red line represents the predicted values of the particle filter. The green and yellow lines represent the mean of open-loop results and the synthetic truth. The grey points represent all the particles.

As shown in Figure 4.3, the predictions of LPR with data assimilation show no significant improvement over the open-loop results. The performance metrics in Table 4.3 indicate a slight decrease in prediction accuracy, although the reduced MRMSE values suggest decreased uncertainty. This is likely because the open-loop simulations already align well with the observations, owing to the MCMC optimization. Additionally, biased estimation during the initial phase of the particle filter may have contributed to the decline in prediction performance. In contrast, the concentration predictions show improved performance

compared to the open-loop predictions. Table 4.3 shows both reduced MRMSE values and increased η values with data assimilation.

Table 4.3.: Prediction performance in synthetic experiment

	Scenario	OL	PF
LPR	$MRMSE[m^3]$	2.935	2.377
	NSE	0.952	0.946
	η	3.043	2.916
C	$MRMSE[g/m^3]$	273.874	94.352
	NSE	0.629	0.673
	η	0.993	1.118

PARAMETERS AND HIDDEN PROCESSES

As shown in Figure 4.4, the mean estimations of most model parameters can converge to the synthetic truth, which indicates good estimation performance. The particle diversity in parameters is well-maintained, which shows the successful application of the MCMC step during resampling. Some parameters like b_{cl} keep high uncertainty after data assimilation, although the mean estimation is improved. It means the information in the observation of these parameters is limited, or there is some correlation between parameters.

Instead of looking into each parameter, we are more interested in the hidden processes in the model controlled by multiple parameters. Figure 4.5 shows the evolution of baseflow with time. The mean estimation of the particle filter aligns well with the synthetic truth, and its uncertainty decreases over time. Figure 4.6 illustrates the percentage of infiltration from the cover layer distributed to mobile cells and bulk, respectively. This reveals the behavior of the travel time distribution in the model. The uncertainties are reduced, and the synthetic truth is within the 95% confidence interval. These results show that we get good estimation results of the hidden processes in the landfill by updating both parameters and states.

4.3.2. REAL CASE STUDY

STATES

As shown in Figure 4.7, the estimation of water storage in the cover layer exhibits behavior similar to the synthetic test, with the mean estimation closely matching the values from open-loop simulations. However, the uncertainty in releasable water storage within the waste body has not significantly decreased compared to its initial status, likely due to large

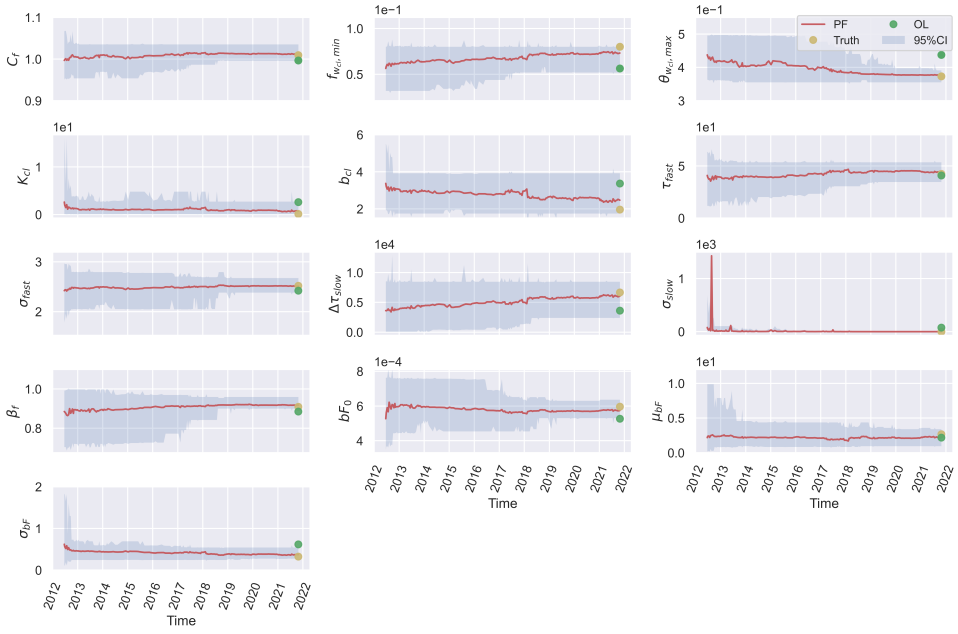

Figure 4.4.: parameter estimation in the synthetic experiment. The red line represents the predicted values of the particle filter. The green and yellow circles represent the mean of open-loop results and synthetic truth. The light grey areas represent 95% confidence intervals.

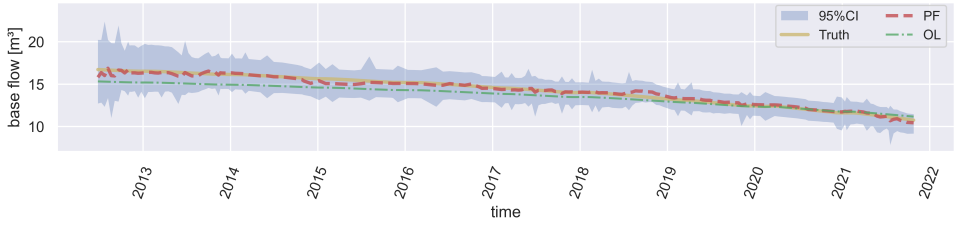

Figure 4.5.: Baseflow estimation in the synthetic experiment. The red line represents the predicted values of the particle filter. The green and yellow lines represent the mean of open-loop results and the synthetic truth. The light grey areas represent 95% confidence intervals.

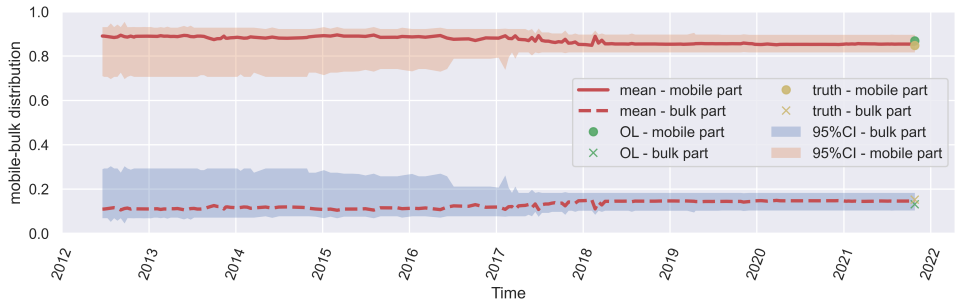

Figure 4.6.: Infiltration distribution estimation in the synthetic experiment. The values indicate the percentage of infiltration water from the cover layer that is distributed to the mobile cells and the bulk of the waste body, respectively. The red lines represent the mean estimations generated by the particle filter. The light orange and blue areas denote the 95% confidence intervals. The yellow circle and cross represent the synthetic truth.

measurement errors. Many initial water storage values in the waste body yield acceptable LPR predictions. The uncertainty in bulk concentration has notably decreased, and the mean estimation shows no significant difference from open-loop results. Similarly, the uncertainty in total releasable chloride mass has been reduced compared to the initial stage, but it remains relatively high due to the substantial uncertainty in water storage estimation.

Since no synthetic truth for hidden states is available in the real case study, we calculate only the performance metrics for predictions. As shown in Table 4.4, the prediction performance of LPR with data assimilation is similar to that of the open-loop predictions, while the concentration predictions show noticeable improvement. Figure 4.8 shows that incorporating data assimilation yields substantially more accurate chloride-concentration forecasts than the open-loop run. As with the synthetic experiment, this is likely because the open-loop simulations already provide accurate predictions for LPR but perform poorly for concentration predictions.

PARAMETERS AND HIDDEN PROCESSES

As shown in Figure 4.9, most parameters exhibit uncertainty ranges similar to their initial distributions, indicating that the current measurements do not significantly reduce these uncertainties. Given that parameter uncertainties were considerably reduced in the synthetic experiment, we believe the remaining uncertainty in the real case study is due to larger measurement errors. Since the parameters are updated based on LPR measurements, this suggests that improving the accuracy of these measurements is necessary to further quantify the uncertainties

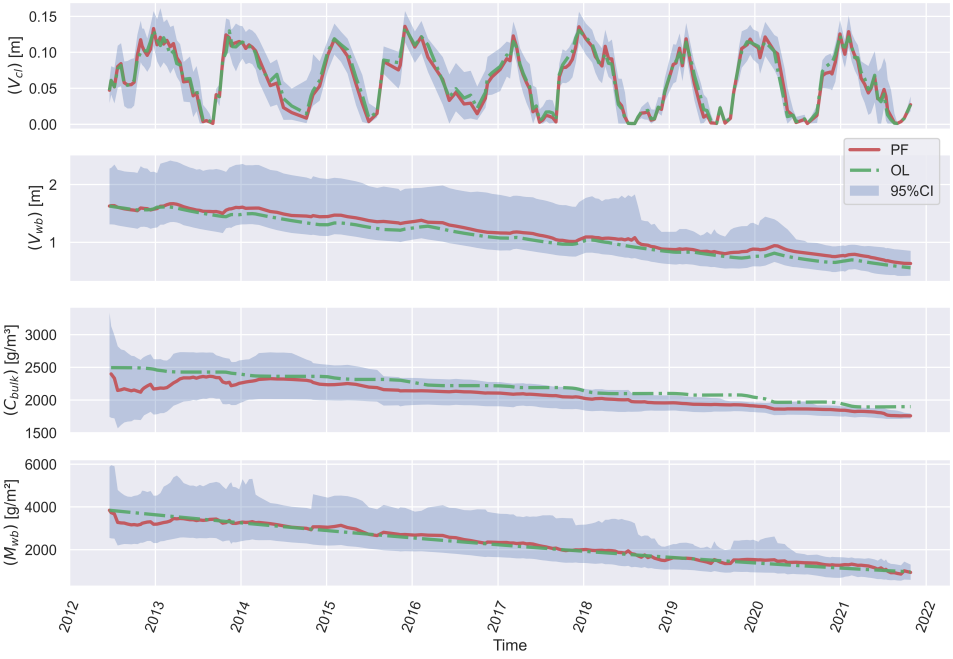

Figure 4.7.: Hidden states estimation in the real case study. The red lines represent the predicted values of the particle filter. The green lines show the behavior of open-loop simulations. The light grey areas represent 95% confidence intervals.

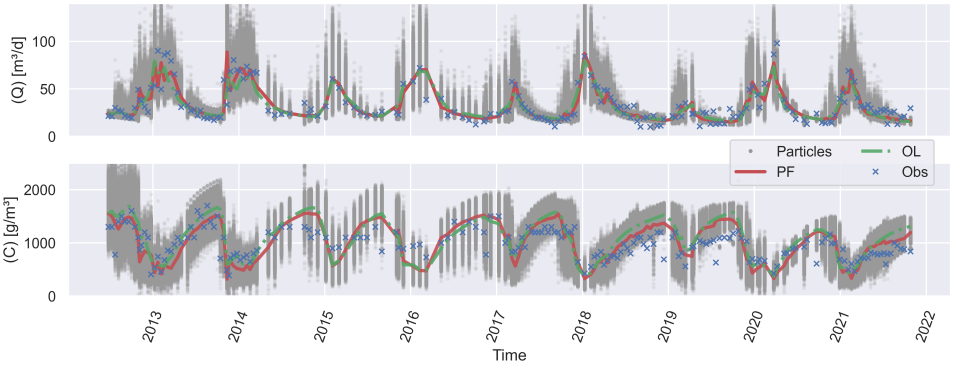

Figure 4.8.: Prediction performance in the real case study. The red line represents the predicted values of the particle filter. The green lines show the behavior of open-loop simulations. The grey points represent all the particles. The blue crosses represent all the measurements.

Table 4.4.: Prediction performance in real case study

	Scenario	OL	PF
LPR	$MRMSE[m^3]$	10.833	9.445
	NSE	0.753	0.714
	η	1.399	1.254
C	$MRMSE[g/m^3]$	361.177	241.729
	NSE	-0.039	0.337
	η	-0.039	0.412

in the model parameters. We observe more fluctuations in parameter estimations in the real case study compared with the synthetic case experiment. It underlines an emerging consensus that time-varying (or "evolving") parameters are often required to compensate for structural errors in long-term landfill models.

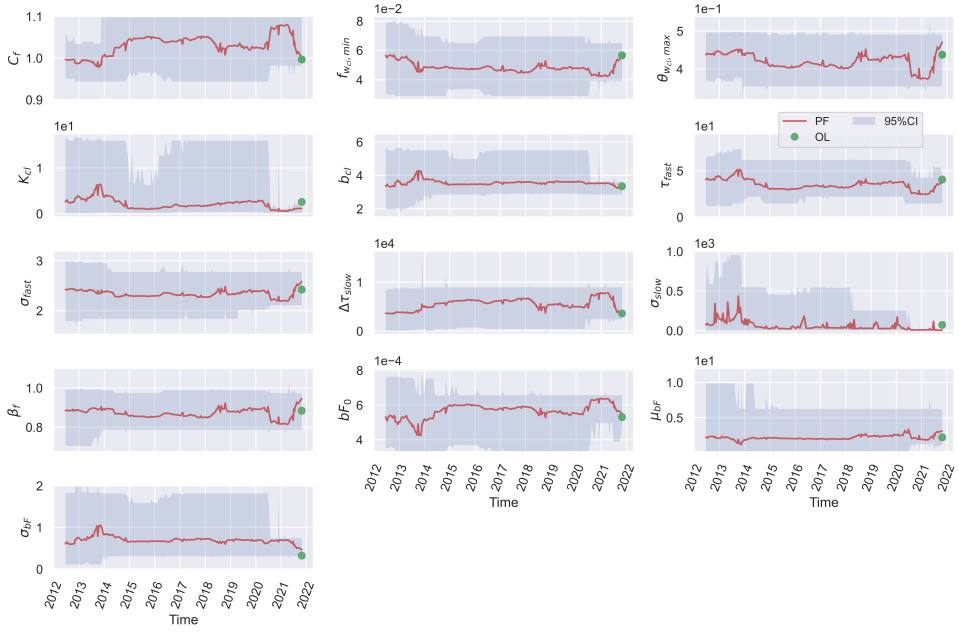

Figure 4.9.: parameter estimation in the real case study. The red line represents the predicted values of the particle filter. The green circles represent the mean of initial parameter distributions in the open-loop scenario. The light grey areas represent 95% confidence intervals.

The estimated behavior of baseflow, illustrated in Figure 4.10, exhibits greater fluctuation compared to the open-loop simulation. This suggests

that the baseflow function in the forward model may be too simplistic to fully capture the system's dynamics. However, the open-loop simulation consistently remains within the estimated 95% confidence interval, indicating that the forward model provides a reasonable average estimate over the entire time period. Based on bulk data, baseflow likely ranges between 10 and 15 m^3/day. Furthermore, a clear and continuous decreasing trend is observed in the baseflow pattern, suggesting a reduced risk of pollution driven by baseflow.

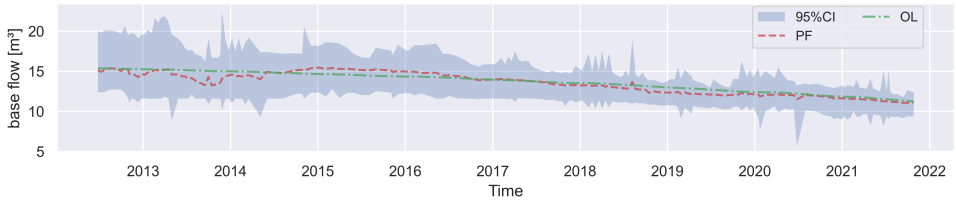

Figure 4.10.: Baseflow estimation in the real case experiment. The red line represents the predicted values of the particle filter. The green line represents the mean of open-loop results. The light grey areas represent 95% confidence intervals.

Figure 4.11 indicates that approximately 90% of water from the cover layer is distributed to the waste body's mobile cells, with around 10% being distributed to the bulk. The uncertainty range in the final stage is significantly narrower than in the prior distributions, primarily due to reduced uncertainty in key parameters of the travel time distribution function. Although there is some fluctuation in the mean estimation, the variation over time is much slower compared to that of baseflow, suggesting that the travel time distribution in the model remains relatively stable over time.

As shown in FIgure 4.12, around 60% of the infiltration from the cover layer goes outside the landfill within 50 days, which lies close to the results from a lab tracer experiment, where between 55 and 70% of the total solute was transported through large pores (Zhang & Yuan, 2019a). It reinforces the view that preferential flow dominates young and mid-aged municipal solid waste bodies, while diffuse pore flow, and thus baseflow, controls pollutant release (Fellner & Brunner, 2010).

4.4. CONCLUSION

This study has introduced and evaluated a PF-MCMC-based weakly coupled data assimilation method to enhance the prediction and estimation of landfill leachate dynamics. Through synthetic and real case experiments, we demonstrated the capability of the proposed

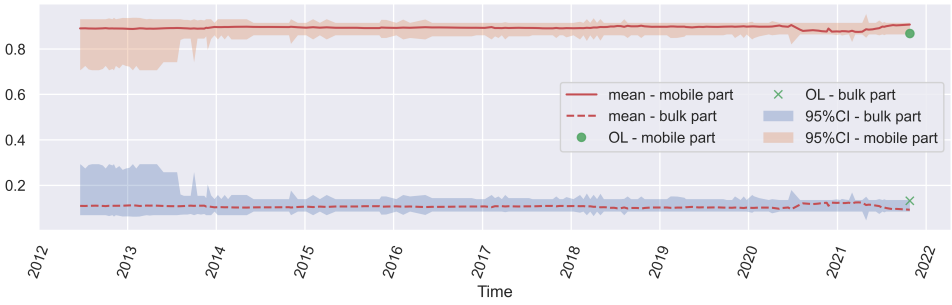

Figure 4.11.: Infiltration distribution estimation in the real experiment. The values indicate the percentage of infiltration water from the cover layer that is distributed to the mobile cells and the bulk of the waste body, respectively. The red lines represent the mean estimations generated by the particle filter. The light orange and blue areas denote the 95% confidence intervals. The green cross and circle represent the open-loop simulation results.

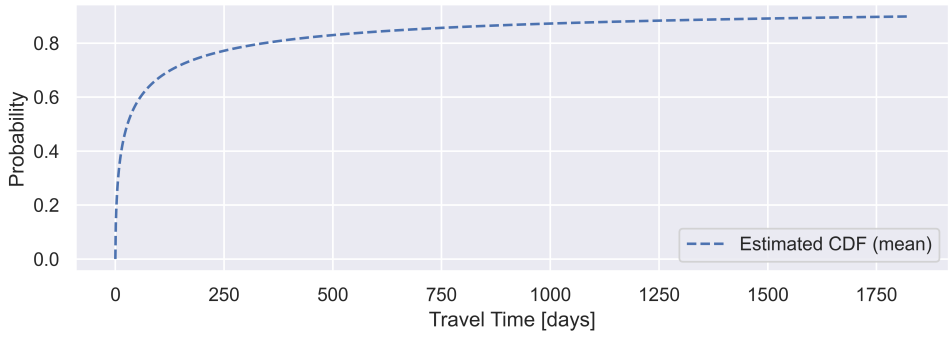

Figure 4.12.: The cumulative distribution of TTD, using the mean estimation of parameters at the last assimilation step in the real case study.

method in uncertainty quantification and gained knowledge about hidden processes in landfills.

Results from the synthetic experiments demonstrated that the PF-MCMC method significantly reduces uncertainty in hidden states, especially in estimating bulk chloride concentrations and solute mass, outperforming open-loop simulations. The method also successfully retrieved the synthetic "truth" for key model parameters and hidden processes such as baseflow and infiltration distribution, illustrating its robustness and reliability under ideal measurement conditions.

In the real case study, the PF-MCMC approach continued to show promising results, particularly in improving concentration predictions and providing plausible ranges for hidden process dynamics, such as baseflow fluctuations and preferential flow behavior. While parameter uncertainties remained relatively wide due to higher measurement errors, the framework demonstrated a unique ability to dynamically adjust parameter estimates over time. This adaptability highlights a key strength of the method: its potential to serve not just as an estimator, but as a diagnostic tool that can identify and correct for conceptual model shortcomings in real time.

Rather than viewing variability in parameter estimates as a weakness, we interpret these fluctuations as valuable information about changes in system behavior or model inadequacy. The PF-MCMC method allows us to monitor and track these changes across time, opening new possibilities for diagnosing and refining conceptual models as more data becomes available. The question that arises is not whether the parameters change, but how robust and meaningful these changes are in relation to the underlying system. This is a central issue that deserves further exploration, both in the present context and more broadly within environmental modeling.

In this light, PF-MCMC emerges not only as a tool for reducing uncertainty but also as a mechanism for enhancing our understanding of complex, dynamic systems. Future work should improve the measurement accuracy and investigate the robustness of temporal parameter changes, explore strategies to extract insights from them, and further develop the framework's potential for adaptive model learning and refinement.

REFERENCES

Abbaszadeh, P., Moradkhani, H., & Daescu, D. N. (2019). The Quest for Model Uncertainty Quantification: A Hybrid Ensemble and Variational Data Assimilation Framework. *Water resources research*, *55*(3), 2407–2431. https://doi.org/10.1029/2018WR023629

Barlaz, M. A., Rooker, A. P., Kjeldsen, P., Gabr, M. A., & Borden, R. C. (2002). Critical Evaluation of Factors Required To Terminate the Postclosure Monitoring Period at Solid Waste Landfills. *Environmental Science & Technology*, *36*(16), 3457–3464. https://doi.org/10.1021/es011245u

De Lannoy, G. J., Houser, P. R., Pauwels, V. R., & Verhoest, N. E. (2006). Assessment of model uncertainty for soil moisture through ensemble verification. *Journal of Geophysical Research: Atmospheres*, *111*(10). https://doi.org/10.1029/2005JD006367

Ercolani, G. (2017). Variational assimilation of streamflow data in distributed flood forecasting. *Water Resources Research*, *53*(1), 158–183. https://doi.org/10.1002/2016WR019208.Received

Eryigit, M. (2021). Estimation of parameters in groundwater modeling by modified Clonalg. *Journal of Hydroinformatics*, *23*(2), 298–306. https://doi.org/10.2166/HYDRO.2021.139

Fatoba, J. O., Eluwole, A. B., Sanuade, O. A., Hammed, O. S., Igboama, W. N., & Amosun, J. O. (2021). Geophysical and geochemical assessments of the environmental impact of Abule-Egba landfill, southwestern Nigeria. *Modeling Earth Systems and Environment*, *7*(2), 695–701. https://doi.org/10.1007/s40808-020-00991-8

Fellner, J., & Brunner, P. H. (2010). Modeling of leachate generation from MSW landfills by a 2-dimensional 2-domain approach. *Waste Management*, *30*(11), 2084–2095. https://doi.org/10.1016/j.wasman.2010.03.020

Gharamti, M. E., Hoteit, I., & Valstar, J. (2013). Dual states estimation of a subsurface flow-transport coupled model using ensemble Kalman filtering. *Advances in water resources*, *60*, 75–88. https://doi.org/10.1016/j.advwatres.2013.07.011

Grugnaletti, M., Pantini, S., Verginelli, I., & Lombardi, F. (2016). An easy-to-use tool for the evaluation of leachate production at landfill sites. *Waste management*, *55*, 204–219. https://doi.org/10.1016/j.wasman.2016.03.030

Gworek, B., Dmuchowski, W., Koda, E., Marecka, M., Baczewska, A. H., Bragoszewska, P., Sieczka, A., & Osiński, P. (2016). Impact of the municipal solid waste lubna landfill on environmental pollution by heavy metals. *Water*, *8*(10), 470. https://doi.org/10.3390/w8100470

Heimovaara, T. J., & Wang, L. (2025). Quantification of Emission Potential of Landfill Waste Bodies Using a Stochastic Leaching Framework. *Water Resources Research*, *61*(3), e2024WR038360. https://doi.org/10.1029/2024WR038360

Kattenberg, W. J., Sloot, H. A. v. d., & Heimovaara, T. J. (2013). *New dutch legislation to allow research of natural biodegradation at landfills* (Vol. 30). CISA Publisher, Italy. http://duurzaamstortbeheer.nl/wp-

content/uploads/2014/06/%20Kattenberg-et-al-Sard2013-652.pdf

KNMI. (2022). Dagwaarden van weerstations. https://www.daggegevens.knmi.nl/klimatologie/daggegevens

Laner, D., Crest, M., Scharff, H., Morris, J. W. F., & Barlaz, M. A. (2012). A review of approaches for the long-term management of municipal solid waste landfills. *Waste Management*, (3). https://doi.org/10.1016/j.wasman.2011.11.010

Liu, Y., Liu, Z., Zhang, S., Jacob, R., Lu, F., Rong, X., & Wu, S. (2014a). Ensemble-based parameter estimation in a coupled general circulation model. *Journal of Climate*, *27*(18), 7151–7162. https://doi.org/10.1175/JCLI-D-13-00406.1

Liu, Y., Liu, Z., Zhang, S., Rong, X., Jacob, R., Wu, S., & Lu, F. (2014b). Ensemble-based parameter estimation in a coupled GCM using the adaptive spatial average method. *Journal of Climate*, *27*(11), 4002–4014. https://doi.org/10.1175/JCLI-D-13-00091.1

Liu, Y., & Gupta, H. V. (2007). Uncertainty in hydrologic modeling: Toward an integrated data assimilation framework. *Water resources research*, *43*(7), 2006WR005756. https://doi.org/10.1029/2006WR005756

Malmström, M. E., Destouni, G., & Martinet, P. (2004). Modeling Expected Solute Concentration in Randomly Heterogeneous Flow Systems with Multicomponent Reactions. *Environmental Science & Technology*, *38*(9), 2673–2679. https://doi.org/10.1021/es030029d

Moradkhani, H., DeChant, C. M., & Sorooshian, S. (2012). Evolution of ensemble data assimilation for uncertainty quantification using the particle filter-markov chain monte carlo method. *Water Resources Research*, *48*(12), 2012WR012144. https://doi.org/10.1029/2012WR012144

Moradkhani, H., Hsu, K. L., Gupta, H., & Sorooshian, S. (2005). Uncertainty assessment of hydrologic model states and parameters: Sequential data assimilation using the particle filter. *Water Resources Research*, *41*(5), 1–17. https://doi.org/10.1029/2004WR003604

Pal, A., Gin, K. Y.-H., Lin, A. Y.-C., & Reinhard, M. (2010). Impacts of emerging organic contaminants on freshwater resources: Review of recent occurrences, sources, fate and effects. *Science of The Total Environment*, *408*(24), 6062–6069. https://doi.org/https://doi.org/10.1016/j.scitotenv.2010.09.026

Plaza Guingla, D. A., De Keyser, R., De Lannoy, G. J., Giustarini, L., Matgen, P., & Pauwels, V. R. (2013). Improving particle filters in rainfall-runoff models: Application of the resample-move step and the ensemble Gaussian particle filter. *Water Resources Research*, *49*(7), 4005–4021. https://doi.org/10.1002/wrcr.20291

Roberts, G. O., & Rosenthal, J. S. (2001). Optimal scaling for various Metropolis-Hastings algorithms. *Statistical Science*, *16*(4), 351–367. https://doi.org/10.1214/ss/1015346320

Rosqvist, H., & Destouni, G. (2000). Solute transport through preferential pathways in municipal solid waste. *Journal of Contaminant Hydrology*, *46*(1), 39–60. https://doi.org/10.1016/S0169-7722(00)00127-3

Stichting Duurzaam Storten. (2017). Biodegradation research programme on dutch landfills. https://duurzaamstortbeheer.nl/english-page/

Tran, V. N., Dwelle, M. C., Sargsyan, K., Ivanov, V. Y., & Kim, J. (2020). A Novel Modeling Framework for Computationally Efficient and Accurate Real-Time Ensemble Flood Forecasting With Uncertainty Quantification. *Water Resources Research*, *56*(3), 1–31. https://doi.org/10.1029/2019WR025727

van Leeuwen, P. J., Künsch, H. R., Nerger, L., Potthast, R., & Reich, S. (2019). Particle filters for high-dimensional geoscience applications: A review. *Quarterly Journal of the Royal Meteorological Society*, (April), 2335–2365. https://doi.org/10.1002/qj.3551

Vrugt, J. A. (2016). Markov chain Monte Carlo simulation using the DREAM software package: Theory, concepts, and MATLAB implementation. *Environmental Modelling & Software*, *75*, 273–316. https://doi.org/10.1016/j.envsoft.2015.08.013

Vrugt, J. A., ter Braak, C. J. F., Diks, C. G. H., & Schoups, G. (2013). Hydrologic data assimilation using particle Markov chain Monte Carlo simulation: Theory, concepts and applications. *Advances in Water Resources*, *51*, 457–478. https://doi.org/10.1016/j.advwatres.2012.04.002

Wang, L., & Heimovaara, T. J. (2025a). Quantifying landfill emission potential using a weakly coupled particle filter. *Water Resources Research*, *61*(2), e2023WR036549. https://doi.org/10.1029/2023WR036549

Wang, L., & Heimovaara, T. J. (2025b). *Understanding hidden processes in landfill emission by applying PF-MCMC in coupled travel time distribution model* [Under review].

Wikle, C. K., & Berliner, L. M. (2007). A Bayesian tutorial for data assimilation. *Physica D: Nonlinear Phenomena*, *230*(1-2), 1–16. https://doi.org/10.1016/j.physd.2006.09.017

Yan, H., DeChant, C. M., & Moradkhani, H. (2015). Improving soil moisture profile prediction with the particle filter-Markov chain Monte Carlo method. *IEEE Transactions on Geoscience and Remote Sensing*, *53*(11), 6134–6147. https://doi.org/10.1109/TGRS.2015.2432067

Yan, H., & Moradkhani, H. (2016). Combined assimilation of streamflow and satellite soil moisture with the particle filter and geostatistical

modeling. *Advances in Water Resources*, *94*, 364–378. https://doi.org/10.1016/j.advwatres.2016.06.002

Zhang, H., Hendricks Franssen, H.-J., Han, X., Vrugt, J. A., & Vereecken, H. (2017). State and parameter estimation of two land surface models using the ensemble Kalman filter and the particle filter. *Hydrology and Earth System Sciences*, *21*(9), 4927–4958. https://doi.org/10.5194/hess-21-4927-2017

Zhang, W., & Yuan, S. (2019a). Characterizing preferential flow in landfilled municipal solid waste. *Waste Management*, *84*, 20–28. https://doi.org/10.1016/j.wasman.2018.11.023

Zhang, W.-j., & Yuan, S.-s. (2019b). Characterizing preferential flow in landfilled municipal solid waste. *Waste Management*, *84*, 20–28. https://doi.org/https://doi.org/10.1016/j.wasman.2018.11.023

Zhang, Z., Pan, X., Fang, Y., Wang, Y., Zhang, Y., & Xu, H. (2020). Laboratory study on the hydraulic characteristics of mechanically and biologically treated waste in China. *Waste Management*, *102*, 686–697. https://doi.org/10.1016/j.wasman.2019.11.026

5

QUANTIFYING WATER CONTENT OF A LANDFILL WITH ERT DATA BY BAYESIAN EVIDENTIAL LEARNING

Accurate water-content estimates in landfills are essential for leachate management, but conventional ERT inversions are ill-posed and uncertain. We present a Bayesian Evidential Learning (BEL) approach that links ERT measurements directly to total water storage (TWS) without explicit inversion. A semi-parametric forward model stochastically samples key parameters (e.g., water-retention and Archie's law coefficients) to generate paired ERT signals and TWS. After validating synthetic data via PCA and one-class SVM falsification, we train a Bayesian Neural Network with Monte Carlo dropout on dimension-reduced ERT features. The BEL framework accurately predicts mid-range TWS with quantified uncertainty but underestimates high-TWS scenarios due to parameter variability. Fixing parameters to deterministic means restores high-end accuracy, demonstrating the critical need to constrain hydro-geophysical parameters. This method provides a robust alternative for landfill moisture monitoring and highlights areas for targeted parameter calibration.

Parts of this chapter appear in Wang and Heimovaara (2025b)

5.1. INTRODUCTION

Modern sanitary engineered landfills are an increasingly important component of waste management strategies in Europe, offering enhanced waste stabilization and energy recovery. However, their effective design, operation, and long-term aftercare are essential to minimize environmental pollution, particularly the risk of groundwater contamination. A critical aspect of landfill management is the prediction of leachate transport within the waste body, which depends heavily on accurately estimating water storage capacity. Water storage influences both leachate generation and contaminant transport, making it a key factor in environmental risk assessment. To address this, researchers have developed a range of numerical models that simulate moisture flow and solute transport in landfill environments (Hu *et al.*, 2020; Li *et al.*, 2021; Lu *et al.*, 2019, 2021). Among these models, dynamic water storage within the waste matrix has emerged as a key parameter for evaluating environmental risks and optimizing waste treatment efficiency.

In previous work, we employed a Travel-Time-Distribution (TTD) model combined with data assimilation techniques to estimate water storage within the landfill (Heimovaara & Wang, 2025; Wang & Heimovaara, 2025a). By conceptualizing water storage as a zero-dimensional state—representing bulk storage without accounting for spatial variability—we avoided the complexities associated with spatially distributed modeling. However, this approach relied exclusively on indirect observations of leachate outflow, making the accuracy of the storage estimates highly dependent on the model's structural assumptions and parameterization. To reduce uncertainty and enhance the robustness of these estimates, we integrate independent, direct measurements of water storage into the modeling framework.

Hydrogeophysical methods have become essential tools for characterizing subsurface hydraulic properties in complex environments such as landfills. Among these, Electrical Resistivity Tomography (ERT) is particularly valuable due to its capacity to infer water content by measuring subsurface electrical resistivity, which correlates with water saturation through Archie's Law. ERT has been widely applied in landfill settings to detect moisture content and monitor the spatial distribution of leachate and gas (Feng *et al.*, 2017; Hu *et al.*, 2019; Neyamadpour, 2019). For instance, Zhan *et al.* (2019) demonstrated the use of ERT to delineate leachate distribution within a controlled landfill cell, while Hu *et al.* (2019) successfully applied time-lapse ERT surveys to monitor landfill dewatering. These studies highlight ERT's potential as a non-invasive, spatially resolved method for tracking hydrological processes within waste bodies.

Another approach involves hydrogeophysical joint inversion, in which water content and related parameters (such as saturation and

petrophysical properties) are estimated directly from ERT measurement data, bypassing the explicit inversion of electrical resistivity (Linde & Doetsch, 2016). This method integrates ERT data into a coupled hydrogeophysical model, employing petrophysical relationships such as Archie's Law to link resistivity to moisture content. By circumventing the traditional resistivity inversion step, joint inversion can reduce uncertainty arising from inversion artifacts and enhance the accuracy of water content estimates. However, its application in landfill settings remains challenging, as it often relies on assumptions, such as a well-defined water table, which rarely holds in the heterogeneous conditions typical of waste bodies.

Since our objective is to estimate the total water storage within the waste body—rather than its spatial distribution—bypassing the ill-posed inversion process allows for a more direct and robust estimation. To achieve this, we introduce a novel approach based on the Bayesian Evidential Learning (BEL) framework (Scheidt *et al.*, 2018), which estimates landfill water storage from ERT measurements without performing conventional inversion. BEL employs a forward model to generate prior samples of both the target variable (water storage) and the observable variable (ERT signals), enabling the statistical learning of their relationship (Thibaut *et al.*, 2021). Unlike traditional inversion techniques, BEL avoids the challenges associated with ill-posedness and regularization artifacts by focusing on learning from ensembles of model realizations. The BEL framework has demonstrated effectiveness across various applications, including seismic data interpretation (Pradhan & Mukerji, 2020), geophysical parameter estimation (Hermans *et al.*, 2019), and experimental design optimization (Thibaut *et al.*, 2021).

In this study, we adapt the Bayesian Evidential Learning (BEL) framework for landfill water storage estimation by developing a semi-parametric forward model that simulates ERT signals as a function of water storage. We then apply a neural network to learn a direct statistical relationship between the simulated ERT measurements and total water storage, effectively bypassing the traditional inversion process. This approach offers a robust alternative for estimating water storage, reducing uncertainties associated with model structural assumptions, ill-posed inversion artifacts, and measurement noise.

5.2. METHODS

5.2.1. BAYESIAN EVIDENTIAL LEARNING

The general objective of data-driven estimation is to obtain the posterior distribution of the target property $p(\mathbf{h}|\mathbf{d_{obs}})$, where $\mathbf{h}$ represents the target variable (e.g., water content) and $\mathbf{d_{obs}}$ represents the available observations (e.g., ERT data). In traditional model-driven approaches, the measured data $\mathbf{d_{obs}}$ are used to optimize the model parameters

m, which include empirical coefficients and subsurface properties used in the forward model. Once the model is optimized, it predicts the target variable **h**. In the context of ERT data analysis, this process involves using $\mathbf{d_{obs}}$ to estimate a resistivity map **m** of the subsurface. A key limitation of this approach is the dimensionality mismatch: the number of unknown model parameters n_m is typically much larger than the number of available observations n_d, making the inversion process ill-posed and prone to uncertainty.

The BEL framework reorganizes this relationship differently by avoiding direct optimization of model parameters. Instead, prior distributions of the model parameters **m** are first defined based on available knowledge. The target variable **h** is computed using a forward model $\mathbf{h} = f_1(\mathbf{m})$, while the observable variable **d** is generated using another forward model $\mathbf{d} = f_2(\mathbf{m})$. This approach enables BEL to learn a direct statistical relationship between the observations **d** and the target variable **h** without explicitly solving an inverse problem, thereby bypassing the need for resistivity inversion.

The conceptual differences between the traditional method and the BEL framework are illustrated in Figure 5.1. Figure 5.2 provides an

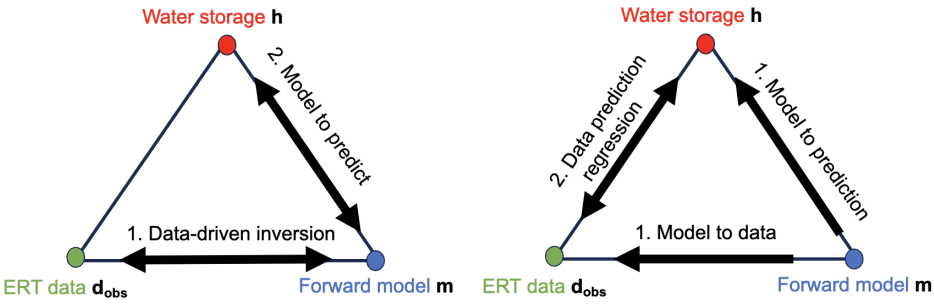

Figure 5.1.: Two paradigms for posterior estimation. The figure is slightly adjusted based on Scheidt *et al.* (2018)

.

overview of the BEL method as applied in this study, including the generation of prior samples, forward modeling of both observable and target variables, and the statistical learning process. In the following sections, we describe these components in detail.

5.2.2. FORWARD MODEL

Forward models are essential in the BEL framework for simulating both ERT data and water storage. Given the high spatial heterogeneity of moisture distribution in landfills, we approximate the three-dimensional waste body with a two-dimensional moisture map. This simplification

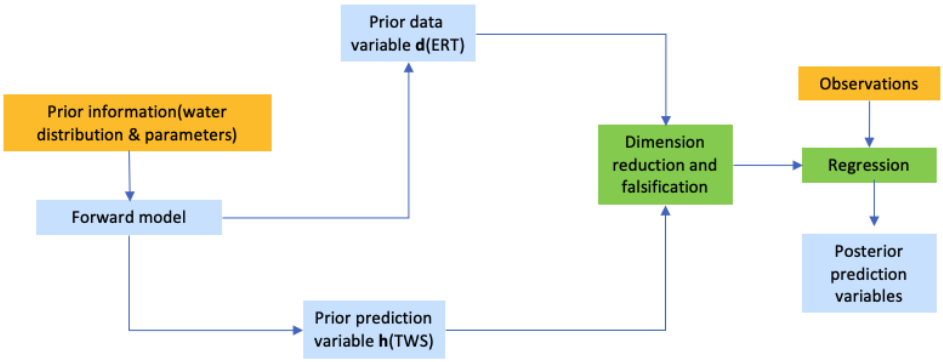

Figure 5.2.: Diagram for BEL method in this study

enables the use of a 2D mesh composed of rectangular grid cells. To further reduce model complexity, we assume hydrostatic conditions within the waste body. Under this assumption, the volumetric water content can be determined if the positions of saturated zones are known. The volumetric water content in the landfill cover layer is represented by the variable θ_{cl}.

To simulate the presence of saturation within the waste body, we developed a stochastic procedure that randomly assigns saturated cells within the 2D mesh. Each cell is treated as a binary variable—either saturated or unsaturated. The generation process begins by sampling a fraction value k, which defines the proportion of saturated cells relative to the total number of cells. This value is drawn from a uniform distribution, $k \sim U(0.01, 0.7)$, with bounds selected based on the minimum and maximum water level measurements observed in the field.

Once the saturated cells are defined, the volumetric water content θ for each grid cell is calculated on a column-wise basis using the water retention curve described by Eqs. (5.1) and (5.2).

$$S_{\text{eff}} = \begin{cases} 1 & \text{if } h_w \geq 0 \\ (1 + (\alpha |h_w|)^n)^{-m} & \text{if } h_w < 0 \end{cases} \tag{5.1}$$

where S_{eff} is the effective saturation, h_w is the pressure head, α is the inverse of the air entry suction (units: L^{-1}), θ_r is the residual water content, θ_s is the saturated water content, θ is the volumetric water content, and n and $m = 1 - 1/n$ are empirical water retention parameters.

The volumetric water content θ is computed as:

$$\theta = \theta_r + S_{\text{eff}}(\theta_s - \theta_r) \tag{5.2}$$

In cases where a column contains no saturated cells, we assume the water table is just below the column due to the presence of a drainage layer. When multiple saturated cells occur in a column, each disconnected saturated region is treated as a localized bottom boundary condition for the unsaturated cells positioned above it. This approach enables a more realistic representation of heterogeneous saturation patterns within the landfill. Figure 5.3 shows an example of a generated water distribution map.

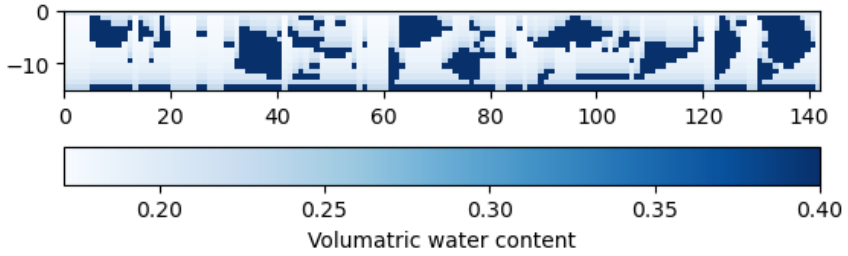

Figure 5.3.: An example of randomly generated volumetric water content distribution map

The total water storage is computed by summing the volumetric water content across all grid cells within the waste body. Because the top cover layer is composed of soil, a separate set of Archie's Law parameters is used to account for its distinct hydrogeophysical properties. The height of the cover layer is set equal to the height of the first layer in the computational mesh. As a simplification, the water retention curve is not applied within the cover layer. Instead, each cell in this layer is assigned a uniform volumetric water content, denoted as θ_{cl}. During the sample generation process, θ_{cl} is randomly sampled from a uniform distribution, with its lower and upper bounds derived from the cover layer saturation estimates $\mathbf{v_{cl}}$ presented in Heimovaara and Wang (2025). Because ERT measurements are most sensitive to resistivity changes near the surface, our choice of a spatially constant θ_{cl} effectively treats the entire cover as a single "effective soil" whose moisture state controls the shallow resistivity response. Sampling θ_{cl} from a narrow prior (based on model estimation obtained from Heimovaara and Wang (2025)) ensures that the cover-layer sensitivity is realistic, so that the BEL model can focus on learning the deeper relationship between resistivity and water storage in the waste body. At this stage, the forward model $f_1(\cdot)$ for computing total water storage is fully defined.

Following the water storage calculation, the electrical resistivity of each cell is determined using Archie's Law, as described in Eq. 5.3.

$$\rho = a_{arc}\rho_w\phi^{-m_{arc}}S_{eff}^{-n_{arc}} \tag{5.3}$$

where ρ is bulk resistivity of the waste, a_{arc} is tortuosity factor, ρ_w is resistivity of the leachate, ϕ is porosity, m_{arc} is cementation exponent, S_{eff} is water saturation, n_{arc} is saturation exponent. Subsequently, the observable ERT signal is simulated using a numerical simulator implemented in PyGIMLi (Rücker *et al.*, 2017). This process defines our model to data $f_2(\cdot)$. Figure 5.4 shows an example of the generated resistivity map using the forward model.

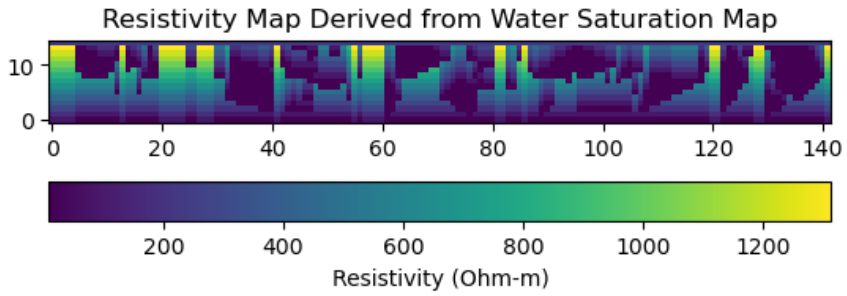

Figure 5.4.: One example of randomly generated resistivity distribution map

5.2.3. PRIORS AND PRIOR FALSIFICATION

The BEL framework aims to directly learn the relationship between observations and target variables by performing statistical regression between $\mathbf{h}$ (e.g., water storage) and $\mathbf{d}_{\text{obs}}$ (e.g., ERT measurements). Training such a model requires a sufficiently large dataset of paired samples $(\mathbf{h}, \mathbf{d}_{\text{obs}})$.

In most real-world applications, however, only a single set of observations $\mathbf{d}_{\text{obs}}$ is available, and the corresponding target variable $\mathbf{h}$ is either unknown or cannot be measured directly. This lack of labeled data renders direct regression based solely on field data impractical. To overcome this, we generate synthetic training samples using the forward models $f_1(\cdot)$ and $f_2(\cdot)$, enabling the construction of a representative statistical relationship between observations and the target variable.

In the standard BEL approach, training samples are generated by running forward simulations $f_1(\mathbf{m})$ and $f_2(\mathbf{m})$ using prior distributions of model parameters $\mathbf{m}$. These prior distributions are typically informed by laboratory and field studies reported in previous research (Saneiyan *et al.*, 2024; Zeng *et al.*, 2017; Zhang *et al.*, 2021).

A key innovation of this study lies in the way moisture distributions within the waste body are generated. Rather than relying on explicit parametric models with fixed equations, we employ a stochastic sampling algorithm to produce diverse training samples. Hyperparameters—such as the fraction of saturated zones—are drawn from

defined probability distributions. Due to the inherent randomness of the sampling process, different spatial saturation patterns can be generated even when hyperparameters remain constant. This non-deterministic approach extends the BEL framework to more complex systems where system states cannot be described by closed-form relationships.

Building a statistical regression model from a limited training set requires caution, as there is no guarantee that the resulting predictions will be statistically or physically feasible. In Bayesian frameworks, the posterior distribution must lie within the support of the prior (Hou & Rubin, 2005; Scheidt *et al.*, 2018). In other words, if the observed data fall outside the range covered by the prior, the prior is considered falsified. While ad-hoc adjustments can be made to broaden the prior distribution, such modifications may result in inaccurate or misleading posterior estimates.

To ensure the validity of regression results, it is essential to verify that the observed measurement data are consistent with the assumed priors and the outputs of the forward models. If inconsistencies are detected, the priors must be revised to more accurately reflect the plausible range of system states.

This verification step, known as *falsification*, is performed in BEL before any regression or prediction step (Hermans *et al.*, 2018; Michel *et al.*, 2020; Pradhan & Mukerji, 2020; Thibaut *et al.*, 2021). It involves comparing the predicted data $\mathbf{d}$, generated via forward modeling, with the observed data $\mathbf{d}_{\text{obs}}$. In low-dimensional cases, this comparison can often be made visually. However, due to the high dimensionality of the ERT data in this study, we first apply a dimensionality reduction technique. The resulting lower-dimensional representation is then used in a classification-based falsification method to assess whether the observed data are statistically consistent with the prior samples. The dimension reduction method is detailed in the following section.

Assuming that all generated samples of $\mathbf{d}$ are drawn from a common underlying distribution, the observed measurement $\mathbf{d}_{\text{obs}}$ is expected to belong to the same distribution. If it is classified as an outlier, the prior is considered falsified. We perform this classification using a one-class Support Vector Machine (SVM) (Bounsiar & Madden, 2014). The parameter $\nu = 0.05$ is chosen to allow up to 5% of synthetic samples to be treated as potential outliers, forming a robust boundary around the dominant structure of the prior distribution.

The prior distributions of the model parameters are iteratively adjusted until the observed measurements are identified as inliers. This ensures that the prior adequately spans the region of observation space where plausible system states exist.

5.2.4. DIMENSION REDUCTION

Regression models are most effective when the number of training samples significantly exceeds the number of unknown parameters. In the context of Bayesian Evidential Learning (BEL), a dimension reduction step is commonly introduced to mitigate the challenges associated with high-dimensional regression. This approach assumes that the high-dimensional observational data or model predictions reflect a set of underlying low-dimensional features that cannot be directly measured.

In this study, where the ERT data are high-dimensional, we apply dimension reduction prior to regression to enhance model efficiency and generalization. We employ Principal Component Analysis (PCA) to extract key features—referred to as principal components—from the dataset by identifying the directions of greatest variance. These components are ordered according to the amount of variance they explain, and the leading components are retained to capture the dominant structure of the data. For instance, in our application, the first 10 principal components explain approximately 98% of the total variance in the dataset. A comprehensive explanation of PCA can be found in Jolliffe and Cadima (2016).

5.2.5. REGRESSION WITH A NEURAL NETWORK

After performing dimension reduction and falsification, we can model the statistical relationship between the dimension-reduced target variable $\mathbf{h}^*$ and the observed data $\mathbf{d}^*$. Since dimension reduction was not performed on the target variable in our case, $\mathbf{h}^*$ is equivalent to $\mathbf{h}$. We used a deep learning method, specifically a Bayesian Neural Network (BNN) with Monte Carlo Dropout, to model this relationship and estimate prediction uncertainty.

BNN is a widely used deep learning method suitable for nonlinear regression problems (Jospin *et al.*, 2022). It is a type of neural network where the weights and biases are probability distributions instead of fixed values. This allows the model to quantify uncertainty in its predictions. We refer readers to (Jospin *et al.*, 2022) for a detailed explanation of the theory. Since it is a well-developed method, we will only describe the model implementation and hyperparameters in the following part.

The input data consists of Dipole-Dipole (DD) and Schlumberger (SLM) apparent resistivity values, which undergo preprocessing via standard scaling and Principal Component Analysis (PCA), retaining 95% of variance for dimensionality reduction. The dataset is split into training (70%), validation (15%), and test (15%) sets.

The network adopts a “last-layer only” Bayesian approach in which the first three layers are deterministic, while the final output layer is modeled probabilistically to capture predictive uncertainty. Only the

final layer is implemented as a Bayesian linear layer with a prior mean of zero and a prior standard deviation of 0.25. This design choice significantly reduces the computational overhead associated with fully Bayesian networks while still enabling uncertainty quantification in the predictions. In detail, the architecture comprises an input layer that receives features transformed by PCA (retaining 98% of the variance), followed by three fully connected layers with 128, 64, and 32 neurons, respectively. Each of these layers is equipped with Batch Normalization and dropout (with rates of 0.05, 0.03, and 0.02, respectively) to ensure robust feature learning and regularization.

The network is trained using a composite loss function that combines the mean squared error (MSE) between predicted and observed total water storage values with a Kullback–Leibler (KL) divergence penalty that regularizes the Bayesian parameters. A KL weight of 1×10^{-5} is used to balance the trade-off between model fit and uncertainty quantification. The total number of generated samples is 5000, and the batch size to train the model is 128. Training is conducted using the Adam optimizer with a learning rate of 3×10^{-5} and a weight decay of 1×10^{-6}, along with a Cosine Annealing learning rate scheduler over 3000 epochs.

For uncertainty estimation, we perform Monte Carlo sampling with 1000 stochastic forward passes during inference, thereby obtaining an empirical predictive distribution. The mean and standard deviation computed from these samples are then used to construct uncertainty intervals for the predicted total water storage. This “last-layer only” Bayesian framework thus provides robust point estimates alongside meaningful uncertainty quantification, which is critical for risk-informed decision-making in geophysical applications. The final results are visualized with confidence intervals to illustrate uncertainty-aware predictions. These hyperparameters are tuned by trial-and-error tests.

5.3. RESULTS

5.3.1. FALSIFICATION

The final selected prior ranges for all model parameters are presented in Table 5.1. Figure 5.5 presents the boxplot of the first five principal components (PCs) derived from the training data, along with the observed test samples overlaid as distinct markers. The boxplots represent the interquartile range (IQR, 25th–75th percentile) of the training data, with whiskers extending to the 5th and 95th percentiles. Black dots beyond the whiskers indicate outliers within the training distribution.

The test samples exhibit strong alignment with the training data distribution. Specifically, all four real samples fall within or very close to the IQR across all principal components, suggesting that their statistical

properties are consistent with the training set. No test sample appears in the extreme outlier region beyond the whiskers, reinforcing the observation that the measured resistivity values are well captured by the simulated dataset. Furthermore, the real samples cluster around the median, indicating that their distributional characteristics are within the expected variability of the training data.

To quantitatively evaluate the similarity between field observations and synthetic simulations, we computed decision function scores from the trained one-class SVM model. The decision function returns the signed distance of each test sample to the learned decision boundary that encloses the distribution of the synthetic data in the PCA-reduced feature space. Positive values indicate that a sample lies inside the learned boundary (classified as an inlier), while negative values suggest an outlier. In our case, all four test samples yielded positive scores: 0.4832, 0.4843, 0.4687, and 0.4735, respectively. These consistently high values indicate that each observed resistivity profile is well within the range of variability represented by the synthetic training data. This strongly supports the validity of the underlying physical model used to generate the synthetic data, as it captures the essential features of the observed resistivity response in the field.

Table 5.1.: Prior distributions of model parameters used in the simulation.

Parameter (Description)	**Range / Distribution**
Global parameters (common layers)	
ϕ (Porosity)	U[0.3, 0.5]
ρ_w (Pore-water resistivity)	U[1, 3]
a_{arc} (Tortuosity factor)	U[0.5, 1.0]
m_{arc} (Cementation exponent)	U[1.6, 2.0]
n_{arc} (Saturation exponent)	$\mathcal{N}(2.0,\ 10\%)$
θ_r (Residual water content)	U[0.15, 0.25]
θ_s (Saturated water content)	Same as ϕ
α (VG inverse air-entry suction)	U[5.0, 10.0]
n (VG pore-size index)	U[1.2, 1.8]
Soil-specific overrides (cover layer only)	
a_{soil} (Soil tortuosity)	U[0.5, 1.5]
m_{soil} (Soil cementation)	U[1.5, 2.5]
n_{soil} (Soil saturation exponent)	U[1.0, 2.0]
$\rho_{w,\text{soil}}$ (Soil water resistivity)	U[5, 15]
$\theta_{s,\text{soil}}$ (Saturated content)	$\mathcal{N}(0.3437,\ 5\%)$
$\theta_{r,\text{soil}}$ (Residual content)	$\mathcal{N}(0.02472 \times \theta_{s,\text{soil}},\ 5\%)$

Note: All random draws are assumed independent. U[a,b] denotes a uniform distribution on $[a, b]$, and $\mathcal{N}$ is a normal distribution with mean μ and standard deviation σ. In rows with $\mathcal{N}(\mu, \text{percentage})$, the second argument indicates $\sigma = (\text{percentage}) \times \mu$.

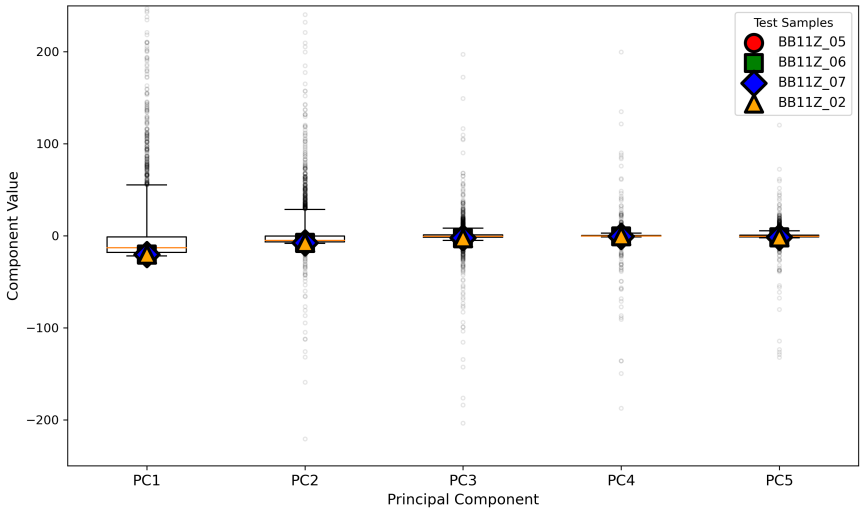

Figure 5.5.: Boxplot of principal components (PC1–PC5) from the training data, with test samples overlaid as distinct markers. The boxes represent the interquartile range (IQR), from the 25th percentile (Q1) to the 75th percentile (Q3). The horizontal line inside each box denotes the median (50th percentile). The whiskers extend to 1.5 times the IQR from Q1 and Q3, respectively, capturing the bulk of the data. Outliers beyond this range are shown as individual points. The four test samples represent real datasets from cell 11Z of Braambergen Landfill measured in different months. The alignment of test samples with the IQR suggests that no significant falsification is detected.

5.3.2. REGRESSION AND PREDICTION

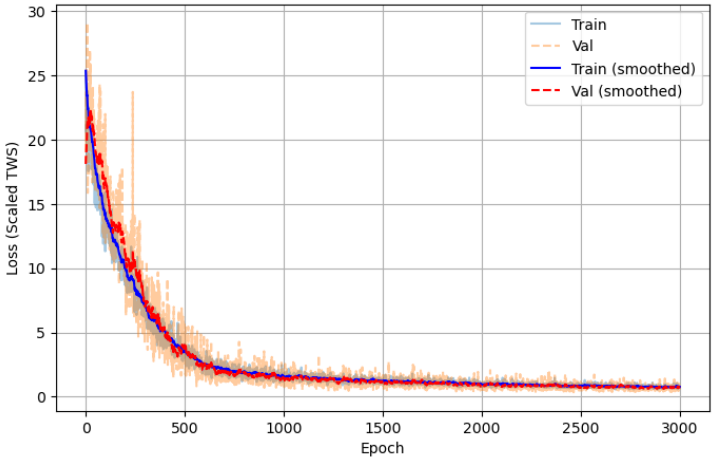

Figure 5.6.: Training and validation loss over 3000 epochs using a Bayesian neural network (BNN). Solid lines show smoothed loss curves, while faded lines show raw epoch-wise losses.

Figure 5.6 shows the evolution of training and validation losses over 3000 epochs for the Bayesian Neural Network (BNN). The loss function combines a mean squared error (MSE) term with a Kullback–Leibler (KL) divergence term, the latter applied only to the final Bayesian layer. Smoothed curves (solid lines) illustrate overall trends, while the faded lines depict raw epoch-wise losses. The steady decrease and convergence of both losses suggest effective learning without significant overfitting.

Figure 5.7 demonstrates the BNN's performance on unseen test samples by comparing its predictive distribution to the sorted ground-truth TWS values. Overall, most of the true TWS values lie within the estimated 95% confidence intervals, indicating that the BNN can capture prediction uncertainties to a reasonable degree. However, the model consistently underestimates TWS in the higher range (e.g., values above 5), suggesting that the network has learned a relatively conservative bias and struggles to extrapolate to these extremes.

Several factors may contribute to this limitation. First, the training dataset contains fewer samples at the upper end of the total water storage (TWS) range. As a result, the Bayesian Neural Network (BNN) learns a distribution that is narrower and biased toward mid-range values. Second, the mesh cells exhibit varying sensitivity to changes in resistivity signals. Some regions may be poorly constrained or even undetectable, given the available ERT data. Third, variations in water retention characteristics and Archie's law parameters can cause similar

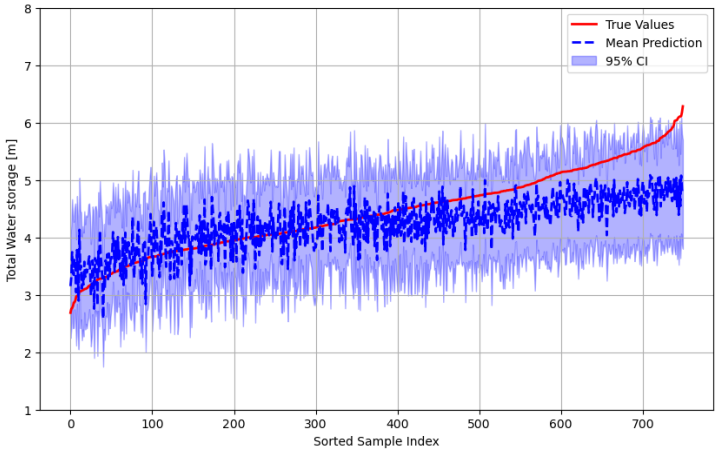

Figure 5.7.: Bayesian neural network predictions with uncertainty on the test dataset. The red curve shows the ground truth total water storage (TWS), sorted in ascending order. The dashed blue line represents the mean prediction from 1000 Monte Carlo samples, and the shaded area shows the predictive uncertainty (95% confidence interval).

resistivity signals to emerge from fundamentally different TWS values during forward simulations.

To isolate the impact of each factor, we conducted a series of targeted experiments. To address the data imbalance, we manually selected samples across a broader range of TWS values to approximate a uniform distribution. For the spatial sensitivity issue, we computed the Jacobian matrix for each cell to quantify its sensitivity, then removed cells with very low sensitivity from the mesh. Both methods are implemented in the provided script. However, preliminary results showed that these adjustments had little effect on prediction accuracy, suggesting that these factors are not the primary sources of the observed underestimation.

Our final experiment focused on parameter variability. We fixed all parameters in Archie's law and the water retention curve to their respective mean values, making them deterministic rather than sampled. The model's resulting performance is shown in Figure 5.8.

Figure 5.8 shows that when trained with deterministic parameters, the BNN more accurately captures high TWS values. With fixed parameters, the relationship between resistivity and TWS becomes more consistent, allowing the model to distinguish truly high TWS scenarios from moderate ones. This reduces the ambiguity seen in the stochastic case, where different parameter realizations can lead to similar resistivity responses.

Together, Figures 5.7 and 5.8 demonstrate the importance of

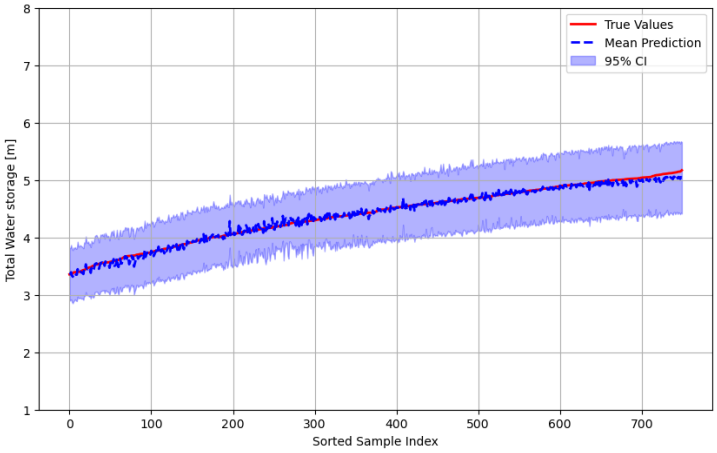

Figure 5.8.: Bayesian neural network predictions with deterministic parameter set. The red curve shows the ground truth total water storage (TWS), sorted in ascending order. The dashed blue line represents the mean prediction from 1000 Monte Carlo samples, and the shaded area shows the predictive uncertainty (95% confidence interval).

parameter variability in shaping model performance. These results highlight the need for better constraints on key subsurface parameters. Additional data collection, particularly aimed at narrowing the plausible range of water retention and Archie's law parameters, would likely reduce predictive uncertainty and improve performance in high-TWS regimes.

Parameter non-uniqueness is a well-recognized limitation in hydrogeophysics, particularly in the interpretation of petrophysical relationships that link electrical resistivity to hydrological state variables (Linde & Doetsch, 2016). This ambiguity arises because multiple combinations of subsurface properties (e.g., porosity, saturation, tortuosity) can yield similar geophysical responses, making it difficult to isolate the true system state from measurements alone (Tso *et al.*, 2019). In our study, we probed this issue by repeating the BEL workflow using fixed (deterministic) values for the Archie and van Genuchten parameters. This experiment effectively removed epistemic parameter uncertainty, allowing us to disentangle its influence from aleatory heterogeneity in the spatial distribution of water content. The improvement in high-TWS prediction accuracy (Fig. 5.8) highlights how parameter variability can mask true differences in total water content by producing overlapping ERT signatures. These findings are consistent with the robustness analysis by Ahmed *et al.* (2024), who demonstrated that constraining petrophysical priors in BEL significantly narrows posterior variance. Together, these results support the view that targeted laboratory

measurements of key parameters (e.g., site-specific Archie exponents) can play a decisive role in reducing predictive uncertainty and improving interpretability in geoelectrical moisture estimation.

In Figure 5.9, we show boxplots of the Bayesian Neural Network's predictive distributions for four field datasets (BB11Z_05, BB11Z_06, BB11Z_07, and BB11Z_02). Each dataset exhibits a spread of Monte Carlo predictions between approximately 3.5 and 6 m^3/m^2, with the median (red line) generally near 5 m^3/m^2. Although there are some fluctuations in the mean values for these real measurements, the variation can be neglected compared with its prediction uncertainty. These patterns mirror our synthetic tests (*cf.* Figures 5.7 and 5.8), where parameter variability can cause ambiguous resistivity signals and lead the network to adopt a conservative bias.

The results clearly show that the real ERT data can be used to quantify the uncertainty of total water storage in the waste body, while its capacity to quantify the water storage change is constrained by the high uncertainty in the model parameters.

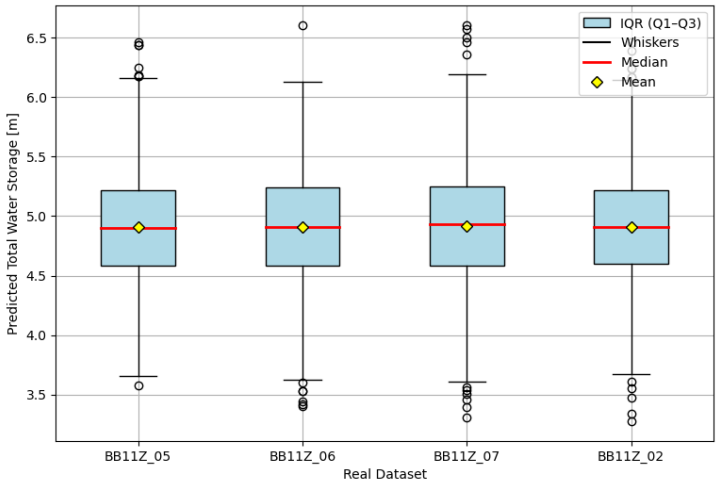

Figure 5.9.: Boxplot of the Bayesian neural network's Monte Carlo predictions for the four real datasets (BB11Z_05, BB11Z_06, BB11Z_07, BB11Z_02). Each box extends from the first quartile (*Q1*) to the third quartile (*Q3*), with the red horizontal line indicating the median. The whiskers represent a conventional range of ±1.5 × IQR from the quartiles, and any samples outside this range are shown as circular outliers. The yellow diamond within each box denotes the mean of the distribution. The light blue shading of the boxes helps visualize the spread and central tendency of the Monte Carlo predictions.

5.4. CONCLUSIONS

This study presents a novel approach to quantify the water content of landfill waste bodies using Electrical Resistivity Tomography (ERT) data within the Bayesian Evidential Learning (BEL) framework. Unlike traditional inversion-based approaches, the BEL method directly learns statistical relationships between resistivity measurements and total water storage (TWS), bypassing the ill-posed resistivity inversion process. This approach significantly reduces model-related uncertainties and offers robust quantification of TWS, accompanied by meaningful uncertainty estimates.

Our results show that the BEL framework successfully incorporates complex hydrogeophysical relationships to provide reliable estimations of landfill water storage. The forward modeling procedure, incorporating stochastic generation of saturation distributions, demonstrated its capability to encompass the observed ERT responses. The falsification tests validated that the prior model and generated synthetic datasets were representative of the actual landfill conditions, as all observed ERT datasets aligned closely with the simulated data distribution.

The Bayesian Neural Network (BNN) predictions demonstrated high accuracy and reliable uncertainty quantification for moderate TWS ranges. However, the BNN tended to underestimate higher TWS values, especially under conditions of parameter uncertainty. Numerical experiments showed that this underestimation primarily arises from uncertainties in hydrogeophysical parameters (e.g., parameters in Archie's law and water retention curves). When these parameters were held deterministic, the prediction accuracy improved substantially, highlighting the critical role parameter uncertainties play in shaping predictive performance.

These insights emphasize that parameter uncertainty poses a significant challenge for accurate quantitative interpretation of ERT data in heterogeneous landfill environments. Reducing uncertainties through targeted experiments or additional complementary measurements would enhance the predictive performance and reliability of the BEL-based approach.

The developed BEL methodology represents a significant step forward in landfill moisture monitoring, providing robust uncertainty quantification and avoiding the inherent challenges associated with traditional inversion methods. Future research should focus on constraining critical hydrogeophysical parameters to further enhance prediction accuracy, particularly in high-water-storage scenarios, thus strengthening its application in environmental risk assessment and landfill management.

REFERENCES

Ahmed, A., Aigner, L., Michel, H., Deleersnyder, W., Dudal, D., Orozco, A. F., & Hermans, T. (2024). Assessing and improving the robustness of Bayesian evidential learning in one dimension for inverting TDEM data: Introducing a new threshold procedure.

Bounsiar, A., & Madden, M. G. (2014). One-Class Support Vector Machines Revisited. *2014 International Conference on Information Science & Applications (ICISA)*, 1–4. https://doi.org/10.1109/ICISA.2014.6847442

Feng, S.-J., Bai, Z.-B., Cao, B.-Y., Lu, S.-F., & Ai, S.-G. (2017). The use of electrical resistivity tomography and borehole to characterize leachate distribution in Laogang landfill, China. *Environmental Science and Pollution Research*, *24*(25), 20811–20817. https://doi.org/10.1007/s11356-017-9853-0

Heimovaara, T. J., & Wang, L. (2025). Quantification of Emission Potential of Landfill Waste Bodies Using a Stochastic Leaching Framework. *Water Resources Research*, *61*(3), e2024WR038360. https://doi.org/10.1029/2024WR038360

Hermans, T., Lesparre, N., de Schepper, G., & Robert, T. (2019). Bayesian evidential learning: A field validation using push-pull tests. *Hydrogeology Journal*, *27*(5), 1661–1672. https://doi.org/10.1007/s10040-019-01962-9

Hermans, T., Nguyen, F., Klepikova, M., Dassargues, A., & Caers, J. (2018). Uncertainty Quantification of Medium-Term Heat Storage From Short-Term Geophysical Experiments Using Bayesian Evidential Learning. *Water Resources Research*, *54*(4), 2931–2948. https://doi.org/10.1002/2017WR022135

Hou, Z., & Rubin, Y. (2005). On minimum relative entropy concepts and prior compatibility issues in vadose zone inverse and forward modeling. *Water Resources Research*, *41*(12). https://doi.org/10.1029/2005WR004082

Hu, J., Ke, H., Lan, J.-W., Chen, Y.-M., & Meng, M. (2020). A dual-porosity model for coupled leachate and gas flow to vertical wells in municipal solid waste landfills. *Géotechnique*, *70*(5), 406–420. https://doi.org/10.1680/jgeot.18.P.193

Hu, J., Wu, X. W., Ke, H., Xu, X. B., Lan, J. W., & Zhan, L. T. (2019). Application of electrical resistivity tomography to monitor the dewatering of vertical and horizontal wells in municipal solid waste landfills. *Engineering Geology*, *254*, 1–12. https://doi.org/10.1016/j.enggeo.2019.03.021

Jolliffe, I. T., & Cadima, J. (2016). Principal component analysis: A review and recent developments. *Philosophical Transactions of the Royal Society A: Mathematical, Physical and Engineering Sciences*, *374*(2065), 20150202. https://doi.org/10.1098/rsta.2015.0202

Jospin, L. V., Buntine, W., Boussaid, F., Laga, H., & Bennamoun, M. (2022). Hands-on Bayesian Neural Networks – a Tutorial for Deep Learning Users. *IEEE Computational Intelligence Magazine*, *17*(2), 29–48. https://doi.org/10.1109/MCI.2022.3155327

Li, K., Chen, Y. M., Xu, W. J., Zhan, L. T., Ling, D. S., Ke, H., Hu, J., & Li, J. L. (2021). A thermo-hydro-mechanical-biochemical coupled model for file:///home/lwang19/Documents/literatures/ES-MDA_TU_Delft_March_2022.pdf landfilled municipal solid waste. *Computers and Geotechnics*, *134*(March). https://doi.org/10.1016/j.compgeo.2021.104090

Linde, N., & Doetsch, J. (2016). Joint Inversion in Hydrogeophysics and Near-Surface Geophysics. In *Integrated Imaging of the Earth* (pp. 117–135). American Geophysical Union (AGU). https://doi.org/10.1002/9781118929063.ch7

Lu, S.-F., Feng, S.-J., Zheng, Q.-T., & Bai, Z.-B. (2021). A multi-phase, multi-component model for coupled processes in anaerobic landfills: Theory, implementation and validation. *Géotechnique*, *71*(9), 826–842. https://doi.org/10.1680/jgeot.20.P.002

Lu, S.-F., Xiong, J.-H., Feng, S.-J., Chen, H.-X., Bai, Z.-B., Fu, W.-D., & Lü, F. (2019). A finite-volume numerical model for bio-hydro-mechanical behaviors of municipal solid waste in landfills. *Computers and Geotechnics*, *109*, 204–219. https://doi.org/10.1016/j.compgeo.2019.01.012

Michel, H., Nguyen, F., Kremer, T., Elen, A., & Hermans, T. (2020). 1D geological imaging of the subsurface from geophysical data with Bayesian Evidential Learning. *Computers & Geosciences*, *138*, 104456. https://doi.org/10.1016/j.cageo.2020.104456

Neyamadpour, A. (2019). 3D monitoring of volumetric water content using electrical resistivity tomography in municipal solid waste landfill. *Environmental Earth Sciences*, *78*(14), 1–9. https://doi.org/10.1007/s12665-019-8436-4

Pradhan, A., & Mukerji, T. (2020). Seismic Bayesian evidential learning: Estimation and uncertainty quantification of sub-resolution reservoir properties. *Computational Geosciences*, *24*(3), 1121–1140. https://doi.org/10.1007/s10596-019-09929-1

Rücker, C., Günther, T., & Wagner, F. M. (2017). pyGIMLi: An open-source library for modelling and inversion in geophysics. *Computers & Geosciences*, *109*, 106–123. https://doi.org/10.1016/j.cageo.2017.07.011

Saneiyan, S., Gimenez, D., Siegenthaler, E., & Slater, L. (2024). On the accuracy of saturation estimation from electrical measurements of soils with high swelling clay content. *Vadose Zone Journal*, *23*(4), e20340. https://doi.org/10.1002/vzj2.20340

Scheidt, C., Li, L., & Caers, J. (2018, June). *Quantifying Uncertainty in Subsurface Systems*. John Wiley & Sons.

Thibaut, R., Laloy, E., & Hermans, T. (2021). A new framework for experimental design using Bayesian Evidential Learning: The case of wellhead protection area. *Journal of Hydrology*, *603*, 126903. https://doi.org/10.1016/j.jhydrol.2021.126903

Tso, C.-H. M., Kuras, O., & Binley, A. (2019). On the field estimation of moisture content using electrical geophysics: The impact of petrophysical model uncertainty. *Water Resources Research*, *55*(8), 7196–7211.

Wang, L., & Heimovaara, T. J. (2025a). Quantifying landfill emission potential using a weakly coupled particle filter. *Water Resources Research*, *61*(2), e2023WR036549. https://doi.org/10.1029/2023WR036549

Wang, L., & Heimovaara, T. J. (2025b). *Quantifying water content of a landfill with ert data by bayesian evidential learning* [Under review].

Zeng, G., Liu, L., Xue, Q., Wan, Y., Ma, J., & Zhao, Y. (2017). Experimental study of the porosity and permeability of municipal solid waste. *Environmental Progress & Sustainable Energy*, *36*. https://doi.org/10.1002/ep.12632

Zhan, L.-t., Xu, H., Jiang, X.-m., Lan, J.-w., Chen, Y.-m., & Zhang, Z.-y. (2019). Use of electrical resistivity tomography for detecting the distribution of leachate and gas in a large-scale MSW landfill cell. *ENVIRONMENTAL SCIENCE AND POLLUTION RESEARCH*, *26*(20), 20325–20343. https://doi.org/10.1007/s11356-019-05308-6

Zhang, C., Liang, B., Liu, L., Wan, Y., & Zhu, Q. (2021). Determination of Unsaturated Hydraulic Properties of Seepage Flow Process in Municipal Solid Waste. *Water*, *13*(8), 1059. https://doi.org/10.3390/w13081059

6

CONCLUSIONS AND RECOMMENDATIONS

6.1. CONCLUSIONS

This thesis set out to enhance our understanding and quantification of landfill emission potential by combining stochastic flow and transport modeling, data assimilation, and hydrogeophysical methods. Drawing on four key chapters, we pursued a progression from model development and validation to advanced data assimilation and finally leveraging hydrogeophysical measurements for water-storage estimation. Below is a concise synthesis of the chief findings in this research.

In the first part of this research, we developed a stochastic travel-time model, based on water life expectancies, to capture the heterogeneous flow pathways within landfill waste bodies. By formulating the *emission potential* for conservative solutes (e.g., chloride), we demonstrated that long-term leachate flux and composition measurements can be used to determine how preferential inflows from the cover layer and a bulk "stagnant" zone both drive outflow concentration. Results showed that preferential flow exerts a dominant influence on leachate release, whereas the stagnant zone significantly affects contaminant discharge during low-flow periods.

Building on that model, we then introduced a *weakly coupled Particle Filter* approach to reduce uncertainties in both water-storage states and the solute mass. By simultaneously assimilating leachate flow (LPR) and concentration data, this method effectively refines estimates of bulk water volume and pollutant mass over time. It emerged that the model's baseflow can only be used to estimate bulk storage if it's sensitive to the bulk storage variations, highlighting the importance of monitoring over sufficiently long time-spans to capture the sensitive range in the baseflow function.

Subsequently, we presented a *PF–MCMC* assimilation method that jointly updates model parameters and states. Synthetic experiments confirmed that this hybrid approach yields lower uncertainties than open-loop simulations, especially regarding bulk chloride concentration and water travel times. It also validates the feasibility of combining several parameters to estimate the hidden processes in the landfill. Real case study in PF-MCMC chapter at the Braambergen landfill reinforced these benefits, while revealing the limitations imposed by measurement error and possible model simplifications. Ensuring accurate parameter estimation and incorporating finer-scale heterogeneity remain key challenges for future refinement.

Finally, we applied a *Bayesian Evidential Learning (BEL)* framework to use Electrical Resistivity Tomography (ERT) data for landfill water-storage estimation. By bypassing conventional inversion in favor of a direct statistical mapping between simulated resistivity signatures and water content, we produced reliable total water storage predictions while quantifying uncertainties. However, uncertainty in the parameter values, like Archie's law exponents, can lead to an underestimation of higher water

contents. Fixing these parameters at deterministic values greatly improved predictive accuracy, underscoring the importance of well-constrained subsurface properties in hydrogeophysical models.

Collectively, this thesis demonstrates that combining Lagrangian-based transport models, advanced data assimilation, and hydrogeophysical surveys can significantly enhance landfill emission potential assessments.

6.2. CONTRIBUTIONS AND IMPLICATIONS

The research presented in this thesis offers several key contributions:

- *Emission Potential Formalization*: By formalizing the term *emission potential* within a stochastic framework, this work provides landfill operators and regulators with a clearer, quantitatively defined metric to support aftercare decisions. Chapter 5 demonstrates that the total water storage estimated from ERT data likely exceeds $5 m^3/m^2$, whereas the water content estimated by the PF-MCMC method in Chapter 4 is lower than $1 m^3/m^2$. Assuming a volumetric residual water content of 0.2, the total residual water in the waste body (with a height of 14m) is approximately $2.8 m^3/m^2$. These findings suggest that more than $1 m^3/m^2$ of water is stored in isolated zones within the waste body. Considering the average concentration for leachable is probably lower than the isolated water, the defined emission potential is substantially smaller than the total pollutant mass, underscoring the importance of distinguishing between leachable and non-leachable water in emission potential assessments.

- *Integrated Assimilation Approaches*: Combining PF–MCMC with a flexible, Lagrangian-based travel time model has proven both tractable and capable of incorporating multiple data streams (e.g., flow rates, concentrations).

- *Reduced Data Requirements*: Stochastic modeling avoids explicit high-resolution characterization of landfill heterogeneity, relying instead on probabilistic distributions of travel times and site-specific data. This reduces the need for large-scale field campaigns, while still capturing the principal controls on leachate generation and pollutant release.

- *Practical Guidance for Landfill Aftercare*: By demonstrating how real-time data assimilation can update model states, the methods developed here can serve as valuable decision-support tools, aiding in the optimization of leachate management, irrigation strategies, and risk assessments.

6.3. RECOMMENDATIONS FOR FUTURE WORK

While this thesis advances the state of the art, several limitations remain. We will discuss these issues and also give suggestions for future research.

- The methods largely focus on conservative solutes (e.g., chloride). Additional complexities arise for reactive species, where chemical transformations and microbial degradation must be considered. Extending the modeling framework to handle reactive and multi-component transport in an integrated manner could give a more comprehensive view of landfill emissions, particularly for ammonium, organic contaminants, or other compounds.

- Data assimilation performance depends heavily on the conceptual model. Structural errors inevitably arise since no model can perfectly capture all real-world processes. In practice, the data assimilation methods used here treat the model's structure as correct so that any missing processes may be artificially compensated for by adjustments to parameters or states. This compensation can introduce estimation bias, reflecting a broader risk in approaches that assume complete and accurate model formulations. Future research could leverage the existing data assimilation framework to understand parameter behaviors and hidden states better, thereby diagnosing and quantifying missing processes. Additionally, we can combine multiple model variants through model averaging or Bayesian model selection instead of relying on a single conceptual model.

- Current research mainly relies on literature-based parameter ranges for the water retention curve and Archie's law. Because these priors can be unnecessarily broad, this will lead to underestimating higher water contents. Moreover, the resulting predictive uncertainty is larger than typical month-to-month fluctuations in landfill water storage, thereby reducing the model's ability to detect real changes over time. To address this, future studies could collect samples from the cover layer and multiple zones within the waste body for laboratory experiments, not to pinpoint deterministic parameter values but to establish more informative prior distributions. Additionally, the ERT measurement array should be deliberately designed to increase sensitivity to water storage variations within the waste mass, for example, by extending current surface-based surveys into deeper landfill regions.

- ERT surveys were intended to reduce uncertainties in landfill water storage. However, the water storage estimated from ERT is often larger than that derived from water balance models, because ERT captures total water, including isolated zones that do not affect leachate outflow. By contrast, the hydraulic model focuses on

the leachable water fraction. Consequently, we cannot simply treat the ERT-based storage as a direct observation in the water balance model. Nevertheless, if the ERT measurements can reliably track changes in storage (rather than just absolute magnitudes), they could serve as an external observation source to further constrain the model's uncertainty. The current relationship between ERT data and total water storage, built by a Bayesian neural network, could be seen as the observation operator in a data assimilation framework. Hence, once issues of accuracy and parameterization are addressed, future work should focus on integrating ERT data into a data assimilation framework to enhance landfill water storage predictions.

6.4. FINAL REMARKS

In closing, this thesis highlights the benefits of combining *stochastic modeling*, *advanced data assimilation*, and *hydrogeophysical surveys* to enhance the quantification of landfill emission potential. By integrating these tools, researchers and practitioners can better address the uncertainties inherent in waste heterogeneity, leading to more robust predictions of leachate and pollutant release and, consequently, improved aftercare strategies.

Yet, several challenges remain. Increased focus on *reactive transport processes*, more precise *parameter constraints* (e.g., via laboratory experiments), and greater *measurement coverage* in hydrogeophysical campaigns are all vital next steps. Refining how ERT-based estimates of total water storage align with hydraulic models, especially regarding non-leachable water fractions, will further improve modeling consistency. Data assimilation methods can be more confidently applied as these technical refinements progress, ultimately reducing both financial and environmental risks associated with long-term landfill management.

NOMENCLATURE

c_{bulk_t}	Chloride concentration in bulk at time t
$c_{cell_t^i}$	Chloride concentration in i th cell at time t
C_{cl_t}	Chloride concentration in cover layer at time t
C_{wb_t}	Chloride concentration in waste body at time t
m_{bulk_t}	Chloride mass in bulk at time t
$m_{cell_t^i}$	Chloride mass in i th cell at time t
M_{cl_t}	Chloride mass in cover layer at time t
M_{wb_t}	Chloride mass in waste body at time t
v_{bulk_t}	Water content in bulk at time t
$v_{cell_t^i}$	Water content in i th cell at time t
V_{cl_t}	Water content in cover layer at time t
V_{wb_t}	Water content in waste body at time t
a_{arc}	Tortuosity factor in Archie's Law
a_{soil}	Tortuosity factor in Archie's Law for soil cover
a_{bF}	Shape parameter of the gamma distribution for base flow life expectancy (dimensionless)
A_{lf}	Surface area of the landfill [m^2]
α	Inverse air entry suction parameter in van Genuchten model (L^{-1})
$a_{\xi,t}$	An independently and identically distributed random error with zero mean and unit standard deviation, described by a skew exponential power (SEP)
b_{cl}	An empirical shape factor for the non-linear flow term of the cover layer [-]
β	Kurtosis parameter for the error distribution in the generalized likelihood function

β_f The fraction of fast flow in the waste body [-]

c_β Nuisance parameter which is calculated as a function of ξ and β.

c_{cl} The solute concentration in the water present in the cover layer [$\mathrm{kg\,m^{-3}}$].

C_f An empirical crop-factor to compensate for different types of crops in order to close the water balance [—]

c_{wb} The solute concentration in the water present in the waste body [$\mathrm{kg\,m^{-3}}$]

DD Dipole-Dipole configuration in ERT measurement

E_{pot} The potential evapotranspiration at the boundary of the cover layer [$\mathrm{m\,d^{-1}}$]

$f(\tau)$ A system function describing how the waste body transforms the infiltration flux to the leachate flux [-]

f_{red} Empirical reduction factor to reduce evpo-transpiration when the cover layer gets too dry [-]

$f_{w_{wb},min}$ Residual volumetric water content in the bulk storage of the waste body [-].

$f_{w_{cl},min}$ Fraction of the maxmum volumetric water content in the cover layer used for parameterization of the minimum storage of the cover layer [-].

H_{lf} Total height of the landfill [m].

H_{cl} The thickness of the cover layer [m].

H_{wb} The height of the waste body [m].

k Fraction of saturated cells in the landfill grid

K_{cl} The saturated hydraulic conductivity of the cover layer [$\mathrm{m\,d^{-1}}$]

$L(t, \tau_i, \sigma_i)$ The log-normal probability density function as a function of time which is characterised by geometric mean travel time t_i and variance σ_i, where i stands for either the fast flow fraction or the slow flow fraction

L_{tot} Sum of the three likelihood functions

m_{arc} Cementation exponent in Archie's Law

m_{soil} Cementation exponent in Archie's Law for soil cover

M_{cl} The mass of solute in the cover layer [kg/m^2]

M_{cl} The solute mass in the cover layer [kg m^{-2}].

μ_{bF} scale factor for the base flow function [m].

M_{wb} The mass of solute in the waste body [kg/m^2]

M_{wb} The solute mass in the waste body [kg m^{-2}]

n Number of observations in a measurement data set [-]

n Pore-size distribution index in van Genuchten model

n Subscript indication time n [-]

n_{arc} Saturation exponent in Archie's Law

n_{soil} Saturation exponent in Archie's Law for soil cover

ν Parameter setting the fraction of outliers in one-class SVM

ω_{ξ} Nuisance parameter which is calculated as a function of ξ and β.

$p_{b_F}(T_E)$ Time invariant probability distribution function of life expectancies of water entering the waste body as base flow.

ϕ Porosity

$p_{q_{inf}}(T_E)$ Time invariant probability distribution function of life expectancies of water infiltrating from the cover layer at time t.

$p_{V_{wb}}(T_E, t)$ Probability distribution function of waste body water storage V_{wb} as a function of life-expectancy T_E at time t.

q_{bF} The 'base' flow from the bulk storage in to the mobile cells. This a function of bulk storage [m/d].

q_{bF_0} Maximum value for the 'base' flow from the bulk storage into the mobile cells. This is a function of bulk storage [m/d].

q_{drain} The leachate flux leaving the drainge system [m d^{-1}]

q_{inf} The water flux infiltrating from the cover layer into the waste body [m d^{-1}]

q_{leach} The leachate flux from the waste body to the drainage system [m d^{-1}]

$\boldsymbol{q_M}$ The solute mass flux [kg m^{-2} d^{-1}]

ρ Bulk electrical resistivity of the waste

ρ_w Resistivity of pore water (leachate)

$\rho_{w,\text{soil}}$ Resistivity of pore water in soil layer

V_{cl} The water storage in the cover layer [m]

$V_{cl_{max}}$ The maximum storage in the cover layer before by pass flow occurs [m]

$V_{cl_{min}}$ The minimum storage in the cover layer that allows infiltration [m]

S_{eff} Effective saturation

S_{eff} The effective saturation of the cover layer [-]

σ_{slow} Standard deviation of the travel time in the slow lognormal travel time distribution [d]

σ_ξ Nuisance parameter which is calculated as a function of ξ and β.

σ_{bF} shape factor for the base flow function [m].

SLM Schlumberger configuration in ERT measurement

V_{total} Water storage in the landfill. Volume water per unit area landfill. [m]

V_{wb} Water storage in the waste body. [m]

τ Time of infiltration in to the waste body (integration parameter) [d]

τ_{fast} Expected value of the fast travel time in the log-normal travel time distribution [d]

τ_{slow} Expected value of the slow travel time in the log-normal travel time distribution [d]

T_E Remaining life expectancy time of a water parcel in the waste body [d].

$\boldsymbol{\theta}$ Vector containing all parameters in the model

θ Volumetric water content

$L(\boldsymbol{\theta} \mid \hat{\mathbf{y}})$ Likelihood of the model assuming model vector $\boldsymbol{\theta}$ and measured data $\hat{\mathbf{y}}$

θ_{cl} Volumetric water content of the cover layer

θ_r Residual volumetric water content

$\theta_{r,\text{soil}}$ Residual volumetric water content in soil

θ_s Saturated volumetric water content

$\theta_{s,\text{soil}}$ Saturated volumetric water content in soil

$\theta_{w_{cl}}$ The volumetric water content in the cover layer [-].

$\theta_{w_{cl},max}$ The maximum volumetric water content in the cover layer used for parameterization of the model [-].

$\theta_{w_{wb}}$ The volumetric water content in the waste body [-].

T_R Residence time of a water parcel in the waste body [d].

T_T Total life time of a water parcel in the waste body [d].

μ_{bF} Scaling factor for the bulk storage in the base flow function [m]

$V_{bulk,min}$ Minimal storage in the bulk of the waste body where baseflow will be zero

V_{lf} Total volume of the landfill [m^3]

S_{total} Volume of water in the landfill [m^3]

$\boldsymbol{x_{dl}}$ path along with a water particle travels through the waste body [m]

ξ Skewness parameter for the error distribution in the generalized likelihood function

$\hat{\mathbf{y}}$ Vector containing measurement data related to simulated output

y_{min} parameter allowing the heteroscedastic part of the measurement error to be zero at a minimum value of the measurement

A

SUPPORTING INFORMATION FOR CHAPTER 2

The main paper applies the model to data from the 11Z cell of the Braambergen landfill near Almere in the Netherlands. In this supporting information, similar results are shown for applying the model to three other landfill cells: Braambergen 11N, Braambergen 12, and cell 6 of the Wieringermeer landfill near Medemblik.

The motivation for providing these results is to demonstrate the general applicability of the Landfill Emission Modelling concept and corresponding estimates of the emission potential for these three additional landfill cells. And strengthen the conclusions drawn in the main paper.

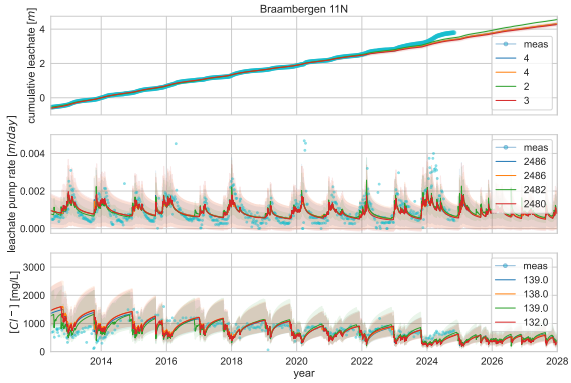

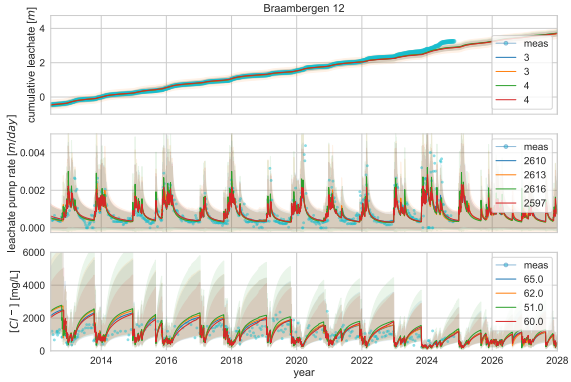

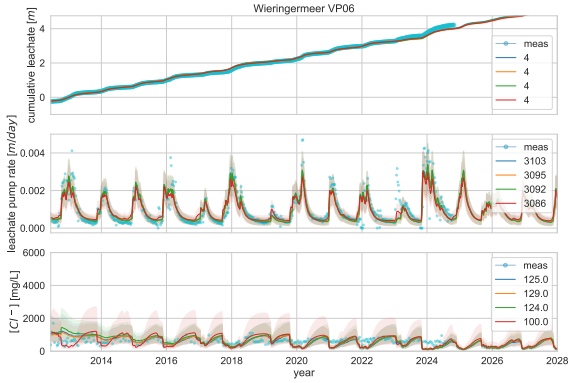

Figure S2.: Simulated and measured values of cumulative leachate production, leachate pump rate and leachate chloride concentration for Braambergen 11N, 12 and Wieringermeer VP06

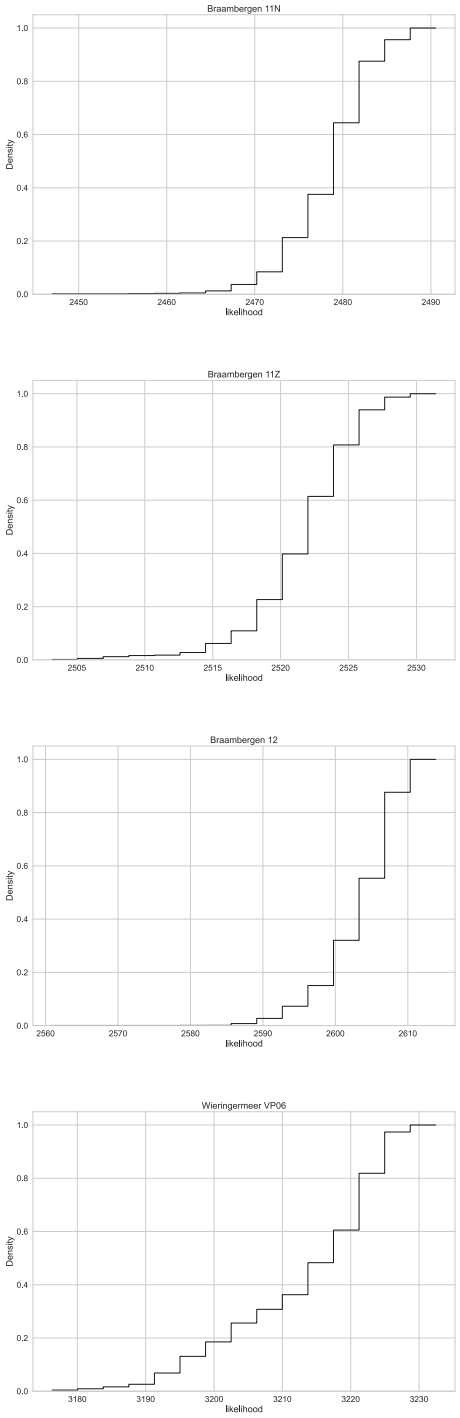

Figure S1.: Posterior likelihood distributions for for Braambergen 11N, 11Z, 12 and Wieringermeer VP06

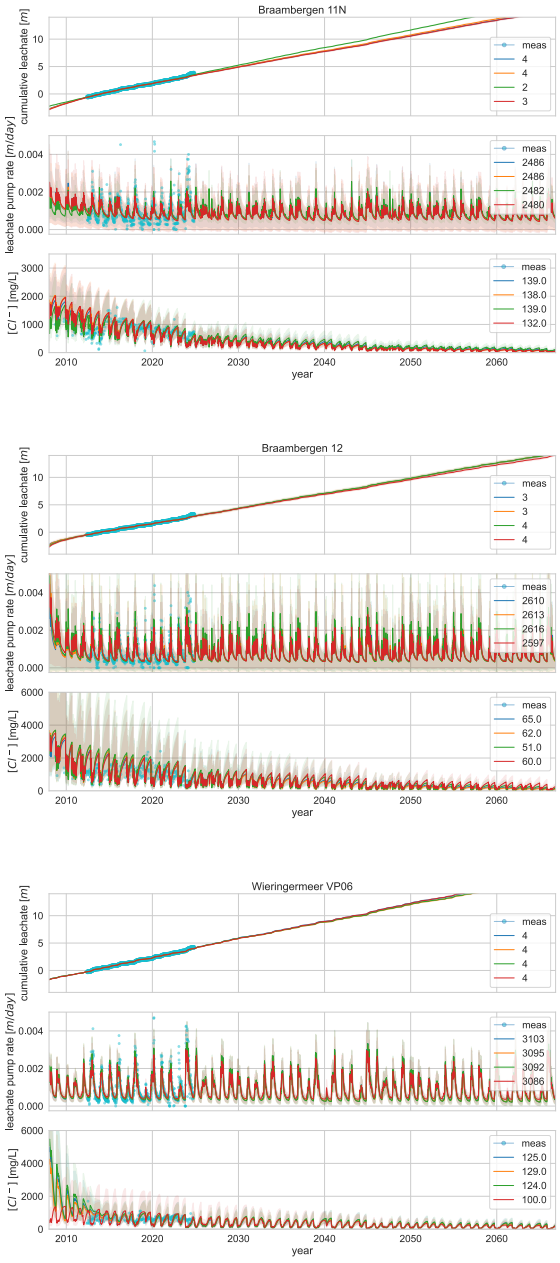

Figure S3.: Long-term extrapolation for Braambergen 11N, 12 and Wieringermeer VP06

ACKNOWLEDGEMENTS

First and foremost, I wish to express my deepest gratitude to my promoter, Prof. Timo Heimovaara, and my co-promotor, Prof. Julia Gebert, for their unwavering support and patient guidance throughout my PhD journey. I am especially indebted to Timo for offering me the opportunity to pursue my doctoral research in Delft. Whenever I encountered challenges, he provided timely and insightful guidance, often presenting perspectives that were unconventional yet profoundly meaningful. These exchanges helped me cultivate a more critical approach to my work and encouraged me to consider problems from a practical standpoint. His enduring optimism has been a constant source of motivation and played a pivotal role in the successful completion of this dissertation. I am equally grateful to Julia for her invaluable advice and steadfast support, particularly in organizing the field experiments. Also, our weekly group meetings will remain a cherished memory and a highlight of this journey.

I would also like to express my sincere thanks to Prof. Femke C. Vossepoel for her generous support in introducing me to the field of data assimilation. Her guidance opened the door to a discipline that became a cornerstone of my research. I am equally grateful for the opportunity to participate in her group's discussions and activities, which not only broadened my academic perspective but also gave me the chance to form many valued friendships.

Many thanks to friends and colleagues in the CURE project: Hans Lammen, Hans Oonk, Carmen, Heijo, Rob, Richard, Tristan, and Anne-Catherine. Their arm support and insightful suggestions make my research life much easier and happier.

I would like to express my heartfelt thanks to the technical staff in Delft, especially Roland, Jens, Cristina, Karel, and Marc, for their tremendous support throughout this project. I am particularly grateful to Roland for his invaluable help during the fieldwork. Whether it was winter or summer, setting up tents in the wind, or even learning how to herd sheep in the field, our shared experiences have left me with countless memorable stories.

I would like to thank my PhD committee members for their valuable time and insightful comments, which have greatly helped me to improve the clarity of my thesis.

Thanks to my friends and colleagues: Nathali, Cristhian, Frank, Nick, Susan, Andre, Leo, Nasim, Bhini, Laura, Nazeir, Tees, Divya, Hamed,

Samantha, Jenny, Mohsan, Meiling, Gabriel, Celine, Max, Dieter, Tilman, Simon, Reuben, Issa, and Sebastijan. I would also like to thank the small but warm-hearted Chinese community both within and beyond the Geo-Engineering section, in particular: Aoxi, Xuehui, Yuen, Zheng, Xiangcou, Weiyuan, Haoyuan, Lexin, Wen, Na Hao, Zhaojiang, Wei, Man, Jiarui, Yidou, Dayu, Hao, Junhan, Na Li, and Ye. Their humor and kindness made this PhD journey much warmer, and I am truly grateful for all the joyful moments we shared together.

This thesis would not have taken its present shape without the unwavering trust, support, and unconditional love of my parents and family, for which I am forever grateful.

CURRICULUM VITæ

Liang Wang

02-01-1994	Born in Changzhou, Jiangsu.

EDUCATION

2024–2025	postdoc researcher in Algorithmics Delft University of Technology, the Netherlands
2019–2024	PhD candidate in Geoengineering Delft University of Technology, the Netherlands
2016–2019	MSc in Geotechnical Engineering Southeast University, China
2012–2016	BSc in Civil Engineering Nanjing Tech University, China

LIST OF PUBLICATIONS

1. Wang, L., & Heimovaara, T. J. (2025). Quantifying landfill emission potential using a weakly coupled particle filter. *Water Resources Research*, *61*(2), e2023WR036549. https://doi.org/10.1029/2023WR036549

2. Heimovaara, T. J., & Wang, L. (2025). Quantification of Emission Potential of Landfill Waste Bodies Using a Stochastic Leaching Framework. *Water Resources Research*, *61*(3), e2024WR038360. https://doi.org/10.1029/2024WR038360

3. Wang, L., & Heimovaara, T. J., Understanding hidden processes in landfill emission by applying PF-MCMC in coupled travel time distribution model. (Under review in WRR)

4. Wang, L., & Heimovaara, T. J., Quantifying water content of a landfill with ERT data by Bayesian evidential learning. (Under review in GRL)